Indian Institute of Science
Department of Physics
Department of Instrumental & Applied Physics

Master of Science in Physics

Quantum-walk based simulations & algorithms

Masters Dissertation of:
Himanshu Sahu

Advisors:
Prof. Subroto Mukerjee & Prof. CM Chandrashekar

Tutor:
Prof.

Supervisor of the MS Program:
Prof. Prateek Sharma

Research is what I'm doing when I don't know what I'm doing.
– Wernher von Braun

Declaration

I, Himanshu Sahu, hereby declare that the content presented in this MS Thesis titled '*Quantum-walk based simulations & algorithms*' represents the culmination of my work conducted at the Department of Instrumental & Applied Physics, Indian Institute of Science, Bangalore, under the guidance of Prof. CM Chandrashekar. This work is original and has not been previously submitted for any degree or diploma. I have duly acknowledged and referenced any findings or insights drawn from the work of others in adherence to academic conventions.

Himanshu Sahu
Bangalore
March 2024

Certification

This is to certify that the work contained in this project report entitled '*Quantum-walk based simulations & algorithms*' submitted by *Himanshu Sahu*, towards the partial fulfillment of the degree of Master in Science in Physics has been carried out by him under my supervision at the Department of Instrumental & Applied Physics, Indian Institute of Science, Bangalore, and no part of it has been previously submitted for a degree, diploma or any other qualification at this university or any other institution.

List of Publications

Listed in the order, their content is discussed in the thesis.

The thesis is based on the following publications:

- H. Sahu & C.M. Chandrashekar, Open system approach to Neutrino oscillations in a quantum walk framework, (2023). Quantum Information Processing 23, 7 (2024).
- H. Sahu & K. Sen, Quantum-walk search in motion. Scientific Reports 14, 2815 (2024).
- A. Bhattacharya, H. Sahu, A. Zahed, and K. Sen, Complexity for one-dimensional Discrete Time Quantum Walk Circuits, (2023). Phys. Rev. A 109, 022223 (2024).

Other Publications

Listed in the order, their appearence in arXiv.

Other publications during MS, not included in thesis

- A. Bhattacharya, P.P. Nath & H. Sahu, Speed limits to the growth of Krylov complexity in open quantum systems, (2024).[1] arXiv:2403.03584 [quant-ph] To be appear in Physical Reivew D Letter
- K.V. Sharma, H. Sahu & S. Mukerjee, Quantum chaos in $\mathcal{PT}$-symmetric Quantum Kicked Rotor, (2024). arXiv:2401.07215 [quant-ph]
- A. Bhattacharya, P.P. Nath & H. Sahu, Krylov complexity for non-local spin chains. Phys. Rev. D 109, 066010 (2024).[1]
- A. Bhattacharya, P. Nandy, P.P. Nath & H. Sahu, On Krylov complexity in open systems: an approach via bi-Lanczos algorithm, (2023). J. High Energ. Phys. 2023, 66 (2023).[1]
- A. Bhattacharya, P. Nandy, P.P. Nath & H. Sahu, H. Operator growth and Krylov construction in dissipative open quantum systems. J. High Energ. Phys. 2022, 81 (2022).[1]

Conferences, Seminar, and Schools

Talks

- Quantum Information Scrambling in non-local systems
  CHEP In-House Symposium, Centre for High Energy Physics, Indian Institute of Science, Bangalore, India 18-19 November 2023

[1] All authors contributed equally in this work. The authors of this paper were ordered alphabetically.

Posters

- Simulating Neutrino Oscillations Using Quantum-walk
  Quantum Information Processing and Applications, Harish-Chandra Research Institute, Prayagraj, India 04-10 December 2023.
- Quantum Information Scrambling in Dissipative Open Quantum Systems
  Emerging Topics in Quantum Technology, Indian Institute of Technology, Palakkad, India 02-04 November 2023.
- Operator Complexity in Open Quantum System
  Condensed Matter meets Quantum Information, International Centre for Theoretical Sciences (ICTS), Bengaluru, India 25 Sep-06 Oct 2023
- Neutrino oscillations in discrete-time quantum walk framework
  Student Conference in Optics and Photonics, Physical Research Laboratory, Ahmedabad, India 27-29 September 2023.
- Exploring Operator Growth and Krylov Complexity in Dissipative Open Quantum Systems
  It from Qubit, Perimeter Institute for Theoretical Physics, Waterloo, Ontario, Canada 31 July-4 August 2023 (Online)

Acknowledgement

"Words do not express thoughts very well. They always become a little different immediately after they are expressed, a little distorted, a little foolish."

-Hermann Hess, Demian

In the Steppenwolf treatise, there is something to the effect that it is only a fancy of his to believe that he has one soul, or two, that he is made up of one or two personalities. Every human being, it says, consists of ten, or hundred, or a thousand souls.

I imagined that I too was very backward in all the little arts of living. I had never known much of this side of life. Himanshu – the thinker – is a decades years old, but Himanshu – the dancer – is scarcely half a day old. In the last three years, its the later which has aged significantly. And he could not have make it so without a lot of support from a people with diverse perspectives, opinions, and wisdom. In my view, I have been very lucky in all aspects of life —specially in terms of people in my life, but it will save time to only list the people who contributed to finish this dissertation.

- CM Chandrashekar, my advisor, has taught me much on the independent research – and how it is done. I will leave aside much of his stories, but list some advice: no work completely solves a problem so read until you find a new way in its ending. Chandrashekar had one stipulation: why this problem is worth doing? This stipulation led me to a lot of practice in trying to come up with the ideas that are interest to a large community.

In fact, I would say this is now stamped in my brain to ask the implementation of the idea. Nevertheless, I still believe in the usefullness of useless knowledge.

- I must say that meeting with Aranya Bhattacharya was rather a coincidence and a gamble on my end. He led me to face-up the research – from its basics, technical writing to research culture, in general. He introduced me many more people (some of whom, I'll mention later), often indirectly who taught me much.

This is because I was so skeptical about giving a try to high-energy physics due to its reputation among my friends. Nevertheless, my early interest in the field led me to ask for a project from Aninda Sinha, who assigned me Aranya as a co-guide.

- Kallol Sen – who introduced to me by Aranya – is someone who is hard to catch up with when it comes to working on a problem. But I was also not someone who could back down easily and the struggle to catch up with him taught me a lot. Specially, shaping an idea that often stems from a naive question.

With him, I shared my first article – the day which any researcher will remember for a long time.

- The friends-side of this list is long, nevertheless, I would like to mention members of Fo-11 sitting place with whom I spend late nights doing assignments and discussing ideas that were not always from a textbook.

Aditi, Banashree, Harsh, Kanad, Kunal, Manish, Manishankar, Mridul, Narayan, Pradipta, Priesh, Prince, Ranju, Subhabhan, Suresh, Trideb, Vaibhav, Vivek (listed in alphabetically order).

It was great to be part of the Integrated Ph.D. 2021 batch — with whom I danced for the first time. I am indebted for the friendship, insight, and caring of an incredible number of them:

Harsh Vardhan Upadhyay, *who knows how to think practically;*
Kunal Shukla, *who remind us to not to take it too seriously;*
Narayan Dutt Sharma, *who is good at cracking bad jokes;*
Mridul Kandpal, *still hard to describe;*

Aditi Choudhary, *who tries not think too hard;*
Manishankar Ailiga, *who outperform us in all aspects;*
Vivek Kumar, *single rebellion for us all;*
Subhabhan Roy, *I'm not that bad, really.*
Kanad Sengupta, *who can take trivial things seriously;*

You all make me happy, miss you all.

There are a number of others who helped me one way or another. Pingal Pratyush Nath – still someone I known from Aranya – and Kshitij Sharma with whom I shared a pain of doing some heavy calculations, and writing papers. Also, there are number of faculties with whom I shared plenty of discussion – Subroto Mukerjee, Sumilan Banerjee.

But none of this could have happened without my family. Looking back, my moman have always encouraged me to pursue my interest and provide me all the help that many a time needed — given without asking. Thank you, moman.

Himanshu Sahu
Bangalore
March 2024

I am certain to fail this acknowledgement.

despite my forgetfullness

Witch!

Preface

This thesis embraces all the efforts that I put during the last three years as a MS student at the Indian Institute of Science. I have been working under the supervision of Prof. CM Chandrashekar, who is also the leader of the research group I am part of. In this time frame I had the wonderful opportunity of being "initiated" to research, which radically changed the way I look at things: I found my natural *"thinking outside the box"* attitude — that was probably well-hidden under a thick layer of lack-of-opportunities, I took part of very interesting joint works — among which the year I spent at the Quantum Optics and Quantum Information Lab at IISc is at the first place, and I discovered the Zen of my life.

While I come to like many a fields in physics, I had to choose one as I too *am horribly limited* just like Plath. So I thought "*why not choose something that lies in between many of my interests*"! My research is all about *quantum computers* and every other thing possibly related to them – physics, computer science, information theory to name few. So, despite my limitation to pursue many a field remain, of course – I thought, *quantum computers might give me opportunities to look now and then into here and there on what others are doing*.

One years later, I must say that quantum computing has not let me down – I explored, all kind of stuff and made this work come to life. There is a humongous amount of people that, directly or indirectly, have contributed to my research and, in particular, to this work. Since my first step into the lab, I will never be thankful enough to Prof. CM Chandrashekar, who, despite my impetuous behavior at times, has always been supportive. I can not thank enough to Aranya – working with whom may initiated by a coincidence, nevertheless, led to list of people to know, to work with and to learn from.

On the colleagues-side of this acknowledgments I put all the fellows of Room A203, the crew of the QOQI lab and, also to Kallol, Ahmadullah and Aranya with whom I shared all the pain of paper writing between Jul'23 and Jan'24 that are main content of this thesis. On the friends-side of this list "Mess D ke Baap log" go first, for being my family during my stay.

notably, Kanad, Kunal, Shafi, Shreyash, Anirudh, Sricharan, Nikitha, Mayank, Adithi.

I have tried to translate in simple words the infinite gratitude I have and will always have to maman and my siblings — whom life I made difficult with my naive love. Obviously, I failed.

Himanshu Sahu
Bangalore
March 2024

Author's Note

Whether this thesis needs any introductory remarks may be open to question. I, however, feel the need of adding a few words to how I try to record my recollection of works done during my MS. In my view, I tried to provide both a comprehensive and detailed review of my work. To the reader, it may sound contradictory and, therefore, requires an explanation from the author. I wrote the overview of this document in a manner so that it is self-contained. It certainly does not elaborate on the methods of the works; nevertheless, it gives a brief introduction to the respected field, followed by the problem of interest. The answers to these affairs, which I tried to resolve up to a certain extent, are therefore provided. For those who might find some of these investigations interesting, a dedicated chapter to each of the works is provided — although I advise the reader to go through the overview of the work.

Now that I have given an account of the structure of this work, there is another thing that may be of some interest. The work contains three separate ideas that are not correlated in the way they are presented. Therefore, each separate chapter can be read independently of the others. Each chapter independently provides motivation for the idea on its own, but the overview provides a sense of completion. These are the limits and only biases of this work. Certain personal experiences urge me to make this clear.

Himanshu Sahu
Bangalore
March 2024

To the experience we never expected,
and the paths that were redirected.
To the friends and family we found along the way.

Abstract

This dissertation details our research on a wide range of ideas from quantum computing – quantum simulation, quantum algorithms, and quantum complexity which are brought together under the umbrella of quantum walks.

- Quantum simulation – whose long-term promises are far-reaching – presents opportunities to solve problems that are not accessible to classical computers, such as many-body quantum systems with large degrees of freedom. Our contribution regarding quantum simulation focuses on a qubit-efficient scheme to simulate quantum-walk-based simulations. This involves isolating the dynamics of the internal state of quantum-walk by probing the effect of the position state as the environment. We explicitly demonstrate the scheme for the simulation of neutrino oscillations and establish a connection between the dynamics of reduced coin state and neutrino phenomenology, enabling one to fix the simulation parameters for a given neutrino experiment.
- Quantum computers have the ability to outclass conventional classical computing by running quantum algorithms. In the last several decades, quantum algorithms have been proposed for computation problems in areas such as cryptography, search and optimization, simulation, and solving large systems of linear equations. Among the early known quantum algorithms is Grover's search algorithm, which searches data points in unstructured data sets. Our contribution regarding the search algorithm focuses on the extension of the algorithm to search for multiple data points, ensuring the homogeneous amplification of probability amplitude for each, as well as the inherent category associated with the points. Our algorithm uses additional qubits to encode the data point category. We extended the scheme to propose a protocol for the search of dynamic marked points. The quantum algorithm is complemented by the explicit construction of the quantum circuit along with its complexity.
- Quantum complexity – in particular, circuit complexity – is a mathematical technique to find the cost of implementing a unitary operation. Vaguely, it meant to quantify the number of gates required to implement a unitary operation. Although, its exact relation to circuit depth is still not known. Our contribution regarding circuit complexity is to establish its relation with circuit depth. In our work, we computed the two quantities – circuit complexity and circuit depth – for a two-qubit system obtained from the purification of the reduced coin state of the quantum walk. We showed that the two quantities obey the same linear scaling.

The aforementioned ideas – which are thoroughly documented in this document – are explored rigorously – and lead to interesting results.

Contents

List of Figures

Colophon

This document was typeset using the XeTeX typesetting system created by the Non-Roman Script Initiative and the memoir class created by Peter Wilson. The body text is set 10pt with EB Garamond. Other fonts include `Envy Code R`, Optima Regular and. Most of the drawings are typeset using the TikZ/PGF packages by Till Tantau or created using InkScape.

Overview 1

"The last pages of a book are already contained in the first pages."

– Albert Camus

A quantum computer is not the next generation of supercomputers; it uses specialized technology, including computer hardware and algorithms that take advantage of quantum mechanics, to solve complex computational problems that are intractable on classical computers or supercomputers. Unfortunately, all the quantum computers that we currently have are good for *absolutely nothing*. Nevertheless, decades of research have brought the goal closer than when Paul Benioff first proposed the idea. The significant challenge in the hardware aspect of quantum computing is scaling the system to a large number of qubits. Moreover, it is essential to make these qubits robust against errors introduced through various environmental interactions such as thermal vibrations and electromagnetic interference.

In 2019, IBM introduced the first circuit-based commercial 20-qubit quantum computer – called IBM Quantum System One. Its successor, IBM Q System Two, was unveiled in 2023 with more than a hundred qubits.

There has also been significant progress in theoretical developments, such as the development of efficient quantum algorithms, quantum simulations for many-body systems, quantum chemistry, etc. In fact, in certain artificial problems, quantum computers have been shown to surpass classical computers, a point known as 'quantum advantage.' It is crucial to leverage this quantum advantage for more practical problems. In this regard, quantum simulators hold long-term promises, particularly analogue quantum simulators, as they can readily scale to large system sizes.

Analogue quantum simulators are special-purpose analogue computers.

This thesis focuses on the development of theoretical ideas surrounding quantum algorithms, quantum simulations, and quantum complexity. The exact problems are stated in the later part of this chapter. In this overview, I will provide a brief description of these three concepts, followed by the exact problems that will be explored in the rest of the thesis. Let's dive in.

1.1 Quantum simulation

In his 1981 lecture 'Simulating physics with computers,' Feynman emphasized the complexity of simulating quantum systems using classical computers. The computational power required to describe even a single quantum system scales exponentially with the number of its constituents. Therefore, simulating quantum systems on classical computers is deemed impractical, as articulated by Feynman.

For instance, to describe the most general (pure) quantum state for N spin-1/2 particles, we would need to store 2^N coefficients on our computer — a task that becomes practically impossible for N greater than around 50. Moreover, predicting the value of a physical quantity would involve adding, multiplying, or otherwise combining all of those coefficients, a process that would require time scaling exponentially with N as well.

Quantum simulation[2] has become a rapidly growing field due to extraordinary development reporting the demonstration of controlling the quantum states in experimental setups [3–11]. Apart from the quantum advantages that come from exploiting the laws of quantum mechanics [12, 13], it allows the study of the system from a quantum information theory perspective [14–20]. There are two ways to approach problems via quantum simulation: digital or analog quantum computers.

- A digital quantum computer – designed in analogy to modern classical computers, manipulates the quantum mechanical state using a series of discrete gate operations and can possibly perform error correction on imperfect operations. So far, only certain aspects of error correction have been demonstrated for very small numbers of qubits and for a limited set of errors, and to make progress, most devices operate without any quantum error correction. This current situation is sometimes referred to as 'noisy intermediate-scale quantum (NISQ) computing'.

- On the other hand, analog quantum computers are built to simulate the dynamics of a particular system or quantum algorithm. These have a significant advantage in that they can be scaled to large system sizes. There are multiple experimental platforms where analog quantum simulations are realized, including neutral atoms, superconducting systems, trapped ions, and photons [3–11].

There are several ways to approach the problem of simulating a quantum system. I'll briefly state the mathematical statement of the quantum simulation problem (also referred to as the Hamiltonian simulation problem) and provide standard techniques to approach the problem.

1.1.1 Problem statement

In the Hamiltonian simulation problem, given a Hamiltonian H ($2^n \times 2^n$ hermitian matrix acting on n qubits), a time t and maximum simulation error ϵ is the ideal evolution, and that approximates U such that $\|U - e^{-iHt}\| \leq \epsilon$, where e^{-iHt} is the ideal evolution and $\|\cdot\|$ is the spectral norm. A special case of the Hamiltonian simulation problem is the local Hamiltonian simulation problem. This is when H is a k-local Hamiltonian on n qubits where $H = \sum_{j=1}^{m} H_j$ and H_j acts non-trivially on at most k

qubits instead of n qubits. The local Hamiltonian simulation problem is important because most Hamiltonians that occur in nature are k-local.

1.1.2 Techniques

Here, I will briefly discuss few techniques used for Hamiltonian simulation.

Trotter-Suzuki decompositions Trotter-Suzuki decompositions simulate the sum-of-terms of a Hamiltonian by simulating each on separately for a small time slice. If $H = H_1 + H_2$, then

$$U = e^{-i(H_1+H_2)T} = \lim_{n\to\infty} \left(e^{-iH_1\delta t} e^{-iH_2\delta t}\right)^n$$

where n is the number of time steps to simulate for and δt is the duration of time-step.. The larger the n, the more accurate the simulation.

Taylor series By the Taylor series expansion:

$$e^{-iHt} = \sum_{n=0}^{\infty} \frac{(-iHt)^n}{n!} = I - iHt - \frac{H^2t^2}{2} + \frac{iH^3t^3}{6} + \cdots \tag{1.1}$$

The series can be truncated $\left(\sum_{n=0}^{N}(-iHt)^n/n!\right)$, choosing sufficiently large N. Next, one decomposes the Hamiltonian $H = \sum_{l=1}^{L} \alpha_l H_l$ such that each H_l is unitary, and so

$$H^n = \sum_{l_1,\ldots,l_n=1}^{L} \alpha_{l_1} \cdots \alpha_{l_n} H_{l_1} \cdots H_{l_n} \tag{1.2}$$

is also a linear combination of unitaries. Therefore, the evolution of a quantum state describe by application of terms H^n.

Quantum walk In the quantum walk, a unitary operation whose spectrum is related to the Hamiltonian is implemented then the Qauntum phase estimation algorithm is used to adjust the eigenvalues. This makes it unnecessary to decompose the Hamiltonian into sum-of-terms like the Trotter-Suzuki methods.

1.2 Quantum algorithms

A quantum algorithm, similar to a classical algorithm, is a step-by-step procedure for solving a problem, and each of the steps can be performed on a quantum computer. What makes these interesting is that they might be able to solve some problems faster than classical algorithms (discussed below in detail) using features of quantum computation – quantum superposition and quantum entanglement. These quantum algorithms have a wide range of practical applications, from cryptography, search and optimization, and quantum system simulation to the resolution of extensive sets of linear equations. I'll briefly discuss some of these.

What is quantum speedup? – when we say that a quantum computer solves a problem faster than a classical computer, we typically mean in terms of computational complexity. In both the classical and quantum settings, we measure runtime by the number of elementary operations used by an algorithm. In the case of quantum computation, this can be measured using the quantum circuit model (See FIG. 1.1), where a quantum circuit is a sequence of elementary quantum operations called quantum gates, each applied to a small number of qubits.

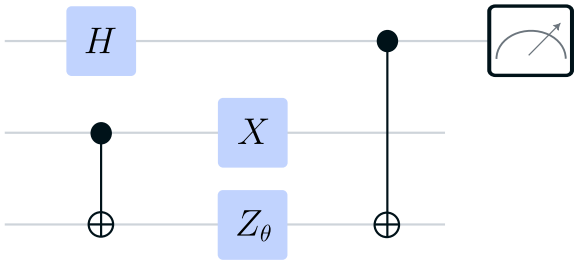

FIGURE 1.1: Quantum circuit model is a generalization of the classical circuit model based on Boolean logical operations. The horizonal lines are quantum wires, representing qubits. The implementation order of operations (quantum gates) runs from left-to-right followed by a measurement at the end.

1.2.1 The hidden subgroup problem

Shor's algorithm for integer factorization is one of the first algorithm in the 'Quantum Algorithm Zoo' that provide substantial quantum speedup. In number theory, integer factorization is the decomposition of a positive integer N into a product of integers $N = p \times q$. Apart from the mathematical interest, it is of great importance since the widely used RSA public-key cryptosystem relies on the difficulty of integer factorization. More specifically, the best classical algorithm has a computational complexity $\exp\left(\mathcal{O}\left(\log N\right)^{1/3}\left(\log\log N\right)^{2/3}\right)$; while Shor's quantum algorithm solves this problem in $\mathcal{O}\left(\left(\log N\right)^3\right)$ – a superpolynomial speedup.

Shor's algorithm for factoring is an instance of the mathematical problem known as the hidden subgroup problem (HSP). In simpler terms, the goal of HSP is to identify a hidden pattern of structure (the hidden subgroup) within the function that exhibits certain periodicity or regularity based on the underlying group G. Shor's algorithm solves the case $G = \mathbb{Z}$, while for the other few groups, polynomial-time quantum algorithms are proposed.

1.2.2 Search algorithm

Search problem is one of the basic problems in computer science. Mathematically, it is formulated as – Suppose we have a function $f : \{0,1\}^n \to \{0,1\}$, find x such that $f(x) = 1$. Classically, one needs to evaluate the function for each input — $N = 2^n$ times in the worst case. Therefore, the classical computer cannot solve the problem in fewer than $\mathcal{O}(N)$ evaluations since, on average, one has to check half of the domain to get a half chance of finding the solution. Remarkably, the quantum search algorithm proposed by Grover can solve the problem using $\mathcal{O}(\sqrt{N})$ evaluations in the worst case. Implementation of this algorithm can be done using a number of gates linear in the number of qubits. The gate complexity of this algorithm is $\mathcal{O}(\log N)$ per iteration or $\mathcal{O}(\sqrt{N}\log N)$. Grover's search algorithm generalized to

the idea known as Amplitude amplification, which gave rise to a family of quantum algorithms.

These includes – finding the minimum of an unsorted list of N integers, determining graph connectivity, and pattern matching.

1.3 On Geometry of Quantum Computation

As we discussed, the implementation of a unitary operation U on a quantum computer involves a sequence of gates acting on a small number of qubits. The implementation is said to be hard or difficult if it requires a large number of gates. Suppose that U is generated by some time-dependent Hamiltonian $H(t)$ according to the Schrödinger equation $dU/dt = -iHU$ and with the requirement that at final time t_f, $U(t_f) = U$. Then, we can characterize the difficulty of the computation by imposing a cost $F[H(t)]$ on the Hamiltonian control $H(t)$. We can choose a cost function on $H(t)$ that defines a Riemannian geometry on the space of unitary operations. Then, finding the optimal control function $H(t)$ for synthesizing a desired unitary U then corresponds to finding minimal geodesics of the Riemannian geometry.

More specifically, implementation is efficient if the number of gates required grows only polynomially with the size of the problem.

The minimal geodesic distance between the identity operation I and U can be shown to be equivalent to the number of gates required to synthesize U. To choose a cost function on the control Hamiltonian $H(t)$, we first write $H(t)$ in terms of the Pauli operator expansion

$$H = \sum_i h_{i_1 i_2} \sigma^{\otimes i_1 i_2} + \sum_i h_{i_1 i_2 \ldots i_n} \sigma^{\otimes i_1 i_2 \ldots i_n} \tag{1.3}$$

assuming the following : (i) In the first sum, σ ranges over all possible one- and two-body interactions. (ii) In the second sum, σ ranges over all other tensor products of Pauli matrices and the identity. (iii) The coefficients h_σ are real. Then, we define a measure of the cost function for the Hamiltonian as

$$F(H) = \sqrt{\sum_i h^2_{i_1 i_2} + p^2 \sum_i h^2_{i_1 i_2 \ldots i_n}} \tag{1.4}$$

The parameter p is a penalty paid for applying non-local interactions (larger than two-body interaction).

This definition of control cost can be used as distance in space $\mathrm{SU}(2^n)$ of n-qubit unitary operators. A curve $[U]$ between the identity operation I and the desired operation U is a smooth function $U : [0, t_f] \to \mathrm{SU}(2^n)$, such that $U(0) = I$ and $U(t_f) = U$. The length of this curve can be defined by the total cost of synthesizing the Hamiltonian that generates evolution along the curve

These are chosen large enough in order to suppress such terms.

$$d([U]) \equiv \int_0^{t_f} dt F[H(t)] \tag{1.5}$$

Since $d([U])$ is invariant with respect to different parameterizations of $[U]$, we can always rescale the Hamiltonian $H(t)$ such that $F[H(t)] = 1$ and the desired unitary

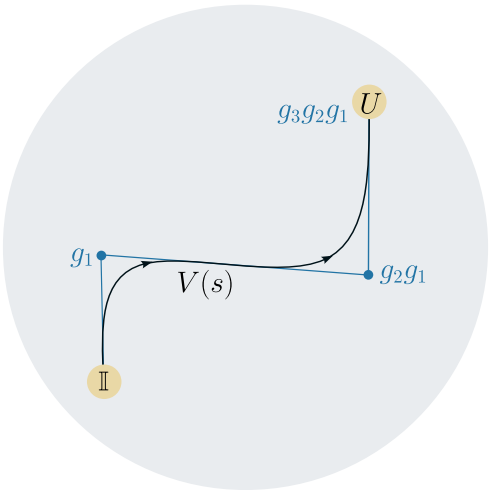

FIGURE 1.2: Illustration of the unitary manifold (gray disk) featuring a geodesic trajectory (depicted in black) from the identity to a specific target unitary U. The blue straight lines symbolize the construction of a circuit utilizing elementary gates g_i, with the final unitary expressed as $U = g_3g_2g_1$. The geodesic path provides a smooth approximation to the circuit by adjusting a control velocity $V(s)$, analogous to an infinitesimal elementary gate. Here, the parameter s serves as a parameterization for the curve.

is generated at time $t_f = d([U])$. Working with such normalized curves, the distance $d(I, U)$ between I and U is defined to be the minimum of $d([U])$ over all curves $[U]$ connecting I and U. The cost function or minimum distance is referred to as Nielsen's Complexity (or simply circuit complexity).

If the distance $d(I, U)$ scales polynomially with n for some family of unitary operators, then it is possible to find a polynomial-sized quantum circuit for that family of unitary operators. Therefore, by recasting the problem of finding the quantum circuits as a geometric problem, the circuit complexity opens up the possibility of using the techniques of Riemannian geometry to suggest new quantum algorithms or to prove the computational limitations of quantum computers.

1.4 The Problem

In this section, I will present three questions that reflect three seemingly unrelated concerns that, nevertheless, are answered using a common tool.

1. Considering the recent theoretical and experimental results on quantum simulation, it appears that the practical quantum advantage might be realized in the near future. However, there are still some problems to be overcome. Experimentally, one demands improved controllability and scalability as most systems (besides optical lattices) still have to handle a large array of qubits. Theoretically, the investigation on control and decoherence becomes important. The optimal requirement for the realization of physical systems, a po-

tential limitation of various schemes, and new applications of quantum simulation through existing ones should be explored.

2. In part of the quantum algorithm, our consideration is on Grover's search algorithm. The algorithm can be extended to the cases where one searches for multiple marked points- in other words, the function $f(x) = 1$ can have multiple solutions. However, such algorithms do not provide homogeneous amplitude amplification to each marked point. On a different line of thought, we can also consider further structured data under consideration. One such consideration could be that the points in the dataset have additional categories. Surprisingly, the solution to these two uncorrelated problems requires the same framework as we will discuss in later sections.

3. The efficient use of quantum computers requires the construction of optimal quantum circuits for solving a problem. As we discussed in §1.3, circuit complexity is a good measure of the difficulty of implementing the operation U on a quantum computer. It can be used to put a lower bound on the number of one- and two-qubit quantum gates required to exactly synthesize U. However, its exact relation with circuit depth is still not clear. A better understanding of a possible link between circuit depth and circuit complexity could provide an analytical handle on the practical circuit build using quantum gates.

1.5 My Thesis

The goal of this dissertation is to improve the state of affairs mentioned above. To that end, the dissertation demonstrates three claims :

> The amount of it, to be sure, is merely a scream, but sometimes a scream is better than a thesis.
>
> – Ralph Waldo Emerson

1. Quantum-walk-based simulations can be made qubit efficient by exploiting the system-environment interactions.

2. Homogeneous amplitude amplification, as well as categorical search, can be made for marked points in the dataset by considering extended Hilbert space dimension.

3. Circuit complexity and circuit depth obey the same scaling law.

We elaborate on each claim in turn –

1.5.1 Claim 1

The Hilbert space of a quantum walk consists of a position space — usually describing the structure of a lattice or graph on which a particle moves — and an internal space — describing the internal state of the particle, such as spin. Therefore, the quantum simulation based on quantum walk requires a large number of qubits that

grow linearly with the lattice size, which makes experimental implementation hard. We can bypass the requirement of lattice space by considering a system that consists of only the internal state interacting with an environment. The interaction between the system and environment is made such that the overall state evolution of the system is the same as that of a complete quantum walk. We will explicitly show the form of this system-environment interaction and demonstrate the scheme for the neutrino oscillation simulation.

1.5.2 Claim 2

In a quantum-walk-based search algorithm, the dataset is considered as a graph that plays the role of position space of the walk. Therefore, the marked points are represented as marked nodes in this graph. The amplitude amplification can be thought of as the localization of wave function at the position of the marked node. In the case of multiple nodes, the wave function localizes at multiple positions, and localization at one position, in general, affects the localization at other positions. This causes the amplitude amplification to be inhomogeneous — in the sense that one point may amplify to high amplitude while the other may not amplify at all. This problem could be resolved if we consider the multi-layered graph structure for the position space of the walk. In this case, the localization occurs in different layers and, therefore, occurs independently of each other, thereby preserving the homogeneity of amplification.

It is further possible to utilize this multi-layered structure to search for categorical datasets. This stems from the fact that these layers can be given labels for the category so that the marked point is a node of a particular layer. The framework of categorical data structure can also be used to consider the search for a dynamic marked node — in which the marked node can change its position in time. In this case, one considers the marked node to be moving from one layer to another. Therefore, the layers play the role of time stamp in tracking the particle or node.

1.5.3 Claim 3

To understand the relation between circuit complexity and circuit depth, we consider a two-way calculation for a two-qubit system evolving in discrete-time steps: 1) Explicit calculation of circuit complexity. 2) Calculation of circuit depth by explicit construction of the quantum circuit. Our results show that the two quantities obey similar scaling with respect to time. Although this does not provide the exact relation between the two quantities, it presents strong evidence of possible relation between the two quantities.

1.6 Organization

Chapter 2 provides the technical background on quantum-walk, particularly discrete-time quantum walks, which will be used in later chapters. The §2.1 lays down the for-

mulation of the discrete-time quantum walk and illustrates its connection with the Dirac Hamiltonian. Later, in §2.2, the formulation is generalized to more generic graphs. We end with providing a brief survey on the experimental implementation of quantum-walk in §2.3.

The rest of the thesis is dedicated to three problems described in §1.4. Chapter 3 begins with describing the phenomena of neutrino oscillation (§3.1). This follows up in §3.2 with the construction of system-environment interaction that probes the position-space effects and explicitly illustrates the case of Hamiltonian dynamics of Dirac particle. §3.3 illustrate the simulation scheme for the neutrino oscillation for two- and three-flavor cases, followed by the presentation of results in §3.4.

Chapter 4 begins with providing the formulation of quantum-walk search algorithm (§4.1) with explicit case of two-dimensional lattice. It then moves on to multi-layered construction in §4.2, providing the numerical results as well as scaling with lattice size. In §4.3, we talk about the quantum tracking problem and our multi-layered approach to solving it. The chapter is concluded in §4.4 by providing the explicit construction of quantum circuit and its complexity.

Chapter 5 starts with the formulation of the definition of circuit-complexity for the geometry of n-qubit system evolving under operation in $\mathrm{SU}(2^n)$. We, then, consider the two-qubit system obtained from the purification of the internal state of quantum-walk and set the target unitary operator (§5.2). The analytic as well as numerical calculation of circuit complexity and circuit depth is done in §5.3 and §5.4, respectively.

Finally, the dissertation concludes with chapter 6, which summarizes the contributions and raises several additional research questions for future investigations.

Quantum walk 2

Consider a particle that moves either to the left or right depending on the result of a coin toss. This process is an example of a random walk or drunkard's walk – a random process that describes a path that consists of a succession of random steps on some mathematical space. Despite its simple structure, random walks have wide applications from physical sciences – physics, chemistry, materials science, and biology to economics and sociology. A quantum analog of the random walk can be formulated by allowing superposition and unitary operations (particle movement and coin toss). Quantum walk [21–24] is a widely successful framework for modeling controlled dynamics in quantum systems [25–30], and for building quantum algorithms [24, 31–33]. There are two broad categories of quantum walks - discrete-time quantum walk (DTQW) and continuous-time quantum walk (CTQW).

- In a discrete-time quantum walk, a quantum particle or a qubit is allowed to move in discrete steps on a lattice governed by unitary evolution operators. At each step, the particle state undergoes a unitary transformation, which can be expressed as a product of two operators, namely the coin and the shift operators. The coin operator acts as a rotation in the qubit space, and the shift operator translates the particle to another vertex on the lattice [21, 34].

- In the case of continuous-time quantum walk, the quantum particle is described by a quantum state that evolves over time according to a time-varying unitary operator. As opposed to discrete-time quantum walk, the continuous-time quantum walk evolution is continuous in time [35].

In what follows, I will discuss discrete-time quantum walk in more detail as it would play a central role in the rest of the thesis.

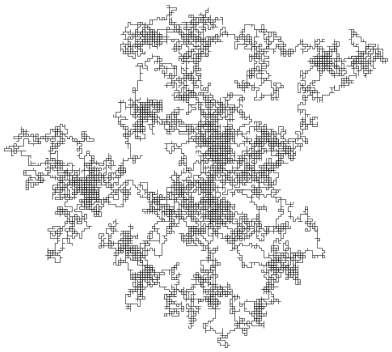

FIGURE 2.1: Random walk in two dimensions with 25 thousand steps[1].

See ref. [21] for a comprehensive review on a continuous-time quantum walk.

2.1 Discrete-time quantum walk

To start with, I am assuming the position space to be one-dimensional. Later in this chapter, I'll talk about extensions to generic graphs.

The discrete-time quantum walk on a line is defined on a Hilbert space $\mathcal{H} = \mathcal{H}_c \otimes \mathcal{H}_p$ where $\mathcal{H}_c$ is coin Hilbert space and $\mathcal{H}_p$ is the position Hilbert space. For a walk in one dimension, $\mathcal{H}_c$ is spanned by the basis set $|\uparrow\rangle$ and $|\downarrow\rangle$ representing the internal degree of the walker, and $\mathcal{H}_p$ is spanned by the basis state of the position $|x\rangle$ where $x \in \mathbb{Z}$ on which the walker evolves. At any time t, the state can be represented by

$$|\Psi(t)\rangle = |\uparrow\rangle \otimes |\Psi^{\uparrow}(t)\rangle + |\downarrow\rangle \otimes |\Psi^{\downarrow}(t)\rangle \tag{2.1}$$

$$= \sum_x \begin{bmatrix} \psi^{\uparrow}_{x,t} \\ \psi^{\downarrow}_{x,t} \end{bmatrix}. \tag{2.2}$$

Each step of the discrete-time quantum walk is defined by a unitary quantum coin operation C on the internal degrees of freedom of the walker, followed by a conditional position shift operation S, which acts on the configuration of the walker and position space. Therefore, the state at time $(t + \tau)$ where τ is the time required to implement one step of the walk will be

$$|\Psi(t+\tau)\rangle = S(C \otimes I)|\Psi(t)\rangle = W|\Psi(t)\rangle. \tag{2.3}$$

The general form of coin operator C, given by

$$\begin{aligned} C = C(\xi, \theta, \varphi, \delta) &= e^{i\xi} e^{-i\theta\sigma_x} e^{-i\varphi\sigma_y} e^{-i\delta\sigma_z} \\ &= e^{i\xi} \begin{pmatrix} e^{-i\delta}(c_\theta c_\varphi - i s_\theta s_\varphi) & -e^{i\delta}(c_\theta s_\varphi + i s_\theta c_\varphi) \\ e^{-i\delta}(c_\theta s_\varphi - i s_\theta c_\varphi) & e^{i\delta}(c_\theta c_\varphi + i s_\theta s_\varphi) \end{pmatrix} \\ &= e^{i\xi} \begin{pmatrix} F_{\theta,\varphi,\delta} & G_{\theta,\varphi,\delta} \\ -G^*_{\theta,\varphi,\delta} & F^*_{\theta,\varphi,\delta} \end{pmatrix} \end{aligned} \tag{2.4}$$

where $c = \cos$, $s = \sin$, ξ is global phase angle, $2\theta, 2\varphi, 2\delta$ are the angles of rotations along x, y and z axes respectively with $\theta, \varphi, \delta \in [0, 2\pi]$, and σ_i is the ith component of the Pauli spin matrices $\{\sigma_x, \sigma_y, \sigma_z\}$, which are generators of SU(2) group. The position shift operator S on the lattice with spacing a is of the form

$$S = |\downarrow\rangle\langle\downarrow| \otimes T_+ + |\uparrow\rangle\langle\uparrow| \otimes T_- = \begin{bmatrix} T_+ & 0 \\ 0 & T_- \end{bmatrix} \tag{2.5}$$

where

$$T_\pm = \sum_{x \in \mathbb{Z}} |x \pm a\rangle\langle x|$$

are translation operators. In momentum basis, these take a diagonal form

$$T_\pm = e^{\mp ipa} = \sum_k e^{\mp ika} |k\rangle\langle k|$$

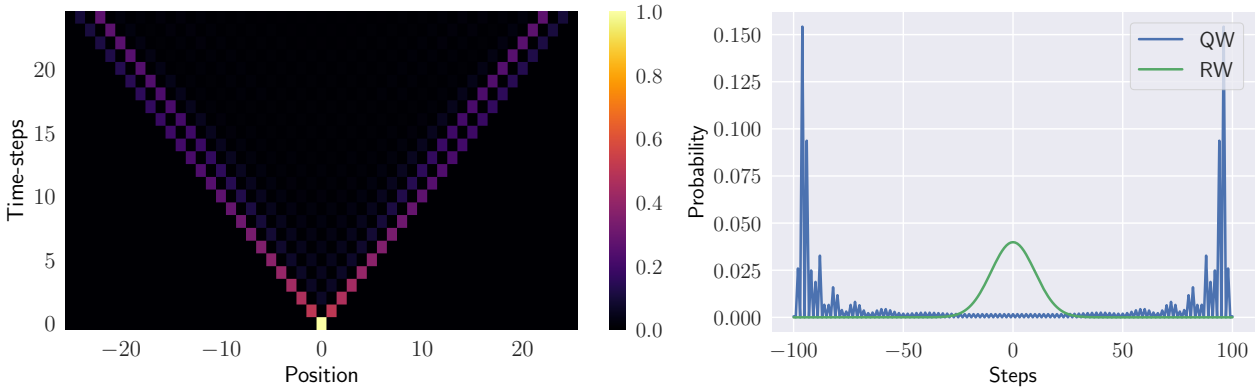

FIGURE 2.2: **Left**: Probability distribution $P(x,t)$ with $t \in [0,25]$ **Right**: Probability distribution $P(x,t_0 = 100)$ of a particle undergoing discrete-time quantum walk with coin angle $\theta = \pi/12$. Figure also shows the probability distribution of the walker in classical setting.

with $|k\rangle$ being momentum eigenstate, given by

$$|k\rangle = \frac{1}{\sqrt{2N+1}} \sum_{x=-N}^{N} e^{-ikx} |x\rangle \tag{2.6}$$

where k is eigenvalue which can take values $2\pi n/(2N+1)$, $n \in \mathbb{Z}$.

2.1.1 Illustration

To illustrate, what does the probability distribution look like for a particle undergoing a discrete-time quantum walk? Consider the initial state of the particle

$$|\Psi(0)\rangle = \left(\frac{|\uparrow\rangle + |\downarrow\rangle}{\sqrt{2}}\right) \otimes |0\rangle$$

with the coin operator defined as in EQ. (2.7). FIG. 2.2 shows the probability distribution defined as

$$P(x,t) = |\psi_{x,t}^{\uparrow}|^2 + |\psi_{x,t}^{\downarrow}|^2 .$$

It is shown that the standard deviation of the probability distribution grows linearly $\sim t$ in contrast to the classical random walk where it grows $\sim \sqrt{t}$. This feature is utilized in quantum algorithms such as search algorithms based on quantum walks.

Quantum walk algorithms take advantage of one of the two ways to outperform random walks — 1) faster hitting time (the time take to spread from a source vertex to a target vertex). 2) faster mixing (the time taken to spread out over all vertices after starting from one source vertex).

2.1.2 Connection with Dirac Hamiltonian

The discrete-time quantum walk can be used to simulate various physical systems. This involves setting up the unitary evolution that has an effective Hamiltonian corresponding to the Hamiltonian of the physical system in question. For the purpose of this thesis, we consider the simulation of Dirac Hamiltonian. In ref. [36], it is shown that for the coin operator

$$\begin{aligned} B &\equiv C(0,\theta,0,3\pi/2) \\ &= \cos\theta|\uparrow\rangle\langle\uparrow| + \sin\theta\,(|\uparrow\rangle\langle\downarrow| - |\downarrow\rangle\langle\uparrow|) + \cos\theta|\downarrow\rangle\langle\downarrow| \end{aligned} \tag{2.7}$$

In ref. [30] discrete-time quantum walks are shown to provide a versatile platform to probe topological phases. This is further demonstrated in various platforms such as with cold atoms [37, 38].

the effective Hamiltonian defined as $W = e^{-iH\tau}$ takes the form of a one spatial dimensional Dirac Hamiltonian for small k and θ with parameter correspondence given by

$$\frac{a}{\tau} = 1 \quad \& \quad \frac{\theta}{\tau} = m. \tag{2.8}$$

The eigenvector of H corresponding to the positive eigenvalue

$$E = \frac{1}{\tau} \arccos(\cos\theta \cos\tilde{k}) \tag{2.9}$$

where $\tilde{k} = ka$ and the corresponding eigenstates are given by

$$|\nu\rangle = \begin{bmatrix} f(\theta,k) & g(\theta,k) \end{bmatrix}^T \otimes |k\rangle \tag{2.10}$$

where

$$\begin{aligned} f(\theta,k) &= \frac{\sin\theta e^{-ik}}{\sqrt{\sin^2\theta + \left[\cos\theta\sin k - (1-\cos^2\theta\cos^2 k)^{1/2}\right]^2}} \\ g(\theta,k) &= \frac{i\left(\cos\theta\sin k - \left(1-\cos^2\theta\cos^2 k\right)^{1/2}\right)}{\sqrt{\sin^2\theta + \left[\cos\theta\sin k - (1-\cos^2\theta\cos^2 k)^{1/2}\right]^2}}. \end{aligned} \tag{2.11}$$

The experimental realization of a Dirac cellular automaton in trapped-ion quantum processor is done in ref. [39] in which space of walker positions and internal state is mapped to multi-qubit states.

This is particularly interesting from quantum simulation point of view as some of the fundamental particles such as electron, neutrino, etc. obeys the Dirac equation.

2.2 Extension to generic graph

Let $G = (V, E)$ be a finite d-regular graph, where V is a set of vertices (nodes), E is the set of edges connecting the nodes, and $N = |V|$ is the number of vertices. The labels of the vertices are 0 to $N-1$, and the label of the edges are 0 to $d-1$. The position space $\mathcal{H}_p$ is spanned by $\{|v\rangle : 0 \le v \le N-1\}$, while coin space is spanned by $\{|a\rangle : 0 \le a \le d-1\}$ represents the internal states associated with each node.

For example, consider a 2D square lattice which have four direction of motion at each lattice point. One of the scheme is to consider four dimensional coin operator with the basis state as $|0\rangle$, $|1\rangle$, $|2\rangle$, and $|3\rangle$ corresponding to each direction of motion. The shift operator can be written as

$$\begin{aligned} S = \sum_{x,y} \big[&|0\rangle\langle 0| \otimes |x-1, z-1\rangle\langle x,z| + |1\rangle\langle 1| \otimes |x-1, z+1\rangle\langle x,z| \\ &+|2\rangle\langle 2| \otimes |x+1, z-1\rangle\langle x,z| + |3\rangle\langle 3| \otimes |x+1, z+1\rangle\langle x,z| \big] . \end{aligned} \tag{2.12}$$

The coin operator, in general, can be the group element of SU(4). A choice could be

$$C = \frac{1}{2}\begin{bmatrix} -1 & 1 & 1 & 1 \\ 1 & -1 & 1 & 1 \\ 1 & 1 & -1 & 1 \\ 1 & 1 & 1 & -1 \end{bmatrix} \tag{2.13}$$

known as the Grover diffusion operator. This plays an important role in quantum-walk based search algorithm – we will come back to this point in chapter 4.

2.3 On experimental implementation & applications

Experimental implementations of discrete-time quantum walks have been realized on various platforms (see ref. [40] for review). To cite but few, these platforms consists of nuclear magnetic resonances [41, 42], trapped ions [43, 44], atoms [45], and a number of photonic platforms [46–51].

As we learned, the discrete-time quantum walk have connection to the Dirac equation. In past developments, variants of discrete-time quantum walk have been used to simulate Dirac equation and its associated dynamics [36, 52–54] which are also experimentally implemented in both analog and digital quantum simulators [39, 55]. These experimental implementation allows the laboratory realization and investigation of a variety of key fundamental phenomena associated with Dirac particle dynamics like Zitterbewegung, simultaneous position and spin oscillations [55–58]. Schemes for quantum simulations of Dirac equation in curved space-time, discrete gauge theories, free quantum field theory, collective neutrino oscillations have been also reported in literature [53, 59–63]. Apart from these, there are other quantum simulation proposed based on discrete-time quantum walks in number of topics such as topological effects [38, 64, 65], recurrence [66], and percolation [67].

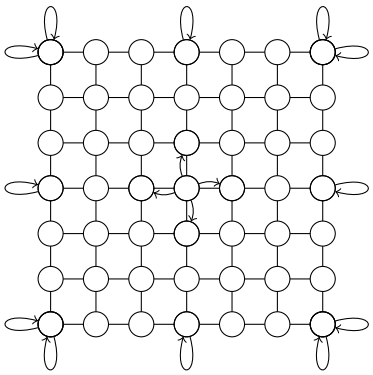

FIGURE 2.3: A 2D square lattice.

A neutrino is a fermion (an elementary particle with a spin of 1/2) that interacts only via weak interaction and gravity. Weak interactions create neutrino in one of three leptonic flavors: electron neutrino ν_e, muon neutrino ν_μ, and tau neutrino ν_τ. *Neutrino oscillations* is a quantum mechanical phenomenon in which a neutrino created with a specific lepton flavor can later be measured to have a different lepton flavor.

Neutrino oscillations have given rise to vibrant phenomena involving supernovae, reactor neutrinos, the early universe, or atmospheric neutrinos, and the solution to the solar neutrino problem [68–74]. A framework to simulate neutrino oscillation with discrete-time quantum walks has been proposed in previous literature [75, 76]. It uses the fact that certain discrete-time quantum walks can be used to simulate the Dirac equation – obeyed by neutrinos. I loosely mentioned this in §2.1.2. Nevertheless, the readers are advised to look at the cited references.

In this chapter, I will approach the problem from the open quantum system perspective by considering the walker's evolution in the reduced coin space, thereby effectively treating the position space as an environment. We consider the reduced dynamics of the coin state obtained by tracing over the position space degrees of freedom of a quantum walker. The Kraus operators we have obtained exhibit a temporal recurrence relation, which allows one to calculate them systematically at any given time. These Kraus operators are shown to describe the dynamics of the Dirac particle. We extended this formalism to describe the dynamics of more than one Dirac particle, thereby establishing a connection between the dynamics of reduced coin state and neutrino phenomenology. The Kraus operators form presented in this work can be used as a guiding framework to model dynamics in other quantum systems where quantum walks, and Dirac equations are used for simulating and modeling the dynamics.

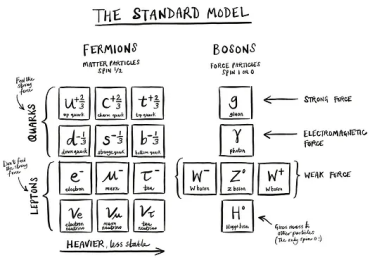

FIGURE 3.1: Elementary particles of the Standard Model [1]

3.1 Neutrino Oscillations

In the theory of electroweak interaction developed by Glashow, Weinberg, and Salam, lepton flavor is conserved, and neutrinos are massless. Therefore, a neutrino of a given flavor created in charged current weak interactions will remain in the same flavor state. However, various experimental observations have shown that the flavor of neutrino changes as it propagates in space-time [77–79]. This disconnection between the theoretical expectation and experimental observation is resolved by a scheme that relies on mixing the three neutrino mass and flavor states. According to this, each of the three neutrino flavor states is a mixture of the three mass eigenstates. As neutrinos move in space-time, each mass eigenstate acquires a different phase. Hence, a definite flavor state evolves into a mixture of three flavors, leading to flavor oscillation called *neutrino oscillation* [80–82].

Defining flavor eigenstates $|\nu_\alpha\rangle$ $(\alpha = e, \mu, \tau)$ and mass eigenstates $|\nu_i\rangle$ $(i = 1, 2, 3)$, then the flavor and mass eigenstates are related by a unitary transformation written as

$$|\nu_\alpha\rangle = \sum_i U_{\alpha i} |\nu_i\rangle \tag{3.1}$$

where $U_{\alpha i}$ is mixing matrix known as the Pontecorvo-Maki-Nakagawa-Sakata (PMNS) matrix [83] given by

$$\begin{aligned} U &= \begin{bmatrix} U_{e1} & U_{e2} & U_{e3} \\ U_{\mu 1} & U_{\mu 2} & U_{\mu 3} \\ U_{\tau 1} & U_{\tau 2} & U_{\tau 3} \end{bmatrix} \\ &= \begin{bmatrix} 1 & 0 & 0 \\ 0 & c_{23} & s_{23} \\ 0 & -s_{23} & c_{23} \end{bmatrix} \begin{bmatrix} c_{13} & 0 & s_{13} e^{-i\delta} \\ 0 & 1 & 0 \\ -s_{13} e^{i\delta} & 0 & c_{13} \end{bmatrix} \\ &\qquad \times \begin{bmatrix} c_{12} & s_{12} & 0 \\ -s_{12} & c_{12} & 0 \\ 0 & 0 & 1 \end{bmatrix} \begin{bmatrix} e^{i\alpha_1/2} & 0 & 0 \\ 0 & e^{i\alpha_2/2} & 0 \\ 0 & 0 & 1 \end{bmatrix} \\ &\equiv U_3 U_2 U_1 U_0 \end{aligned} \tag{3.2}$$

where $c_{ij} \equiv \cos\phi_{ij}$, and $s_{ij} \equiv \sin\phi_{ij}$ with ϕ_{ij} being the mixing angle. The phase factor α_1, α_2 are physically meaningful only if neutrinos are Majorana particles. The state $|\nu_i\rangle$ is the mass eigenstate of the free Dirac Hamiltonian (in natural units)

$$H_i = \vec{\xi} \cdot \vec{p}_i + \beta m_i \tag{3.3}$$

where m_i is the mass, $\vec{p}_i$ is momentum operator. The propagation of eigenstate $|\nu_i\rangle$ can be described by plane wave solutions of the form

$$|\nu_i(t)\rangle = e^{-i\left(E_i t - \vec{k}_i \cdot \vec{x}\right)} |\nu_i(0)\rangle \tag{3.4}$$

where $\vec{k}_i$ is the three dimensional momentum, with $E_i = \sqrt{|\vec{k}_i|^2 + m_i^2}$ being the positive energy of mass-eigenstate.

Suppose that at time $t = 0$ a flavor neutrino $|\nu_\alpha\rangle$ is produced, then at time t the neutrino state given by

$$|\nu_\alpha(t)\rangle = \sum_i U_{\alpha i}|\nu_i(t)\rangle = \sum_i U_{\alpha i}e^{-iE_i t}|\nu_i(0)\rangle. \tag{3.5}$$

Therefore, the probability of transition $\nu_\alpha \to \nu_\beta$ after a time t is given by

$$P(\nu_\alpha \to \nu_\beta; t) = \left|\sum_j U^*_{\alpha j}U_{\beta j}e^{-iE_j t}\right|. \tag{3.6}$$

To illustrate EQ. (3.6), let us consider the simpler case with only two neutrino state. In this case, the mixing matrix U can be written as

$$U = \begin{bmatrix} \cos\phi & \sin\phi \\ -\sin\phi & \cos\phi \end{bmatrix} \tag{3.7}$$

where ϕ is the mixing angle. In ultra-relativistic limit, $|\vec{k}_i| \gg m_i$ so that we can approximate energy as

$$E_i = \sqrt{|\vec{k}_i|^2 + m_i^2} \simeq |\vec{k}_i| + \frac{m_i^2}{2|\vec{k}_i|} \approx E + \frac{m_i^2}{2E} \tag{3.8}$$

where $E \approx |\vec{k}_i|$ for all i. The transition probability from flavor states $|\nu_\alpha\rangle$ to $|\nu_\beta\rangle$ in ultra-relativistic limit then, given by

$$P(\nu_\alpha \to \nu_\beta; t) = \sin^2(2\phi)\sin^2\left(\frac{\Delta m^2 L}{4E}\right) \tag{3.9}$$

with $\Delta m^2 = m_2^2 - m_1^2$ and $L \approx t$ is the distance traveled by the neutrinos from the production to the detection point.

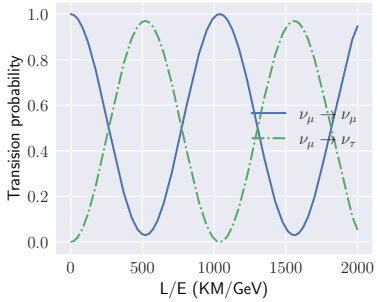

FIGURE 3.2: Two flavor neutrino oscillation. The blue curve shows the probability of the original neutrino retaining its identity. The green curve shows the probability of conversion to the other neutrino. The maximum probability of conversion is equal to $\sin^2\phi$. The frequency of the oscillation is controlled by Δm^2.

In atmospheric neutrino oscillations, the electron plays almost no role; hence EQ. (3.9) is appropriate for flavor transition [84]. It is also appropriate for the solar case of $\nu_e \leftrightarrow \nu_X$ where ν_X is the superposition of ν_μ and ν_τ. These approximations are possible since the mixing angle θ_{13} is very small and because two of the three mass eigenstates are very close in mass compared to the third [85].

3.2 Reduced dynamics of a coin

In this section, we will consider the reduced dynamics of a coin in a DTQW, which previously has been studied in the context of non-markovian characteristics of the dynamics [86]. Although, in contrast to previous work, we will derive a temporal recurrence relation for Kraus operator which allows one to find these at any time for a generic initial quantum state.

Consider the initial state of the walker to be

$$|\Psi(0)\rangle = |\chi\rangle \otimes |\psi_x\rangle. \tag{3.10}$$

consisting of an internal spin state

$$|\chi\rangle \in \mathscr{H}_c = \{a_\uparrow|\uparrow\rangle + a_\downarrow|\downarrow\rangle : a_{\uparrow/\downarrow} \in \mathbb{C}\} \tag{3.11}$$

and a position state

$$|\psi_x\rangle \in \mathscr{H}_p = \left\{\sum_{x\in\mathbb{Z}} c_x|x\rangle : \sum_{x\in\mathbb{Z}} |c_x|^2 < \infty\right\}. \tag{3.12}$$

After t steps, this becomes

$$|\Psi(t)\rangle = W^t|\Psi(0)\rangle = W^t\left(|\chi\rangle \otimes |\psi_x\rangle\right). \tag{3.13}$$

The density matrix representation of the above state is given by

$$\rho(t) = |\Psi(t)\rangle\langle\Psi(t)| \tag{3.14}$$

$$= W^t|\Psi(0)\rangle\langle\Psi(0)|(W^\dagger)^t. \tag{3.15}$$

Now, we can trace over the position space to get

$$\begin{aligned}\rho_c(t) &= \sum_{x=-t}^{t}\langle x|W^t|\Psi(0)\rangle\langle\Psi(0)|(W^\dagger)^t|x\rangle \\ &= \sum_{x=-t}^{t}\langle x|W^t|\psi_x\rangle|\chi\rangle\langle\chi|\langle\psi_x|(W^\dagger)^t|x\rangle \\ &= \sum_{x=-t}^{t}\tilde{K}_x(t)\rho_c(0)\tilde{K}_x^\dagger(t)\end{aligned} \tag{3.16}$$

where

$$\tilde{K}_x(t) \equiv \langle x|W^t|\psi_x\rangle \tag{3.17}$$

are called Kraus operators that describes the density operator evolution in open quantum systems. In general, these operators $\{K_n : 1 \le n \le N\}$ obeys the completeness property

$$\sum_n K_n^\dagger K_n = I\,. \tag{3.18}$$

To verify that $\tilde{K}_x(t)$ obeys the completeness :

$$\begin{aligned}&\sum_x \tilde{K}_x^\dagger(t)\tilde{K}_x(t) \\ &= \sum_x \langle\psi_x|(W^t)^\dagger|x\rangle\langle x|W^t|\psi_x\rangle \\ &= \langle\psi_x|(W^t)^\dagger W^t|\psi_x\rangle \\ &= I\end{aligned}$$

as required.

3.2.1 Temporal recurrence relation

For simplicity, let's take the initial state to be $|\psi_x\rangle = |0\rangle$ so that

$$K_x(t) = \langle x|W^t|0\rangle. \tag{3.19}$$

To make further progress, we break down the evolution operator W in shift and coin operator as

$$\begin{aligned}W &= S(C\otimes I) \\ &= \left[|\uparrow\rangle\langle\uparrow| \otimes T_- + |\downarrow\rangle\langle\downarrow| \otimes T_+\right][C\otimes 1] \\ &= |\uparrow\rangle\langle\uparrow|C\otimes T_- + |\downarrow\rangle\langle\downarrow|C\otimes T_+ \\ &= C_\uparrow \otimes T_- + C_\downarrow \otimes T_+.\end{aligned}$$

where

$$\begin{aligned} C_\uparrow &\equiv |\uparrow\rangle\langle\uparrow| C = e^{i\xi}\begin{pmatrix} F_{\theta,\varphi,\delta} & G_{\theta,\varphi,\delta} \\ 0 & 0 \end{pmatrix} \\ C_\downarrow &\equiv |\downarrow\rangle\langle\downarrow| C = e^{i\xi}\begin{pmatrix} 0 & 0 \\ -G^*_{\theta,\varphi,\delta} & F^*_{\theta,\varphi,\delta} \end{pmatrix}. \end{aligned} \tag{3.20}$$

With this, consider Kraus operator at $t+1$

$$\begin{aligned} K_x(t+1) &= \langle x|W^{t+1}|0\rangle = \langle x|WW^t|0\rangle \\ &= \sum_{x'} \langle x|W|x'\rangle\langle x'|W^t|0\rangle \\ &= \sum_{x'} \langle x|W|x'\rangle K_{x'}(t). \end{aligned} \tag{3.21}$$

Now consider the first term in the expression

$$\begin{aligned} \langle x|W|x'\rangle &= C_\uparrow\langle x|T_-|x'\rangle + C_\downarrow\langle x|T_+|x'\rangle \\ &= C_\uparrow\langle x|x'-a\rangle + C_\downarrow\langle x|x'+1\rangle \\ &= C_\uparrow\delta_{x,x'-a} + C_\downarrow\delta_{x,x'+a} \end{aligned}$$

putting this into EQ. (3.21), we get

$$\begin{aligned} K_x(t+1) &= \sum_{x'}\left[C_\uparrow\delta_{x,x'-a} + C_\downarrow\delta_{x,x'+a}\right]K_{x'}(t) \\ &= C_\uparrow K_{x+a}(t) + C_\downarrow K_{x-a}(t). \end{aligned}$$

Therefore, we get a recurrence relation for the Kraus operator given by

$$K_x(t+1) = C_\uparrow K_{x+a}(t) + C_\downarrow K_{x-a}(t). \tag{3.22}$$

The initial Kraus operator at $t=0$ given by, using the definition given in EQ. (3.19)

$$K_x(0) = \langle x|0\rangle = \delta_{x,0}.$$

If we start with initial position state to be $|x'\rangle$ then Kraus operators $K_{xx'}(t)$ are related to $K_x(t)$ by

$$K_{xx'}(t) \equiv \langle x|W^t|x'\rangle = K_{x-x'}(t) \tag{3.23}$$

and therefore for a generic extended initial position state $|\psi_x\rangle = \sum_{x'} c_{x'}|x'\rangle$, we have

$$\tilde{K}_x(t) = \sum_{x'} c_{x'}K_{xx'}(t) = \sum_{x'} c_{x'}K_{x-x'}(t). \tag{3.24}$$

Hence, for general position state $|\psi_x\rangle$, the Kraus operators are simply a linear combination of Kraus operators for initial state $|0\rangle$.

3.2.2 Example : Dirac Hamiltonian

To illustrate EQ. (3.22), we derive the expression for the Kraus operator corresponding to coin operator in EQ. (2.7) which describes the Dirac Hamiltonian for initial position state $|0\rangle$. The operators $C_{\uparrow/\downarrow}$ for the coin operator EQ. (2.7) have the form

$$\begin{aligned} B_{\uparrow} &\equiv |\uparrow\rangle\langle\uparrow| B = \begin{pmatrix} \cos\theta & \sin\theta \\ 0 & 0 \end{pmatrix} \\ B_{\downarrow} &\equiv |\downarrow\rangle\langle\downarrow| B = \begin{pmatrix} 0 & 0 \\ -\sin\theta & \cos\theta \end{pmatrix}. \end{aligned} \tag{3.25}$$

For a one-step walk, $t = 1$

$$\begin{aligned} K_x(1) &= B_{\uparrow} K_{x+a}(0) + B_{\downarrow} K_{x-a}(0) \\ &= B_{\uparrow}\delta_{x+a,0} + B_{\downarrow}\delta_{x-a,0}. \end{aligned} \tag{3.26}$$

Hence, for a one-step walk, we have two Kraus operators given by

$$\begin{aligned} K_{-a}(1) &= B_{\uparrow} = \begin{pmatrix} \cos\theta & \sin\theta \\ 0 & 0 \end{pmatrix} \\ K_{a}(1) &= B_{\downarrow} = \begin{pmatrix} 0 & 0 \\ -\sin\theta & \cos\theta \end{pmatrix}. \end{aligned} \tag{3.27}$$

For a two-step walk i.e. $t = 2$

$$\begin{aligned} K_x(2) &= B_{\uparrow} K_{x+a}(1) + B_{\downarrow} K_{x-a}(1) \\ &= B_{\uparrow}\left(B_{\uparrow} K_{x+2a}(0) + B_{\downarrow} K_x(0)\right) + B_{\downarrow}\left(B_{\uparrow} K_x(0) + B_{\downarrow} K_{x-2a}(0)\right) \\ &= B_{\uparrow}\left(B_{\uparrow}\delta_{x+2a,0} + B_{\downarrow}\delta_{x,0}\right) + B_{\downarrow}\left(B_{\uparrow}\delta_{x,0} + B_{\downarrow}\delta_{x-2a,0}\right) \\ &= B_{\uparrow}B_{\uparrow}\delta_{x+2a,0} + (B_{\uparrow}B_{\downarrow} + B_{\downarrow}B_{\uparrow})\delta_{x,0} + B_{\downarrow}B_{\downarrow}\delta_{x-2a,0} \end{aligned} \tag{3.28}$$

Therefore, for a two-step walk, we have three Kraus operators, given by

$$\begin{aligned} K_{-2a}(2) &= B_{\uparrow}B_{\uparrow} = \begin{pmatrix} \cos^2(\theta) & \sin(\theta)\cos(\theta) \\ 0 & 0 \end{pmatrix} \\ K_{0}(2) &= B_{\uparrow}B_{\downarrow} + B_{\downarrow}B_{\uparrow} = \begin{pmatrix} -\sin^2(\theta) & \sin(\theta)\cos(\theta) \\ -\sin(\theta)\cos(\theta) & \sin^2(\theta) \end{pmatrix} \\ K_{2a}(2) &= B_{\downarrow}B_{\downarrow} = \begin{pmatrix} 0 & 0 \\ -\sin(\theta)\cos(\theta) & \cos^2(\theta) \end{pmatrix}. \end{aligned} \tag{3.29}$$

In the similar manner, we can find the Kraus operator for a t-steps walk using the recurrence relation EQ. (3.22). These set of operators describes the spin dynamics of Dirac particle. This is important as the evolution of neutrino mass eigenstates is describe using Dirac equation with correspondence as in EQ. (2.8).

3.3 Simulating neutrino oscillations

In this section, we will consider the simulation of neutrino oscillation. We begin with considering the quantum circuit construction associated with mixing matrix EQ. (3.2) and then move on to simulation two-flavor neutrino oscillations and later generalize to the three flavor cases.

3.3.1 Quantum circuit construction of PMNS Matrix

Firstly, we map the neutrino flavor states $|\nu_\alpha\rangle$ into a three-qubit system [87] so that the correspondence between the two systems looks like :

$$|\nu_e\rangle \to |100\rangle \qquad |\nu_\mu\rangle \to |010\rangle \qquad |\nu_\tau\rangle \to |001\rangle. \tag{3.30}$$

With this, we can also write the mass-eigenstates using the mixing matrix as

$$|\nu_i\rangle = U^*_{ei}|100\rangle + U^*_{\mu i}|010\rangle + U^*_{\tau i}|001\rangle. \tag{3.31}$$

Consider now the representation of the mixing matrix on this basis. In the three-qubit system, the mixing matrix would be a 8×8 matrix. To see the explicit form of these, consider the term U_1 in mixing matrix EQ. (3.2)

$$U_1 = \begin{bmatrix} c_{12} & s_{12} & 0 \\ -s_{12} & c_{12} & 0 \\ 0 & 0 & 1 \end{bmatrix} = \begin{array}{c|ccc} & |100\rangle & |010\rangle & |001\rangle \\ \hline |100\rangle & c_{12} & s_{12} & 0 \\ |010\rangle & -s_{12} & c_{12} & 0 \\ |001\rangle & 0 & 0 & 1 \end{array} \tag{3.32}$$

which has a three-qubit representation

$$U_1 \to \begin{bmatrix} 1 & 0 & 0 & 0 & 0 & 0 & 0 & 0 \\ 0 & 1 & 0 & 0 & 0 & 0 & 0 & 0 \\ 0 & 0 & c_{12} & 0 & -s_{12} & 0 & 0 & 0 \\ 0 & 0 & 0 & 1 & 0 & 0 & 0 & 0 \\ 0 & 0 & s_{12} & 0 & c_{12} & 0 & 0 & 0 \\ 0 & 0 & 0 & 0 & 0 & 1 & 0 & 0 \\ 0 & 0 & 0 & 0 & 0 & 0 & 1 & 0 \\ 0 & 0 & 0 & 0 & 0 & 0 & 0 & 1 \end{bmatrix}. \tag{3.33}$$

so that there's a mixing between the terms $|100\rangle$ and $|010\rangle$ while the other remains the same. In the similar manner, we can write a three-qubit representation for other

terms $U_i (i = 0, 1, 2, 3)$ as follows :

$$U_0 \rightarrow \begin{bmatrix} 1 & 0 & 0 & 0 & 0 & 0 & 0 & 0 \\ 0 & 1 & 0 & 0 & 0 & 0 & 0 & 0 \\ 0 & 0 & e^{i\alpha_2/2} & 0 & 0 & 0 & 0 & 0 \\ 0 & 0 & 0 & 1 & 0 & 0 & 0 & 0 \\ 0 & 0 & 0 & 0 & e^{i\alpha_1/2} & 0 & 0 & 0 \\ 0 & 0 & 0 & 0 & 0 & 1 & 0 & 0 \\ 0 & 0 & 0 & 0 & 0 & 0 & 1 & 0 \\ 0 & 0 & 0 & 0 & 0 & 0 & 0 & 1 \end{bmatrix} \tag{3.34}$$

$$U_2 \rightarrow \begin{bmatrix} 1 & 0 & 0 & 0 & 0 & 0 & 0 & 0 \\ 0 & c_{13} & 0 & 0 & -s_{13}e^{i\delta} & 0 & 0 & 0 \\ 0 & 0 & 1 & 0 & 0 & 0 & 0 & 0 \\ 0 & 0 & 0 & 1 & 0 & 0 & 0 & 0 \\ 0 & s_{13}e^{-i\delta} & 0 & 0 & c_{13} & 0 & 0 & 0 \\ 0 & 0 & 0 & 0 & 0 & 1 & 0 & 0 \\ 0 & 0 & 0 & 0 & 0 & 0 & 1 & 0 \\ 0 & 0 & 0 & 0 & 0 & 0 & 0 & 1 \end{bmatrix} \tag{3.35}$$

$$U_3 \rightarrow \begin{bmatrix} 1 & 0 & 0 & 0 & 0 & 0 & 0 & 0 \\ 0 & c_{23} & -s_{23} & 0 & 0 & 0 & 0 & 0 \\ 0 & s_{23} & c_{23} & 0 & 0 & 0 & 0 & 0 \\ 0 & 0 & 0 & 1 & 0 & 0 & 0 & 0 \\ 0 & 0 & 0 & 0 & 1 & 0 & 0 & 0 \\ 0 & 0 & 0 & 0 & 0 & 1 & 0 & 0 \\ 0 & 0 & 0 & 0 & 0 & 0 & 1 & 0 \\ 0 & 0 & 0 & 0 & 0 & 0 & 0 & 1 \end{bmatrix}. \tag{3.36}$$

The unitary operations U_i can be thought of as controlled unitary operators. To illustrate this, consider on our earlier example of U_3, which is a controlled operation on the third qubit (counting from left in $|ijk\rangle$). To see this, we can rewrite the unitary U_3 as :

	000	001	010	011	100	101	110	111
000	1	0	0	0	0	0	0	0
001	0	1	0	0	0	0	0	0
010	0	0	c_{12}	0	$-s_{12}$	0	0	0
011	0	0	0	1	0	0	0	0
100	0	0	s_{12}	0	c_{12}	0	0	0
101	0	0	0	0	0	1	0	0
110	0	0	0	0	0	0	1	0
111	0	0	0	0	0	0	0	1

Or more explicitly, if we define a unitary matrix

$$\mathcal{U}_3 = \begin{bmatrix} 1 & 0 & 0 & 0 \\ 0 & c_{12} & -s_{12} & 0 \\ 0 & s_{12} & c_{12} & 0 \\ 0 & 0 & 0 & 1 \end{bmatrix} \tag{3.37}$$

Then controlled operation look like :

$$\begin{aligned} |ij1\rangle &\rightarrow |ij1\rangle \\ |ij0\rangle &\rightarrow \mathcal{U}_3|ij\rangle \otimes |0\rangle \end{aligned} \tag{3.38}$$

The similar construction can be done for U_0, U_2, U_3.

3.3.2 Passage to more than one particle

In §3.2.2, we learned on how a set of Kraus operators corresponding to coin operator EQ. (2.7) can be used to describe to Dirac particle. We can extend this coin operator to reproduce a set of Dirac equations, hence describing the dynamics of more than one Dirac particle. To this end, consider a discrete-time quantum walk with $2n$-dimensional coin Hilbert space $\mathscr{H}_c$ spanned by basis $\bigoplus_{f=1,n}\{|f,\uparrow\rangle, |f,\downarrow\rangle\}$ and coin operator

$$B_n = \bigoplus_{f=1,n} B_f(\theta_f) \tag{3.39}$$

where

$$\begin{aligned} B_f = \cos\theta_f |f,\uparrow\rangle\langle f,\uparrow| + \sin\theta_f \left(|f,\uparrow\rangle\langle f,\downarrow| - |f,\downarrow\rangle\langle f,\uparrow|\right) \\ + \cos\theta_f |f,\downarrow\rangle\langle f,\downarrow|. \end{aligned} \tag{3.40}$$

In this basis, the evolution operator takes the block diagonal form given by

$$W = S(B_n \otimes I) = \bigoplus_{f=1,n} W_f = \bigoplus_{f=1,n} S_f(B_f \otimes I) \tag{3.41}$$

with

$$S_f = T_+ \otimes |f,\uparrow\rangle\langle f,\uparrow| + T_- \otimes |f,\downarrow\rangle\langle f,\downarrow|. \tag{3.42}$$

Analogous to coin operator EQ. (2.7), coin operator in EQ. (3.39) reproduces a set of n Dirac equations with parameter correspondence

$$\frac{a}{\tau} = 1 \quad \& \quad \frac{\theta_f}{\tau} = m_f, \quad f = 1, \dots, n \tag{3.43}$$

with f being the particle number with internal degree of freedom $\{|f,\uparrow\rangle, |f,\downarrow\rangle\}$ and mass m_f. The Kraus operator formalism that we developed in **??** can easily be extended for coin operator in EQ. (3.39) as follows

$$\tilde{\mathcal{K}}_x^{(n)}(t) = \bigoplus_{f=1,n} \langle x|W_f|\psi_x\rangle = \bigoplus_{f=1,n} \tilde{K}_x(\theta_f, t). \tag{3.44}$$

where extended Kraus operator $\tilde{K}_x(\theta_f, t)$ follow from EQ. (3.24)

$$\tilde{K}_x(\theta_f, t) = \sum_{x'} c_{x'} K_{x-x'}(\theta_f, t) \tag{3.45}$$

with $K_{x-x'}(\theta_f, t) = \langle x|W_f^t|x'\rangle$. With the formalism for simulating dynamics of n Dirac particle at hand, in the next section, we will see how to simulate neutrino oscillations.

3.3.3 Two-flavor neutrino oscillations

In case of two-flavor neutrino oscillations, we need to mimic the dynamics of two Dirac particles and therefore the coin hilbert space is four dimensional space spanned by $\bigoplus_{f=1,2}\{|f,\uparrow\rangle, |f,\downarrow\rangle\}$. The evolution operator W has a block diagonal form given by

$$W = \bigoplus_{f=1,2} W_f = S(B_2 \otimes I) = \bigoplus_{f=1,2} S_f(B_f \otimes I) \tag{3.46}$$

where the quantum coin operator and shift operator are as in EQ. (3.40) and EQ. (3.42). The mass eigenstates given by

$$\begin{aligned} |\nu_1\rangle &= \begin{bmatrix} f(\theta_1,k) & g(\theta_1,k) & 0 & 0 \end{bmatrix}^T \otimes |k\rangle \equiv |\nu_1\rangle_c \otimes |k\rangle \\ |\nu_2\rangle &= \begin{bmatrix} 0 & 0 & f(\theta_2,k) & g(\theta_2,k) \end{bmatrix}^T \otimes |k\rangle \equiv |\nu_2\rangle_c \otimes |k\rangle \end{aligned}. \tag{3.47}$$

The initial state $|\Psi(0)\rangle$ of the neutrino corresponding to α flavor using the mixing matrix acting on each sector

$$|\Psi(0)\rangle = |\nu_\alpha\rangle = \sum_{i=1,2} U_{\alpha i}|\nu_i\rangle. \tag{3.48}$$

The associated reduced coin density matrix given by

$$\rho_c(0) = \sum_{i,j} U_{\alpha i} U^*_{\alpha j} |\nu_i\rangle_c \langle\nu_j|_c. \tag{3.49}$$

The Kraus operator for two particle given by

$$\tilde{\mathcal{K}}_x(t) = \bigoplus_{f=1,2} \langle x|W_f|\psi_x\rangle = \bigoplus_{f=1,2} \tilde{K}_x(\theta_f, t)$$

where state $|\psi_x\rangle$ is momentum eigenstate k in position space representation EQ. (2.6). At any time t, the reduced density matrix is written as

$$\rho_c(t) = \sum_x \tilde{\mathcal{K}}_x^{(2)}(t)\rho_c(0)(\tilde{\mathcal{K}}_x^{(2)})^\dagger(t). \tag{3.50}$$

The probability of the $\nu_\alpha \to \nu_\beta$ transition after a time t is then given by expectation value of the projection operator $|\nu_\beta\rangle_c\langle\nu_\beta|_c$ i.e.

$$P(\nu_\alpha \to \nu_\beta; t) = \mathrm{Tr}\left[|\nu_\beta\rangle_c\langle\nu_\beta|_c \rho_c(t)\right] \tag{3.51}$$

where

$$|\nu_\beta\rangle_c = \sum_{i=1,2} U_{\beta i}|\nu_i\rangle_c \tag{3.52}$$

so that

$$|\nu_\beta\rangle_c\langle\nu_\beta|_c = \sum_{i,j=1,2} U_{\beta i}U^*_{\beta j}|\nu_i\rangle_c\langle\nu_j|_c. \tag{3.53}$$

3.3.4 Three-flavor neutrino oscillations

We can trivially extend the two-flavor neutrino oscillations to three-flavor neutrino oscillation by considering the coin operator, EQ. (3.39) with $n = 3$. The mass eigenstates associated with three-particles are given by

$$\begin{aligned}
|\nu_1\rangle &= \begin{bmatrix} f(\theta_1,k) & g(\theta_1,k) & 0 & 0 & 0 & 0\end{bmatrix}^T \otimes |k\rangle \equiv |\nu_1\rangle_c \otimes |k\rangle \\
|\nu_2\rangle &= \begin{bmatrix} 0 & 0 & f(\theta_2,k) & g(\theta_2,k) & 0 & 0\end{bmatrix}^T \otimes |k\rangle \equiv |\nu_2\rangle_c \otimes |k\rangle. \\
|\nu_2\rangle &= \begin{bmatrix} 0 & 0 & 0 & 0 & f(\theta_3,k) & g(\theta_3,k)\end{bmatrix}^T \otimes |k\rangle \equiv |\nu_3\rangle_c \otimes |k\rangle
\end{aligned} \tag{3.54}$$

The initial state $|\Psi(0)\rangle$ of the neutrino corresponding to α flavor using the mixing matrix acting on each sector

$$|\Psi(0)\rangle = |\nu_\alpha\rangle = \sum_{i=1,2,3} U_{\alpha i}|\nu_i\rangle. \tag{3.55}$$

The associated reduced coin density matrix given by

$$\rho_c(0) = \sum_{i,j=1,2,3} U_{\alpha i}U^*_{\alpha j}|\nu_i\rangle_c\langle\nu_j|_c. \tag{3.56}$$

The Kraus operator for three particle given by

$$\tilde{\mathcal{K}}_x(t) = \bigoplus_{f=1,2,3} \langle x|W_f|\psi_x\rangle = \bigoplus_{f=1,2,3} \tilde{K}_x(\theta_f,t)$$

where state $|\psi_x\rangle$ is momentum eigenstate k in position space representation EQ. (2.6). At any time t, the reduced density matrix is written as

$$\rho_c(t) = \sum_x \tilde{\mathcal{K}}^{(3)}_x(t)\rho_c(0)(\tilde{\mathcal{K}}^{(3)}_x)^\dagger(t). \tag{3.57}$$

The probability of the $\nu_\alpha \to \nu_\beta$ transition after a time t is then given by expectation value of the projection operator $|\nu_\beta\rangle_c\langle\nu_\beta|_c$ i.e.

$$P(\nu_\alpha \to \nu_\beta; t) = \mathrm{Tr}\left[|\nu_\beta\rangle_c\langle\nu_\beta|_c\rho_c(t)\right] \tag{3.58}$$

where

$$|\nu_\beta\rangle_c = \sum_{i=1,2,3} U_{\beta i}|\nu_i\rangle_c \tag{3.59}$$

so that

$$|\nu_\beta\rangle_c\langle\nu_\beta|_c = \sum_{i,j=1,2,3} U_{\beta i}U^*_{\beta j}|\nu_i\rangle_c\langle\nu_j|_c. \tag{3.60}$$

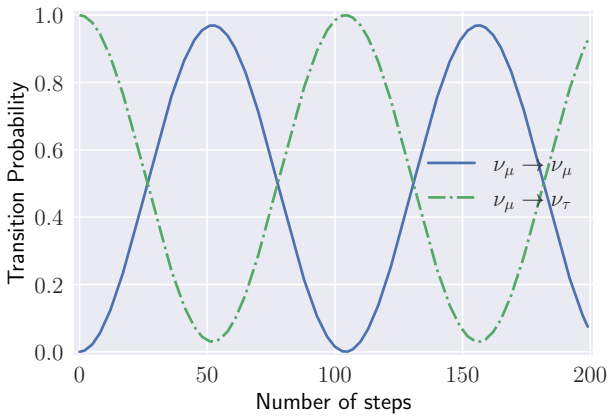

FIGURE 3.3: Transition probabilities of two flavor neutrino oscillation obtained from numerical simulation using the Kraus operator associated with the DTQW with initial state $|\nu_\mu\rangle$. The coin angles are $\theta_1 = 0.001$ rad., $\theta_2 = 0.0986$ rad., and the mixing angle $\phi = 0.698$ rad. with $\tilde{k} = 0.05$.

3.4 Results

In §3.3.2, we have seen that evolution operator in EQ. (3.46) describes the set of Dirac equations that describes neutrino flavor oscillations and, we can make use this to establish a map with neutrino phenomenology, therefore allowing one to fix the QW parameters for a given neutrino experiment. More explicitly, using the correspondence made between quantum walk and Dirac equation in EQ. (2.8), we can write the oscillation frequency in EQ. (3.9) in terms of quantum parameters as

$$\frac{\Delta m_{ij}^2 L}{4E} = \frac{\Delta\theta_{ij}^2}{4\tilde{k}}\frac{t}{\tau} \tag{3.61}$$

where $\Delta\theta_{ij}^2 = \theta_i^2 - \theta_j^2$ and $\Delta m_{ij}^2 = m_i^2 - m_j^2$. FIG. 3.3 and 3.4 shows the transition probability as a function of the number of steps of DTQW for two-flavor and three-flavor neutrino oscillations, respectively obtained from evolution describe by the Kraus operators. We can observe the oscillatory behavior of flavors. One can observe that the plot reproduces the one corresponding to actual calculations of neutrino oscillations (see for example [88]) with taken mass values

$$\begin{aligned}\Delta m_{21}^2 &= 7.50 \times 10^{-5}\ \text{eV}^2\\ \Delta m_{31}^2 &= 2.457 \times 10^{-3}\ \text{eV}^2.\\ \Delta m_{32}^2 &= 2.382 \times 10^{-3}\ \text{eV}^2\end{aligned} \tag{3.62}$$

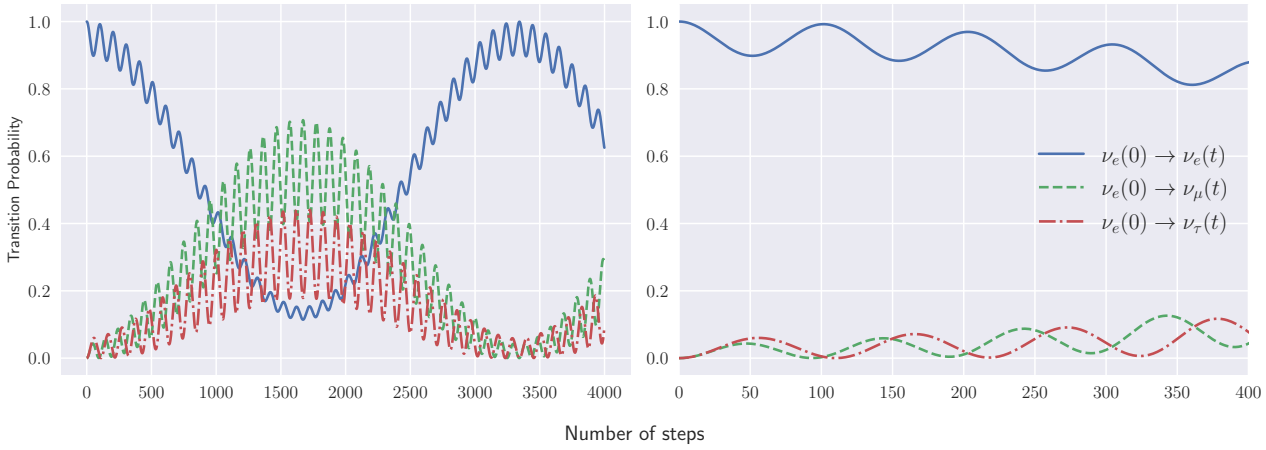

FIGURE 3.4: Transition probabilities of three flavor neutrino oscillation obtained from numerical simulation using the Kraus operator associated with the DTQW **Left** for long time steps and **Right** short time steps with initial state $|\nu_e\rangle$.. The coin angles are $\theta_1 = 0.001$ rad., $\theta_2 = 0.01963$ rad. $\theta_3 = 0.12797$ rad., and the mixing angle $\phi_{13} = 0.16087$ rad., $\phi_{23} = 0.69835$, $\phi_{12} = 0.59437$, and $\delta = 0$ with $\tilde{k} = 0.1$.

3.4.1 Linear Entropy

Among various measures of degree of entanglement [89], the linear entropy is shown to be useful in studying entanglement in neutrino oscillations [90]. The linear entropy associated with a bipartite system is defined as

$$S_j = \frac{d}{d-1}\left(1 - \mathrm{Tr}(\rho_j^2)\right), \quad j = 1, 2. \tag{3.63}$$

where ρ_j represent the reduced density matrix of system j and d is dimension of density matrix ρ_j.

In case of two flavor neutrino oscillations, we can write the state shown in EQ. (3.5) as the Bell-like superposition

$$|\nu_\alpha(t)\rangle = \tilde{U}_{\alpha\mu}(t)|1\rangle_{\nu_\mu}|0\rangle_{\nu_\tau} + \tilde{U}_{\alpha\tau}|0\rangle_{\nu_\mu}|1\rangle_{\nu_\tau} \tag{3.64}$$

where

$$\tilde{U}_{\alpha\beta}(t) = \sum_j U_{\alpha j} U^*_{\beta j} e^{-iE_j t}. \tag{3.65}$$

The linear entropies can found by straightforward calculation using associated density matrix of state $|\nu_\alpha(t)\rangle$, and are given by

$$S_\mu = S_\tau = 4|\tilde{U}_{\alpha e}(t)|^2 |\tilde{U}_{\alpha\mu}(t)|^2. \tag{3.66}$$

Therefore, the linear entropies can be written in term of transition probabilities which continues to be true for three flavor case [90]. FIG. 3.5 shows the linear entropy S_μ obtained from transition probabilities given by EQ. (3.51) using EQ. (3.66). We find that degree of entanglement is largest when both transition probabilities are equals to 0.5 which corresponds to maximally entangled Bell pair state and minimum when one of the transition probability is zero which corresponds to unentangled state. For three-flavor case, we can write three-flavor state as

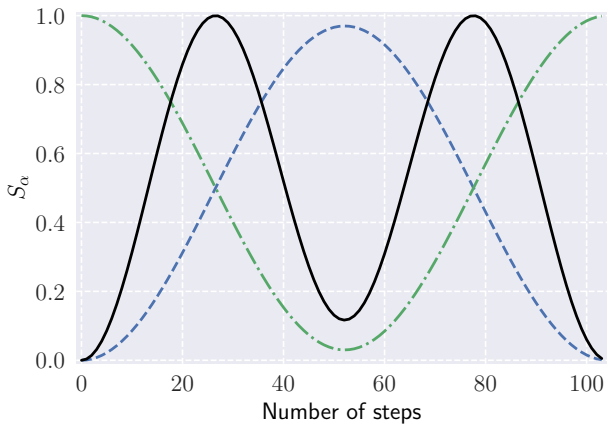

FIGURE 3.5: Linear entropy $S\mu$ (full line) as a function of number of steps (shown for single cycle) along with transition probabilities (dashed lines) $P(\nu_\mu \rightarrow \nu_\mu)$ (red) and $P(\nu_\mu \rightarrow \nu_\tau)$ (blue).

$$|\nu_\alpha(t)\rangle = \tilde{U}_{\alpha e}|1\rangle_{\nu_e}|0\rangle_{\nu_\mu}|0\rangle_{\nu_\tau} + \tilde{U}_{\alpha\mu}|0\rangle_{\nu_e}|1\rangle_{\nu_\mu}|0\rangle_{\nu_\tau} + \tilde{U}_{\alpha\tau}|0\rangle_{\nu_e}|0\rangle_{\nu_\mu}|1\rangle_{\nu_\tau}. \tag{3.67}$$

In case of multipartite system, we can define partial linear entropies corresponding to various bipartition of total system [90]. We adopt the notation $S_\zeta^{(\alpha,\beta;\gamma)}$ for linear entropy of reduced density matrix $\rho_\zeta^{(\alpha,\beta)} = \mathrm{Tr}_\gamma(\rho_\zeta)$ where ζ corresponds to initial flavor state. Similar to two flavor case, the partial linear entropies can be written in terms of transition probabilities and given by

$$S_\alpha^{(e,\mu;\tau)} = 4|\tilde{U}_{\alpha\tau}(t)|^2\left(1 - |\tilde{U}_{\alpha\tau}(t)|^2\right). \tag{3.68}$$

The remaining two partial entropies can be found by simply permuting e, μ, τ. Fig. 3.6 shows the partial linear entropies for initial state $|\nu_e(0)\rangle$. The maximum of these partial shows the point at which maximum entanglement exist between those two flavors. To understand the behavior of overall degree of entanglement, we can define average linear entropy as mean value of partial entropies, given by

$$\langle S_\alpha\rangle = \frac{8}{3}\left(|\tilde{U}_{\alpha e}|^2|\tilde{U}_{\alpha\mu}|^2 + |\tilde{U}_{\alpha e}(t)|^2|\tilde{U}_{\alpha\tau}|^2 + |\tilde{U}_{\alpha\mu}|^2|\tilde{U}_{\alpha e\tau}|^2\right). \tag{3.69}$$

FIG. 3.6 shows behavior of average linear entropy $\langle S_e\rangle$, we observe similar behavior as in case of two-flavor neutrino oscillations. This shows strong correlation between the components ν_μ and ν_τ.

3.5 Outlook

In this work, we proposed a novel scheme to simulate neutrino oscillations using DTQW formalism. We considered the evolution of reduced dynamics of coin density matrix using set of Kraus operators obtained from tracing out the position space.

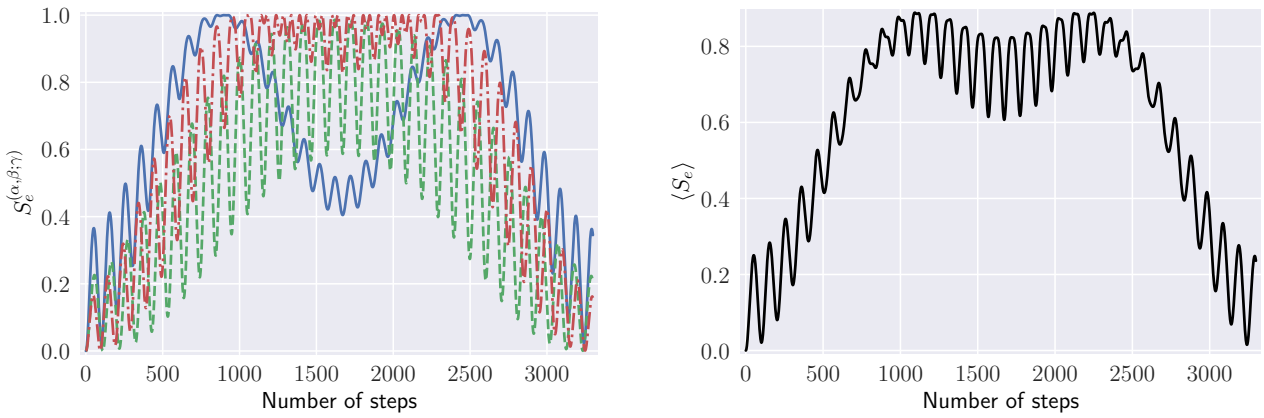

FIGURE 3.6: **Left** Partial linear entropies $S_e^{(\alpha,\beta;\gamma)}$ as a function of number of steps (shown for a single cycle) with black corresponds to $S_e^{(\mu,\tau;e)}$, blue corresponds to $S_e^{(\tau,e;\mu)}$, and red corresponds to $S_e^{(e,\mu;\tau)}$. **Right**: Average linear entropy $\langle S_e \rangle$ as a function of number of steps (shown for a single cycle).

This in turn means effectively treating dynamics in position space as environmental effect. We obtained the transition probabilities of neutrino flavor states in the same framework. To study the degree of entanglement between different flavors, we considered linear entropy which found to be maximum for bell-pair state.

We conclude with a few interesting future directions for this work. Firstly, given the recent development in simulating open system dynamics in quantum devices [91, 92], the demonstration of a quantum algorithm of open system approach to neutrino oscillation on a near-term quantum device would give laboratory verification of the phenomenon. Furthermore, in previous studies, possible decoherence effects induced by new physics (e.g., quantum gravity, string theory) in neutrino oscillations have been studied by considering the open system framework [93], and bounds on dissipative parameters are obtained for various neutrino experiments [94, 95]. Our scheme is open to incorporating these dissipation effects, which may provide an exciting direction for investigating non-standard effects.

Search algorithm 4

"Even after studying quantum algorithms for quite some time, they continue to surprise me."

– Shelby Kimmel

Quantum computers are engineered with the purpose of surpassing the computational capabilities of conventional computers through the execution of quantum algorithms [96–98]. These quantum algorithms have a wide range of practical applications from cryptography, search and optimization, and quantum system simulation to the resolution of extensive sets of linear equations [99–110]. Notably, Grover's search algorithm stands out as a widely recognized quantum algorithm capable of searching unsorted databases with a quadratic speed advantage over its classical counterparts [111]. Grover's algorithm, combined with quantum walk, has motivated the foundation and development of the commonly known research venture of *Quantum walk search algorithms* for searching and sorting unstructured spatial data [100, 112–114]. Quantum search algorithms have an asymptotic quadratic acceleration in terms of oracle calls, unlike their classical cousins [112, 115].

Quantum-walk search with multiple points has been extensively studied in previous literature [116–121]. While the algorithm can locate multiple nodes within a graph, however not all the marked points are equally amplified. Further, the algorithm completely ignores a chronological ordering or category of the marked nodes, if any. In this chapter, we specifically address these issues regarding the QWSA. To resolve these issues, we consider the multilayered graph structure (See FIG. 4.1) which amounts to extension of Hilbert space. Each marked point, then, is associated with a different layer of the graph. As we will see, this multilayer structure of the graph avoids the possible interference between different search operations of marked points. We can further use this multilayer structure to consider the search on categorical datasets. In this case, we regard each layer as a different category to which a marked point might be associated with. The search algorithm, therefore, looks for the marked point along with its category — multilayer search algorithm.

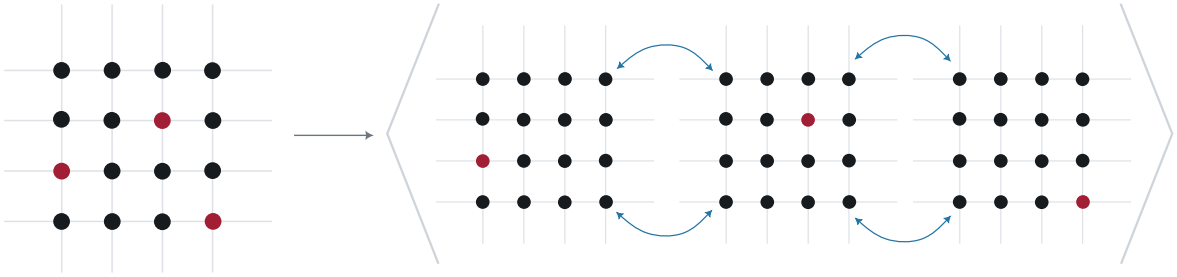

figure 4.1: Consider a graph (on the left) – a two-dimensional lattice – consists of three marked nodes (in red). Our algorithm copies the graph into multiple copies where each copy consists of a single marked point. The multiple copies can be utilize as additional label for the marked nodes as well. We call the labeling static labeling if the probability amplitude can not flow between the layers and dynamical labeling if the probability amplitude can flow between the layers (shown in blue).

The distinction between static and dynamic labeling relies on whether there is a flow of probability between various sheets. Our refined algorithm can address a variety of applications, including real-time object tracking, trajectory prediction, financial market analysis, dynamic optimization problems, and network management and routing that includes dynamical components. The labeling concept is not new and has been applied to element distinctness problems in quantum algorithms. However, to our knowledge, we are not aware of the application of the labeling concept in the context of quantum search algorithms. As a concrete illustration of the scope of applicability of our algorithm, we consider a particle moving in a two-dimensional lattice with time and show that the algorithm is capable of detecting the coordinates of the particle as it moves with time. Further, to properly connect with the idea of integrating our QWSA with state-of-the-art quantum hardware, we construct an equivalent quantum circuit that can implement the algorithm.

4.1 Quantum walk search algorithm

Let $G = (V, E)$ be a finite d-regular graph, where V is a set of vertices (nodes), E is the set of edges connecting the nodes, and $N = |V|$ is the number of vertices. The labels of the vertices are 0 to $N-1$, and the labels of the edges are 0 to $d-1$. A discrete-time quantum walk on the graph G generates a unitary evolution operator in the Hilbert space $\mathcal{H}_U = \mathcal{H}_{\text{pos}} \otimes \mathcal{H}_{\text{coin}}$: the position space $\mathcal{H}_{\text{pos}}$ and the coin space $\mathcal{H}_{\text{coin}}$. $\mathcal{H}_{\text{pos}}$ is spanned by $\{|v\rangle\colon 0 \le v \le N-1\}$, while $\mathcal{H}_{\text{coin}}$ is spanned by $\{|a\rangle : 0 \le a \le d-1\}$ represents the internal states (often called "coin states") associated with each node. At any time t, the state can be represented by

$$|\Psi(t)\rangle = \sum_{a,v} \phi_{a,v}(t)\,|a, v\rangle\,. \tag{4.1}$$

Each step of the DTQW is generated by a unitary operator consisting of coin operation C on the internal degrees of freedom followed by a conditional position shift operation S on the configuration space. Therefore, the state at time t and $(t+\tau)$ (where τ is the time required to implement one step of the walk) satisfies the relation,

$$|\Psi(t+\tau)\rangle = U|\Psi(t)\rangle = S(C \otimes I)|\Psi(t)\rangle\,, \tag{4.2}$$

whereby imposing the operator form of the evolution operator $U = S(C \otimes I)$. With this information, we are set to address the QWSA. Consider that the walker starts from an initial state, which is a uniform superposition of all states over internal and external degrees of freedom,

$$|\Psi(0)\rangle = |\psi_c^{(d)}\rangle \otimes \frac{1}{N} \sum |v\rangle\,, \quad \text{where } |\psi_c^{(d)}\rangle = \frac{1}{\sqrt{d}} \sum_{a=0}^{d-1} |a\rangle\,. \tag{4.3}$$

where $|\psi_c^{(d)}\rangle$ is uniform superposition state in coin space. The idea behind the QWSA is starting with EQ. (4.3), can we define a unitary operator that localizes the state to a certain point (say $|v_0\rangle$) on the grid. This operation is mathematically represented as

$$|\Psi(t)\rangle = \left(U'\right)^t |\Psi(0)\rangle\,, \;\; P_v(t) = |\langle v|\Psi(t)\rangle|^2_{\max\ @\ v=v_0}\,. \tag{4.4}$$

The mathematical equation above states simply that after t such operations of a unitary operator U', the wave function localizes at the point $|v_0\rangle$ where the time t is related to the size of the grid and the marked node configuration. The probability of success is the maximal probability for locating the node $|v_0\rangle$ and is related to the number of times t, the U' operator has been applied on the initial state. For a single marked node, the operator U' is related to the unitary operator for the DTQW $U = S \cdot (C \otimes I)$ by the relation,

$$U' = U \cdot R\,, \tag{4.5}$$

where R is called "Search Oracle" and contains the information about the marked node(s). In essence, it is a phase shift operator that reverses the phase of all but one node (*i.e.* the marked node) by $e^{i\pi}$. For a single marked node, the Search Oracle has a simple functional form [114, 121]

$$R = I - 2|\psi_c^{(d)}\rangle\langle\psi_c^{(d)}| \otimes |v_0\rangle\langle v_0|\,. \tag{4.6}$$

Without the coin state, this form coincides with the Grover Search Oracle [122]

$$U_f = I - 2|v_0\rangle\langle v_0|\,. \tag{4.7}$$

The search oracle R can be easily generalized for multiple marked nodes,

$$R = I - 2\,|\psi_c^{(d)}\rangle\langle\psi_c^{(d)}| \otimes \sum_{v\in M} |v\rangle\langle v| \tag{4.8}$$

where M is set of marked multiple marked node. To illustrate the concrete structure of the algorithm, we will consider a finite two-dimensional lattice with open and periodic boundary conditions.

4.1.1 Finite two-dimensional lattice

Consider the quantum-walk search algorithm in the $\sqrt{N}\times\sqrt{N}$ square lattice. We will consider both open and periodic boundary conditions. The quantum state spanned by $\{|i,j\rangle \otimes |x,y\rangle : i,j \in [0,1] \,\&\, 0 \le x,y \le \sqrt{N}-1\}$ where $|i,j\rangle$ represents coin state, and $|x,y\rangle$ represents position state. The shift operator S is the flip-flop shift operator given by

$$S|i,j\rangle \otimes |x,y\rangle = |1-i,1-j\rangle \otimes |x+(-1)^i\delta_{ij}, y+(-1)^j(1-\delta_{ij})\rangle\,. \tag{4.9}$$

The flip-flop shift operator invert the coin state as it shift the position state. This inversion in the con state is important for speeding up search algorithms on the two-dimensional lattice [114, 121]. In explicit notation, we can write coin state as

$$\begin{aligned} |\uparrow\rangle = |00\rangle = \begin{bmatrix}1\\0\\0\\0\end{bmatrix}, \qquad |\downarrow\rangle = |11\rangle = \begin{bmatrix}0\\0\\0\\1\end{bmatrix}, \\ |\leftarrow\rangle = |01\rangle = \begin{bmatrix}0\\1\\0\\0\end{bmatrix}, \qquad |\rightarrow\rangle = |10\rangle = \begin{bmatrix}0\\0\\1\\0\end{bmatrix}. \end{aligned} \tag{4.10}$$

In this notation, the flip-flop ship operator for the periodic boundary condition given by

$$\begin{aligned} S_c^{(2)} = |\downarrow\rangle\langle\uparrow| \otimes \sum_{x,y} |x,y+1\rangle\langle x,y| + |\uparrow\rangle\langle\downarrow| \otimes \sum_{x,y} |x,y-1\rangle\langle x,y| \\ + |\leftarrow\rangle\langle\rightarrow| \otimes \sum_{x,y} |x+1,y\rangle\langle x,y| + |\rightarrow\rangle\langle\leftarrow| \otimes \sum_{x,y} |x-1,y\rangle\langle x,y| \end{aligned} \tag{4.11}$$

To unclutter the notation, we define set of points $\phi_1 = \{0,1,\ldots\sqrt{N}-2\}$ and $\phi_2 = \{1,2,\ldots,\sqrt{N}-1\}$.

where superscript in $S_c^{(2)}$ is to emphasize that there are two directions of motion. In periodic boundary condition, the position state obey the cyclic property $|x+\sqrt{N}\rangle = |x\rangle$ and $|y+\sqrt{N}\rangle = |y\rangle$. Therefore, the geometry of two-dimensional lattice with periodic boundary condition is equivalent to torus. For open boundary condition, the shift operator is defined as the sum of interior term (see FIG. 4.2).

$$\begin{aligned} S_{\text{int}}^{(2)} = |\downarrow\rangle\langle\uparrow| \otimes \sum_{x,y\in\phi_1} |x,y+1\rangle\langle x,y| + |\uparrow\rangle\langle\downarrow| \otimes \sum_{x,y\in\phi_2} |x,y-1\rangle\langle x,y| \\ + |\leftarrow\rangle\langle\rightarrow| \otimes \sum_{x\in\phi_1,y} |x+1,y\rangle\langle x,y| + |\rightarrow\rangle\langle\leftarrow| \otimes \sum_{x\in\phi_2,y} |x-1,y\rangle\langle x,y| \end{aligned} \tag{4.12}$$

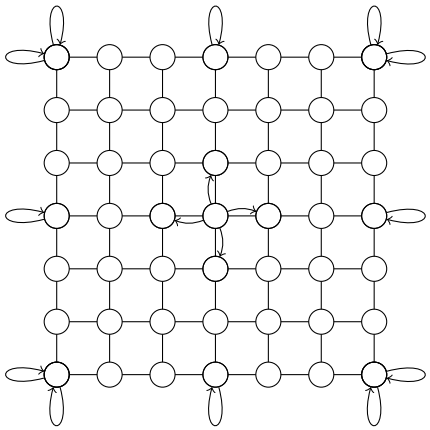

FIGURE 4.2: The structure of the shift operator in the case of open boundary conditions is different in the interior and exterior of the grid. The figure shows the self-loop at the boundary point of the lattice which ensures the unitarity of the shift operator.

and boundary (exterior)

$$\begin{aligned} S_{\text{ext}}^{(2)} = |\uparrow\rangle\langle\uparrow| \otimes \sum_{x,y=\sqrt{N}-1} |x,y\rangle\langle x,y| + |\downarrow\rangle\langle\downarrow| \otimes \sum_{x,y=0} |x,y\rangle\langle x,y| \\ + |\rightarrow\rangle\langle\rightarrow| \otimes \sum_{x=\sqrt{N}-1,y} |x,y\rangle\langle x,y| + |\leftarrow\rangle\langle\leftarrow| \otimes \sum_{x=0,y} |x,y\rangle\langle x,y| \end{aligned} \tag{4.13}$$

as $S_{\text{o}}^{(2)} = S_{\text{int}}^{(2)} + S_{\text{ext}}^{(2)}$. The explicity form of $S_{\text{int}}^{(2)}$ and $S_{\text{ext}}^{(2)}$ is chosen so that the shift operator $S_{\text{o}}^{(2)}$ is unitary i.e. $S_{\text{o}}^{(2)}(S_{\text{o}}^{(2)})^\dagger = (S_{\text{o}}^{(2)})^\dagger S_{\text{o}}^{(2)} = I$ (see appendix 6). The coin operator in the quantum-walk search is chosen to be the Grover diffusion operator [123, 124]

$$G^{(2)} = 2|\psi_c^{(2)}\rangle\langle\psi_c^{(2)}| - I = \frac{1}{2}\begin{bmatrix} -1 & 1 & 1 & 1 \\ 1 & -1 & 1 & 1 \\ 1 & 1 & -1 & 1 \\ 1 & 1 & 1 & -1 \end{bmatrix}. \tag{4.14}$$

The state is initialized as an equal superposition in coin and position space, given by

$$|\Psi(0)\rangle = \frac{1}{2}\sum_{i,j} |i,j\rangle \otimes \frac{1}{N}\sum_{x,y} |x,y\rangle = |\chi\rangle \otimes \frac{1}{N}\sum_{x,y} |x,y\rangle \tag{4.15}$$

The modified unitary operator in Eq. EQ. (4.5) is applied optimal time t_{op} times to initial state

$$|\Psi(t_{\text{op}})\rangle = (U')^{t_{\text{op}}}|\Psi(0)\rangle \tag{4.16}$$

which amplifies the probability amplitude of target states. For the two-dimensional lattice, the complexity of the algorithm is given by $\mathcal{O}(\ln N)$. The running time is $t_{\text{op}} = \mathcal{O}(\sqrt{N \ln N})$ and the success probability is $p_{\text{succ}} = \mathcal{O}(1/\ln N)$ [114].

4.2 QWSA for ordered marked nodes

In previous literature [116–121], quantum-walk search with multiple marked points has been extensively studied. In a general QWSA, multiple marked points can indeed exist on the graph, and there is no inherent (chronological) ordering associated with these marked points. The algorithm's objective is to efficiently locate any one of these marked points without any preference for their order. In this section, we consider that there is an additional (and preferably a chronological) ordering associated with marked points, and devise a refined algorithm that addresses this ordering. More generally, our refined algorithm will address the case where we have multiple marked points belonging to different categories and we will be searching for the point along with its category.

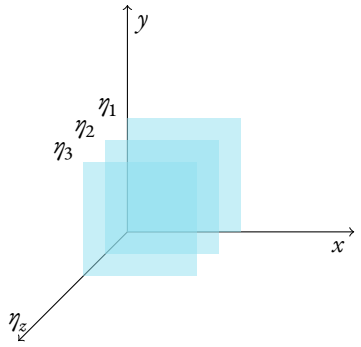

Figure 4.3: Schematic diagram of the structure of Hilbert space for quantum-walk search for ordered marked nodes.

For starters, consider a total of m different categories η_z where $z = 0, 1, \ldots, m-1$. Further, we assume that a particular category η_z has a unique marked point. To represent this system, we introduce additional label states $|\eta_z\rangle$ with $0 \le z \le m-1$, adding an extra dimension to the Hilbert space. We consider a finite two-dimensional lattice, although our method can be easily generalized to arbitrary graphs and dimensions. FIG. 4.3 shows the schematic diagram of Hilbert space for the search algorithm, which shows replicated layers of the $2d$ lattice representing different categories η_z. Depending on whether the motion between different layers (categories) is allowed or not, we have two different scenarios: Static labeling and Dynamic labeling.

4.2.1 Static Labelling

Consider the case where the walker is not allowed to move between the layers. The Hilbert space is spanned by basis $\{|i,j\rangle \otimes |x,y\rangle \otimes |\eta_z\rangle : i,j \in [0,1] \,\&\, 0 \le x,y \le N-1 \,\&\, 0 \le z \le m-1\}$. The oracle can be written as

$$R = I - 2|\psi_c^{(2)}\rangle\langle\psi_c^{(2)}| \otimes \sum_z \sum_{\mathcal{X}\in M_z} |x,y\rangle\langle x,y| \otimes |\eta_z\rangle\langle\eta_z| \tag{4.17}$$

where M_z is set of marked nodes in layer z, and $\mathcal{X} \equiv (x,y)$ to unclutter the notations. Since the walker doesn't move between the layers, the shift and coin operator are the same as the unordered marked case as described in **??**. Note that the Hilbert space for this case is reducible to a direct sum of Hilbert spaces associated with different layers. Therefore, the algorithm boils down to a set of independent reduced QWSA on each layer. Following the reducibility of the Hilbert space, we can write the evolution

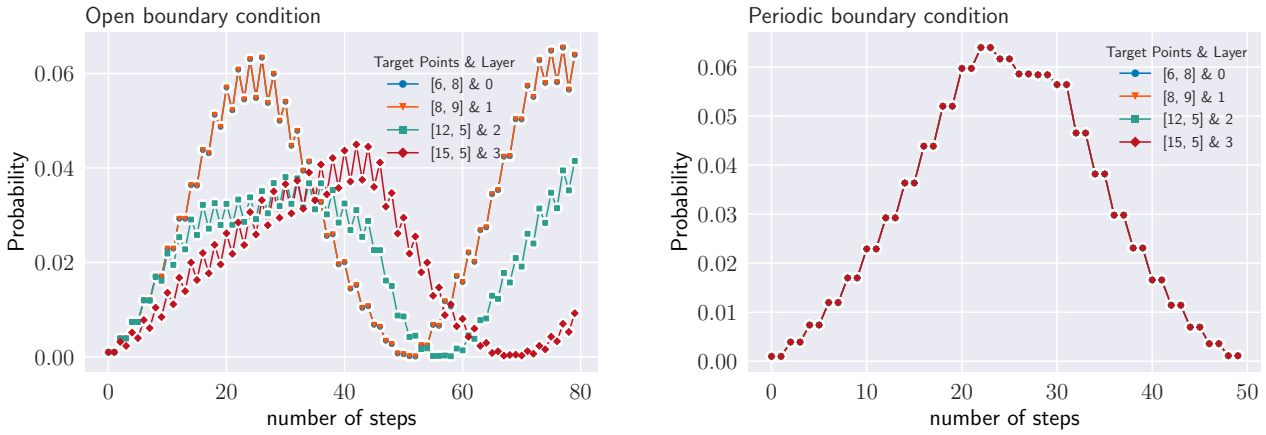

FIGURE 4.4: Amplification of marked nodes with steps for static labelling in the case of **(a)** open grid and **(b)** torus. In case of open grid, the probability of marked nodes [6, 8] and [8, 9] coincides, while in case of torus, the probability of all marked nodes coincide with each other.

operator as a direct sum of evolution operators of individual layers

$$U' = U \cdot R = \bigoplus_z U'_z = \bigoplus_z \left(U_z \cdot R_z\right) , \tag{4.18}$$

where $U_z = S_z(C_z \otimes I)$ and

$$R_z = I - 2|\psi_c^{(2)}\rangle\langle\psi_c^{(2)}| \otimes \sum_{x \in M_z} |x, y\rangle\langle x, y| . \tag{4.19}$$

The initial state is an equal superposition in coin, position, and label space, given by

$$|\Psi(0)\rangle = \frac{1}{2}\sum_{i,j} |i, j\rangle \otimes \frac{1}{N\sqrt{m}} \sum_{x,y,z} |x, y\rangle \otimes |\eta_z\rangle \tag{4.20}$$

The modified operator U' is applied t_{op} times to the state, which amplifies the marked points and their associated labels. To illustrate the algorithm, we perform a numerical simulation of the algorithm on 16×16 grid under both open and periodic boundary conditions. The simulation includes four marked nodes at position $\{(6, 8), (8, 9), (12, 5), (15, 5)\}$, which necessitates four layers or label states.

FIG. 4.4 shows the probability of finding a labeled marked node as a function of the number of steps taken by the algorithm. Figure 4.5 displays the probability distribution at the optimal time step. For the periodic boundary condition, we observe that the probabilities of finding each marked node coincide. This results from the translational symmetry inherent in the toroidal geometry of the lattice. In contrast, under the open boundary condition, the probability of finding a marked node generally depends on its location due to boundary effects. Increasing the system size would lead us to anticipate the disappearance of boundary effects. Consequently, we expect the two probability distributions to converge as the number of nodes N approaches infinity.

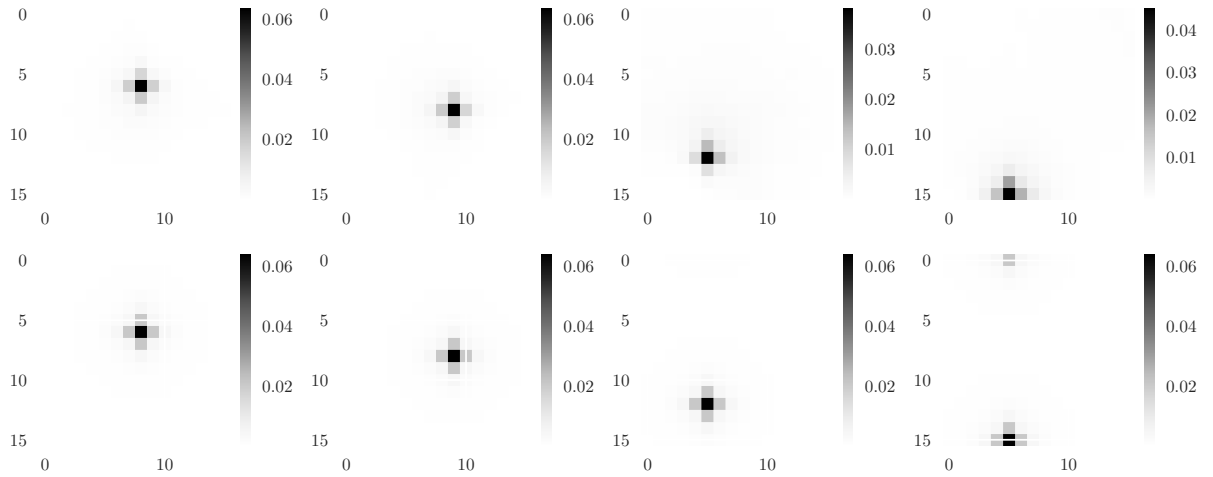

FIGURE 4.5: Probability distribution at t_{op} step for different layers with a single marked point in each layer found using quantum-search algorithm with static labelling **Top**: Open boundary condition **Below** Periodic boundary condition

As a consequence of separability of algorithm to independent QWSA on each layer, the optimal time t_{op} is the same as that for a conentional QWSA. Although, since the probability weight of wavefunction on each layer is scaled down by the factor of number of layers, as a result the success probability p_{succ} is also scaled down by the number of the same factor. Therefore, the success probability associated with each layer is $\mathcal{O}(1/(m \ln N))$.

4.2.2 Dynamic Labelling

For the dynamical labeling, where we allow for inter-layer transition, the coin space includes an additional direction to facilitate such motion (along the direction of the labels). The corresponding Hilbert space is spanned by a basis $\{|i,j,k\rangle \otimes |x,y\rangle \otimes |\eta_l\rangle : i,j,k \in [0,1] \,\&\, 0 \le x,y \le N-1 \,\&\, 0 \le k \le m-1\}$ which has dimension $8mN^2$. The Grover diffusion operator G_3 is elevated to a three-qubit operator. There can be further analogous extensions to open and periodic boundary conditions along the label direction, but we will stick to open boundary along the label direction. Similarly, the shift operator becomes,

$$\begin{aligned} S|i,j,k\rangle \otimes |x,y,\eta_z\rangle = |1-i,1-j,1-k\rangle \otimes \\ |x+(-1)^i(1-\delta_{ij}), y+(-1)^i\delta_{ij}, \eta_{z+(-1)^k}\rangle \end{aligned} \tag{4.21}$$

The modified unitary evolution for the search given by

$$U' = U \cdot R = S(G_3 \otimes I) \cdot R \tag{4.22}$$

where the search oracle is given by

$$R = I - 2|\psi_c^{(3)}\rangle\langle\psi_c^{(3)}| \otimes \sum_z \sum_{\mathcal{X}\in M_z} |x,y\rangle\langle x,y| \otimes |\eta_z\rangle\langle\eta_z| \,. \tag{4.23}$$

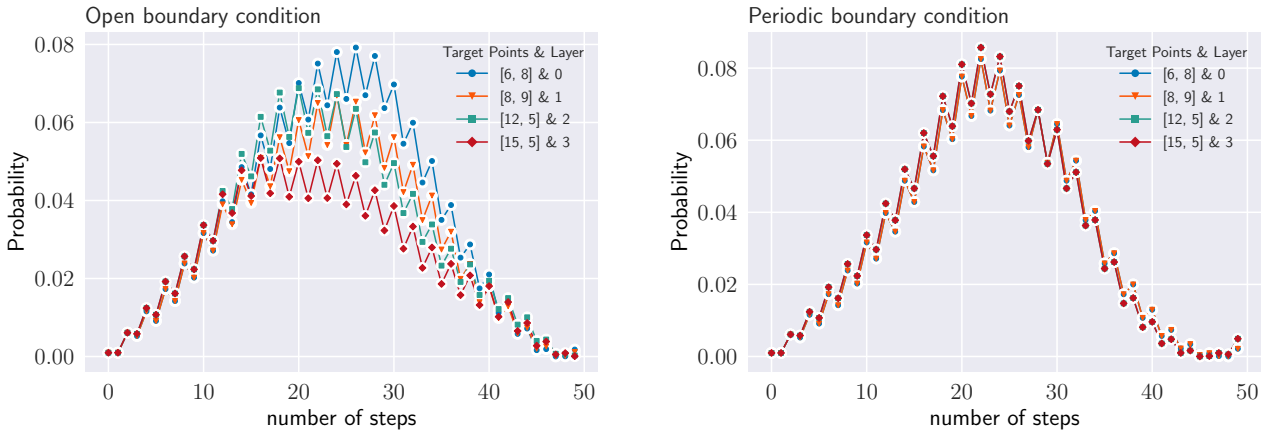

FIGURE 4.6: Amplification of marked nodes with steps for dynamic labelling in the case of **(a)** open grid and **(b)** torus.

The initial state is a uniform superposition in Hilbert space. The modified operator U' is applied t_{op} times on this state, which amplifies the marked point along with labels.

We demonstrate the amplification due to dynamic labeling for the case of the open grid and torus with the same parameters as static case in FIG. 4.6, and probability distribution at optimal time-step in FIG. 4.7. Note that in this case, the torus (as in the case of static labeling) has a unique t_{op}. While the open grid performs much better than the static labeling and possesses a close to unique t_{op} where all the marked nodes are simultaneously amplified.

4.2.3 Scaling

This section investigates how the success probability of our search algorithm scales with the lattice size. We illustrate this by considering the algorithm with two marked nodes, $\{[0,0],[1,1]\}$, on lattices of varying sizes. In FIG. 4.8 presents the success probability of individual marked points and the collective success probability (sum of all individual success probabilities) for both static and dynamical cases. We fit the curve $a/\log(bN)$, which indicating that the algorithm exhibits similar scaling behavior as the conventional QWSA in two-dimensional lattices [114]. Therefore, the collective sucess probability of our search algorithm scales as $\mathcal{O}(1/\ln(N))$, while the success probability of individual marked point scales as $\mathcal{O}(1/m\ln(N))$.

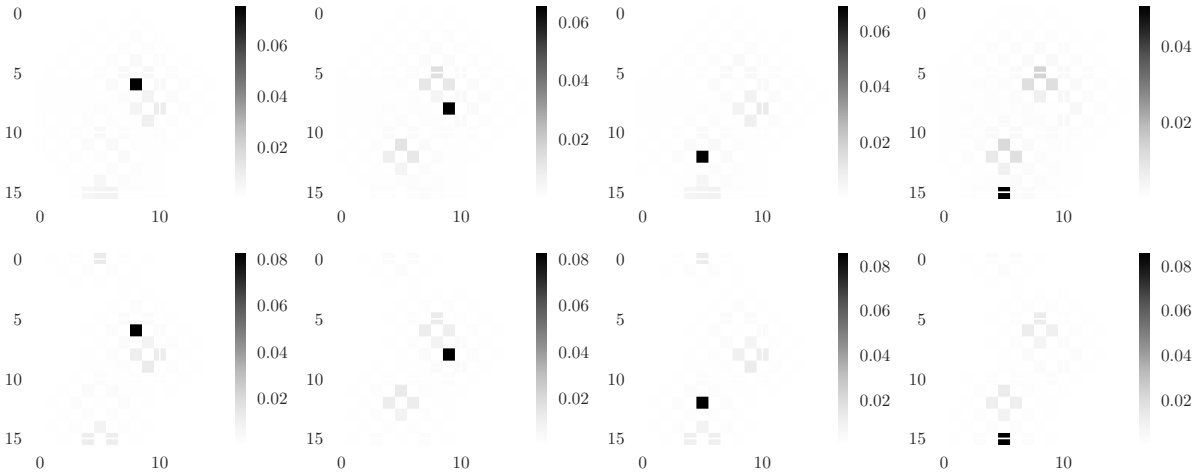

figure 4.7: Probability distribution at t_{op} step for different layers with a single marked point in each layer found using quantum-search algorithm with dynamic labelling **Top**: Open boundary condition **Below** Periodic boundary condition

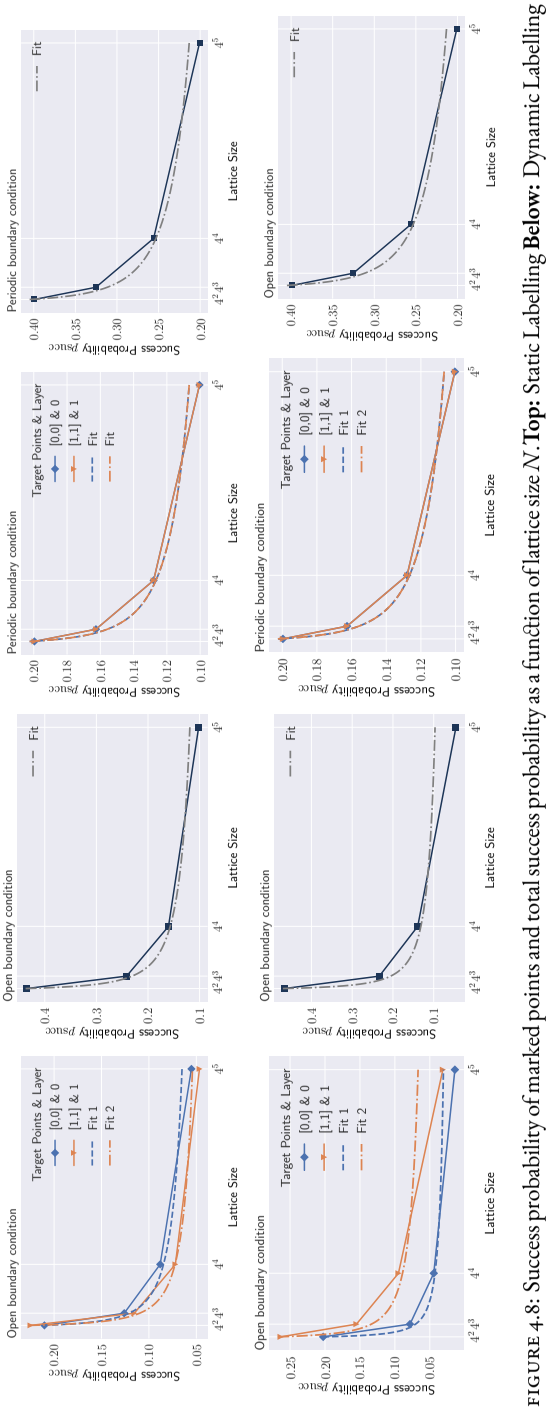

FIGURE 4.8: Success probability of marked points and total success probability as a function of lattice size N. **Top:** Static Labelling **Below:** Dynamic Labelling

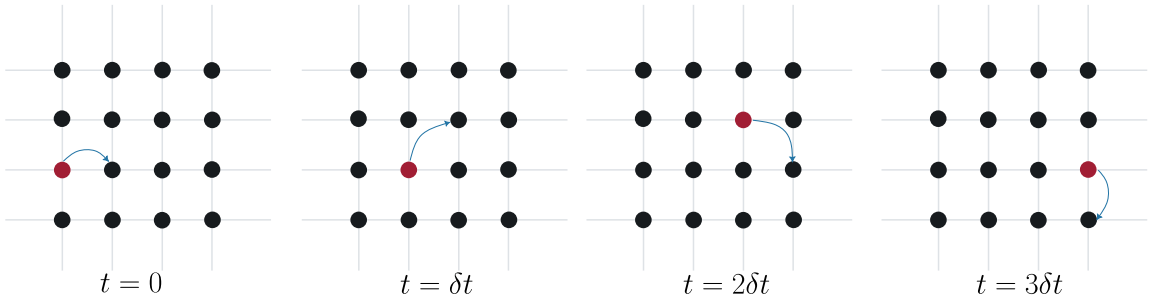

FIGURE 4.9: Particle moving in two-dimensional lattice in discrete-time steps.

4.3 Quantum tracking problem

So far, we have examined our refined QWSA for searches on $2d$ surfaces using open and periodic boundary conditions. We have established that in most cases, the algorithm works better for simultaneous amplification of multiple marked nodes at a unique time t_{op}. In simple terms, this implies that there exists a unitary operator U such that $U^{t_{\text{op}}}$ acting on a maximally superposed initial state can maximize the probability of the marked nodes. In this section we demonstrate a practical application of the algorithm introduced in §4.2 for tracking a particle moving in real-time. We consider a particle moving on a $2d$ surface and the time taken by the particle to move one step is δt (See FIG. 4.9). Let us assume that position of particle at an instance of time $t_z = z\delta t$ with $z = 0, 1, 2, \ldots$ is $\mathcal{X}_z = (x_z, y_z)$. Our aim is to find the trajectory of the particle i.e. $\mathcal{X}_z$.

A two-dimensional lattice represents the particle's configuration space and labels represent time steps. For example $\mathcal{X}_z = (x_z, y_z)$ represents the coordinates of the particle at time $t = z\delta t$. However, it would seem that associating labels with time has an obvious disadvantage in terms of resources, since the time variable continues to increase and so does the labels, hinting at a requirement of potentially infinite resource well. This in turn makes our labeling algorithm practically inapplicable owing to our limited resources. To overcome this problem, we will recycle our labels. Let's understand this in more detail. Let us define layers $l_0, l_1, l_2, \ldots$ representing the configuration space of a particle at time $0, \delta t, 2\delta t, \ldots$. Furthermore, we assume that the probability amplification takes computational time (s_i) such that $s_0, s_1, s_2, \ldots \ll O(T)$. In general, the maximum time of amplification T is greater than the time step δt. Therefore, the information about the particle's appearance must remain in the constructed oracle for at most time T. Let us define m as $m = [T/\delta t]$ which is the number of steps that particles take in time T which is the least number of layers required. Therefore, we can write the oracle as

$$
\begin{aligned}
R &= I - 2|\psi_c^{(2)}\rangle\langle\psi_c^{(2)}| \otimes \big[f(0,T)|x_0,y_0,\eta_0\rangle\langle x_0,y_0,\eta_0| + f(\delta t, T+\delta t)|x_1,y_1,\eta_1\rangle\langle x_1,y_1,\eta_1| + \cdots \\
&\quad + f(m\delta t, T+m\delta t)|x_m,y_m,\eta_m\rangle\langle x_m,y_m,\eta_m| + f((m+1)\delta t, T+(m+1)\delta t)|x_{m+1},y_{m+1},\eta_0\rangle\langle x_{m+1},y_{m+1},\eta_0| + \cdots\big] \\
&= I - 2|\psi_c^{(2)}\rangle\langle\psi_c^{(2)}| \otimes \big[f(0,T)|x_0,y_0,\eta_0\rangle\langle x_0,y_0,\eta_0| + f(\delta t, T+\delta t)|x_1,y_1,\eta_1\rangle\langle x_1,y_1,\eta_1| + \cdots \\
&\quad + f(T,2T)|x_m,y_m,\eta_m\rangle\langle x_m,y_m,\eta_m| + f(T+\delta t, 2T+\delta t)|x_{m+1},y_{m+1},\eta_0\rangle\langle x_{m+1},y_{m+1},\eta_0| + \cdots\big] \\
&= I - 2|\psi_c^{(2)}\rangle\langle\psi_c^{(2)}| \otimes \sum_{n\in\mathbb{Z}} f(n\delta t, n\delta t + T)|x_n,y_n,\eta_{n \bmod m}\rangle\langle x_n,y_n,\eta_{n \bmod m}|
\end{aligned}
\tag{4.24}
$$

where $f(x,y) = \Theta(x) - \Theta(y)$, and $\Theta(x)$ is Heaviside step function. The shift-operator is used in accord with boundary conditions, and the coin-operator is the Grover diffusion operator G_2 as we are considering single-layer amplification. The time profile of probability distribution for different layers is provided in supplementary material.

4.4 Quantum circuit implementation

In this section, we will propose quantum circuit implementation for quantum walk search for ordered marked nodes as well as quantum tracking problems that have a similar structure. In FIG. 4.10, we show a schematic of a quantum circuit for quantum walk search. The qubits $q_0, q_1, \ldots, q_D$ represents position space so that $2^D = N$, and c_1, c_2 represents coin space. The initial state which is a uniform superposition in position and coin space is constructed through the Hadamard operator. The modified unitary operator is then applied t_{op} times which gives probability amplitude amplification for marked points.

For our QWSA with labelled marked points, we introduce extra qubits for the layers. FIG. 4.10 represents a schematic of a quantum circuit for static labelling with additional $Q_1, Q_2, \ldots, Q_{D'}$ qubits for $2^{D'} = m$ layers (or labels). The circuit for dynamic labelling is similar except we have three qubits for coin space. The equivalent circuit for quantum tracking is also similar to that for QWSA with static labelling. The specific structure of the oracle and other elements depends on configurations of marked points and turns out to be control unitary operations. We construct the coin, shift and the oracle operator, explicitly below.

4.4.1 Coin-Operator

The explicit implementation of coin and shift operator, and complexity in the discrete-time quantum walk has been previously done in [39, 125–127]. In QWSA, the coin operator is a Grover diffusion operator in two qubits. The optimal circuit construction for a qubit real unitary operator requires at most 2 CNOT and 12 one-qubit gates [128]. Although, the Grover diffusion operator can be implemented with 1 CNOT and 4 one-qubits gates (See FIG. 4.11). Another way to implement

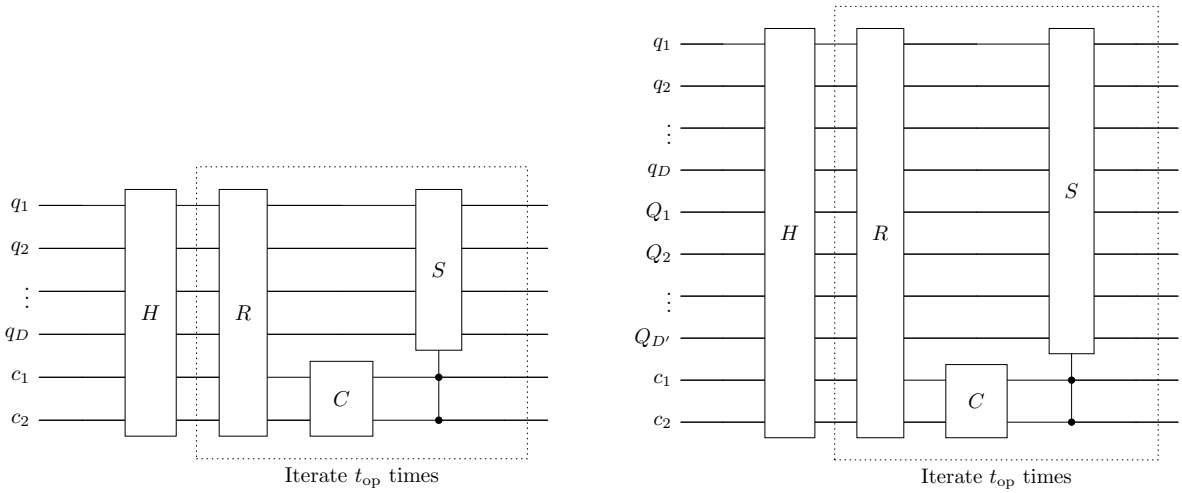

FIGURE 4.10: Schematic of the quantum circuit for **Left** quantum-walk search **Right** quantum-walk search for ordered marked points.

the Grover diffusion operator is to write it in Hadmard basis, in which, it is given by [129]

$$A = \begin{bmatrix} 1 & 0 & 0 & 0 \\ 0 & -1 & 0 & 0 \\ 0 & 0 & -1 & 0 \\ 0 & 0 & 0 & -1 \end{bmatrix} \tag{4.25}$$

Implementing the operator A as a quantum circuit becomes straightforward by incorporating ancilla qubits. These ancilla qubits serve to verify whether the input comprises entirely of o's, allowing for the inversion of the phase if it does not.

4.4.2 Shift-Operator

The flip-flop shift operator is a conditional incrementor over position space qubits. To explicitly implement this, we start with mapping computational basis associated with position $x = 0, 1, 2, \ldots, \sqrt{N} - 1$ into qubit basis by representing state $|x\rangle$ into its binary representation (similar for y direction). As discussed in [126], we can construct an incrementor circuit as shown in FIG. 4.12 using a series of multi-qubit CNOT gates. A n-qubit CNOT gate can be decompose into $\approx 16n$ Toffoli gates, achieving $\mathcal{O}(n)$ bound [130]. An analogous circuit of decrementor can also be constructed using a multi-qubit CNOT gate by changing the control qubits as shown in FIG. 4.12. We can, therefore, construct a flip-flop shift operator using a conditional operator over coin qubits as shown in FIG. 4.13.

In case of multiple layers, the translation operator couples with qubit representing layers depending on static or dynamic labelling. As we seen in §4.2, the algorithm decouples for static labelling, therefore the shift operator remains the same. In case

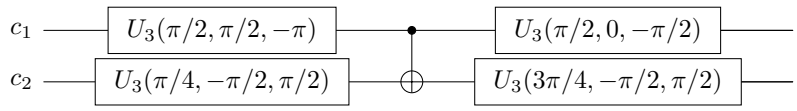

FIGURE 4.11: Implementation of Grover's diffusion operator for 2-qubits done using Qiskit

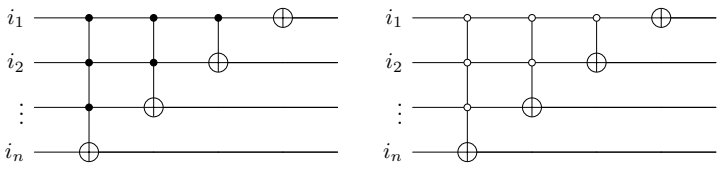

FIGURE 4.12: Translation operator for qubits in position space. **Left**: n-qubit incrementor circuit. **Right**: n-qubit decrementor circuit.

of dynamic labelling, we add an extra coin-qubit to allow inter-layer flow, as shown in FIG. 4.13.

4.4.3 Oracle

Finally, consider the oracle R which we claim to be a controlled Grover diffusion operator (up to a phase), where control qubits are marked states. To prove this, consider the form of oracle in EQ. (4.8). This operator acts trivially (as identity) on the states which does not belong to set of marked nodes M, while it acts as $I \otimes (I - 2|\psi_c^{(d)}\rangle\langle\psi_c^{(d)}|)$ if the state belongs to M. The operator $I - 2|\psi_c^{(d)}\rangle\langle\psi_c^{(d)}| = -G^{(d)}$ is Grover diffusion operator up to a phase of $e^{i\pi}$. This is results follows for the case of multilayer search oracle except the control operation is over state $|x, y, \eta_z\rangle$ where $(x, y) \in M_z$.

To illustrate this result, consider a quantum-walk search on 2×2 lattice with a marked point chosen to be $(0, 0)$ without the loss of generality. We map the position states in qubit states as shown in FIG. 4.14. The oracle can be written as

$$R = I - 2|\psi_c^{(2)}\rangle\langle\psi_c^{(2)}| \otimes |00\rangle\langle 00| \tag{4.26}$$

The first term doesn't affect the state and the second term only contributes when the

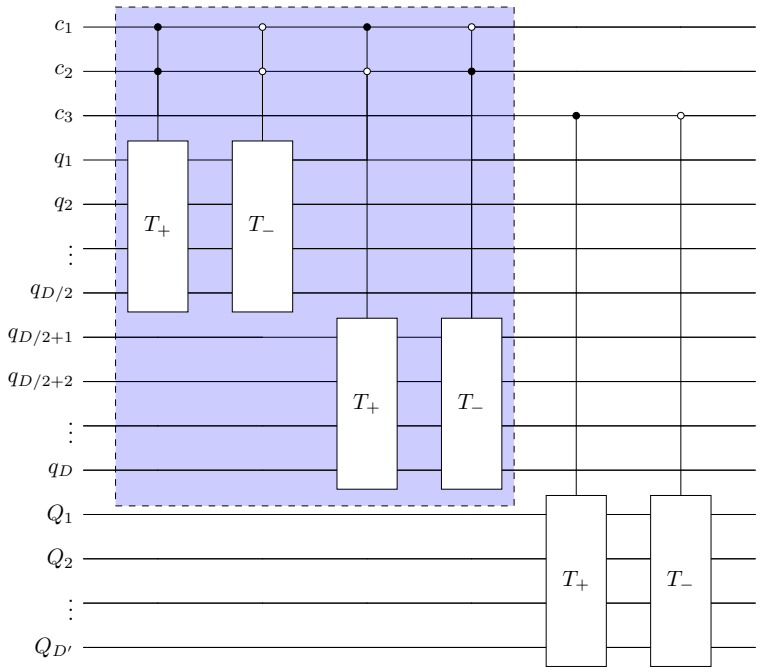

FIGURE 4.13: Quantum circuit for flip-flop shift operator where T_+ and T_- represent translation operators (incrementor and decrementor respectively). The qubits $q_1, q_2, \dots, q_{D/2}$ and $q_{D/2+1}, q_{D/2+2}, \dots q_D$ represents position space qubits associated x and y-direction respectively, c_1, c_2 are coin-space qubits, and $Q_1, Q_2, \dots, Q_{D'}$ represent layer states. The dotted part represents the circuit needed for static labelling.

position state is a marked state $|00\rangle$. More explicitly,

$$\begin{aligned}
|0000\rangle &\to \frac{1}{2}(|00\rangle - |01\rangle - |10\rangle - |11\rangle)|00\rangle \\
|0100\rangle &\to \frac{1}{2}(-|00\rangle + |01\rangle - |10\rangle - |11\rangle)|00\rangle \\
|1000\rangle &\to \frac{1}{2}(-|00\rangle - |01\rangle + |10\rangle - |11\rangle)|00\rangle \\
|1100\rangle &\to \frac{1}{2}(|-00\rangle - |01\rangle - |10\rangle + |11\rangle)|00\rangle\,.
\end{aligned} \tag{4.27}$$

Therefore, it's a control operation over marked state $|00\rangle$ with controlled operation $-G^{(2)}$. FIG. 4.14 shows the quantum circuit implementation of this Oracle. Consider the case of ordered marked points with two categories, therefore, we require one additional qubit for two layers. Further, we assume that the two categories contain marked points $|00\rangle$ and $|11\rangle$ (See FIG. 4.15). The oracle operator R can be written as

$$R = I - 2|\psi_c^{(2)}\rangle\langle\psi_c^{(2)}| \otimes [|00\rangle\langle 00| \otimes |0\rangle\langle 0| + |11\rangle\langle 11| \otimes |1\rangle\langle 1|] \tag{4.28}$$

where we assumed static labelling (but easily generalized to dynamic case). Following the similar argument as before, the oracle operator only acts non-trivially to marked labelled states which belong to set $\mathcal{M}_z$, in this case, $|000\rangle$ and $|111\rangle$. More explicitly,

$$\begin{aligned}
|00\rangle|x,y,\eta_z\rangle &\to \frac{1}{2}(|00\rangle - |01\rangle - |10\rangle - |11\rangle)|x,y,\eta_z\rangle \\
|01\rangle|x,y,\eta_z\rangle &\to \frac{1}{2}(-|00\rangle + |01\rangle - |10\rangle - |11\rangle)|x,y,\eta_z\rangle \\
|10\rangle|x,y,\eta_z\rangle &\to \frac{1}{2}(-|00\rangle - |01\rangle + |10\rangle - |11\rangle)|x,y,\eta_z\rangle \\
|11\rangle|x,y,\eta_z\rangle &\to \frac{1}{2}(|-00\rangle - |01\rangle - |10\rangle + |11\rangle)|x,y,\eta_z\rangle
\end{aligned} \tag{4.29}$$

where $|x,y,\eta_z\rangle = |000\rangle, |111\rangle$. As before, this is controlled Grover diffusion operator over marked position states acting on coin state.

4.4.4 The complexity scaling

In this section, we analyze the complexity scaling (resource required) of the quantum algorithm both with system size. We will focus on quantum-walk search with ordered marked points from which the complexity of the quantum tracking problem can easily be derived.

As we previously seen the Hilbert space dimensions of single and multi-layer amplification algorithms are $4mN$ and $8mN$ respectively, where N is the number of lattice points and m is the number of categories or layers. Therefore, the qubit requirement scale is $\mathcal{O}(\log(mN))$ with system size. The major cost of the operator in the algorithm comes from the flip-flop shift operator. We can find how many Toffoli gates required for the flip-flop shift operator for single-layer amplification

$$4 \times \sum_{n=1}^{D/2} 16\frac{n}{2} \approx 4(D^2 + D)$$

which is $\mathcal{O}(4D^2)$. For the multi-layer amplification case, this modifies to $\approx 4(D^2 + D) + 8D'(D' + 1)$ due to the additional operator needed for hopping between layers. The n-qubit Toffoli gate requires at least $2n$ CNOT gates [131], therefore, the number of CNOT gates required is approximately of order $\mathcal{O}(8D^2)$. The construction of the oracle requires control operation of Grover's diffusion operator as many times as the number of marked points. For a large data set and a small number of marked points, we expect the cost due to shift operator to dominate, and therefore resource requirement is polynomial in the number of gates required for a single step. Therefore, the complete algorithm requires at least $\approx t_{\text{op}}\mathcal{O}(D^2)$ CNOT gates.

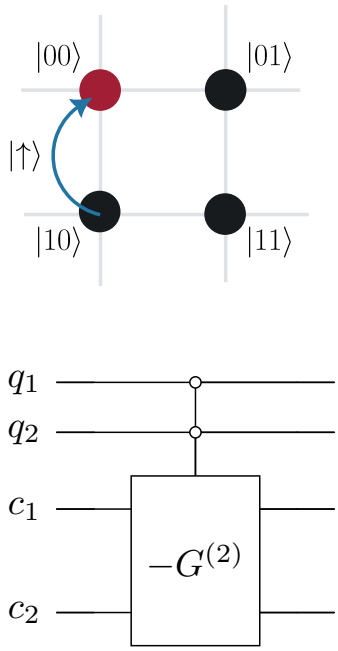

FIGURE 4.14: **Left**: The qubit space for 2 × 2 lattice along with coin basis. **Right**: Quantum circuit implementation of Oracle for 2 × 2 lattice. The Pauli X operator is used to flip the bit to implement control operation over $|00\rangle$ position basis.

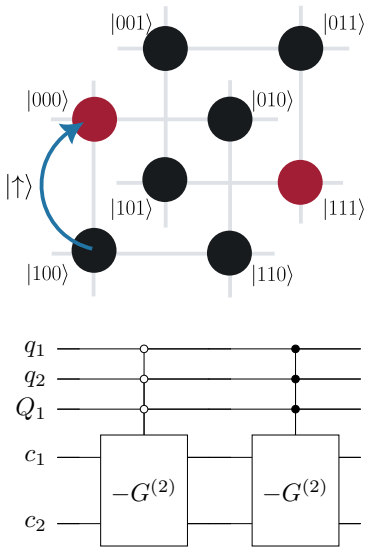

Figure 4.15: (a) The qubit space for 2 × 2 lattice with two layers with coin basis. The marked nodes are shown with blue color. (b) Quantum circuit of oracle for 2 × 2 lattice with two layers for marked nodes |000⟩ and |111⟩.

4.5 Outlook

The conventional QWSA is aimed at finding a marked node in a graph but lacks the ability to characterize the nodes when more than one is present. We propose a modification that locates multiple marked nodes and characterizes them with respect to an existing (chronological) ordering. Clearly, our algorithm can also be extended to cases where the categorization of marked nodes is based on some attribute other than temporal. This involves the introduction of extra qubits associated with categories. We give an explicit form of oracle in two separate cases depending upon whether there's an inter-flow of probability between categories. As a concrete application, we used our formulation for particle tracking in real-time. Finally, we also construct an equivalent quantum circuit for the algorithm, with the prospect of integration with the contemporary quantum hardware. However, this is a beginning step, where we have just scratched the tip of the iceberg, and a lot more needs to be amended in the algorithm before it gets market-ready. We will point out some immediate follow-up questions that we intend to resolve and extend the scope of the algorithm:

- **More generic geometries:** We have considered the algorithm on a simple two-dimensional lattice w/o boundary conditions. The immediate generalization would be to consider more generic and perhaps non-trivial geometries with intricacies. For example, we would consider a percolation lattice in $2d$ with different weighted edges and on-site potentials. These geometries represent various scenarios in real-time systems. Another direction worth pursuing is the search on graphs themselves. A part of the problem is already addressed in §4.3 where we considered the simpler version of [132] where the authors discuss searches on temporal (time-varying) graphs. We would like to see if our algorithm can be extended to address multiple temporal graphs with intersecting vertices. This would be helpful in elevating the predictability of the algorithm from a tracking to a tracking-intercepting algorithm.

- **Localization and Quantum State transfer:** These two concepts are seemingly disconnected. Localization explains how particle propagation (plane waves) can be restricted (localized distribution) in the presence of disorder in the media [133]. In particular, it is demonstrated in the context of DTQW in various settings [134–136]. Quantum State transfer concerns the propagation of a specific quantum state from one node (origin) to another (target) through a complex network (e.g., a spin chain) [137, 138]. These two ideas are not quite connected with each other and are more disconnected from the QWSA. The question, however, is whether we can establish a connection between the search algorithm and the localization aspect by thinking of the search oracle as a disorder in an otherwise non-chaotic media. Similarly, instead of taking a complete superposition for an initial state, can we single out the marked nodes with any biased (a specific) initial state? The real question in both scenarios is to interpret the "Search Oracle" R as a disorder operator

from the physics point of view, which in turn can help understand the search oracle better and amend it for other purposes based on insights from physics.

Nielson's complexity meets circuit depth 5

Although quantum computers are capable of solving interesting computational problems, but it remains a challenge to find efficient quantum circuits that can perform these computational tasks. It is, therefore, of great interest to ask, *What is a optimal quantum circuit for the implementation of a unitary operation?* The answered to this question led to the concept of Nielson's complexity, which will be central topic of this chapter. In their paper [139, 140], Nielsen et al. recasted the problem of finding optimal quantum circuits to finding the shortest path between two points in certain curved geometry, thereby, opened the possibility of using the mathematical techniques of Riemannian geometry to suggest new quantum algorithms or to prove limitations on the power of quantum computers.

Nielsen's Complexity (NC) is conjectured to quantify the optimal number of quantum gates needed to construct the optimal number of quantum gates needed to construct a target state starting from a reference state. Therefore, in an optimal quantum circuit, one would expect a some relation between the NC and circuit depth – an integer number that counts the maximum length in the circuit between the input and the output. However, much we wanted otherwise, the exact connection of the NC and circuit depth in quantum circuits is far from being fully understood. The reason is the ambiguity of precisely mapping the complexity measure to the quantum circuit picture. A better understanding of a possible link between circuit depth and NC proposal could provide an analytical handle on the practical circuits build using quantum gates and ask whether the circuit in question is optimal. From the reverse point of view, it is only logical to bring the analytically well-defined notion of circuit complexity proposal closer to actual quantum circuits. Otherwise, relating the mathematically computed NC to something physically meaningful becomes hard.

This length is usually defined in terms of layers of gates acting in parallel.

In this chapter, we will try to fill in this gap between the NC and circuit depth.

To this end, I'll compute the NC for the unitary evolution of the discrete-time quantum walk as well as the circuit depth by explicit quantum circuit construction. Our results shows that the both quantities follow the identical behavior in terms of number of walk steps.

5.1 Geometry of SU(2^n)

In this section, we consider the explicit formulation of circuit complexity in space SU(2^n) of n-qubit unitary operators. We begin with a basis for the Lie algebra with some notion of locality which is essential to identify some generators in the Lie algebra as local or "simple", and the rest as "complex". In the geodesic framework, it is natural to choose a k-local subspace of the Lie algebra of the unitary group manifold to correspond to "simple directions". We may think of the elementary gates of the quantum computation viewpoint as being exponentials of these simple generators. For the qubit case SU(2^n), there are a couple of natural ways to proceed. We could pick the "Pauli basis", namely products of Pauli matrices acting on individual qubits, as our basis of generators. The second choice is to consider the gamma matrices γ_a with $a \in \{0, \cdots, 2n-1\}$ which satisfy the Clifford algebra (with $\gamma_a^\dagger = \gamma_a$):

$$\{\gamma_a, \gamma_b\} = 2\delta_{ab} \,. \tag{5.1}$$

The Hilbert space of n qubits has a natural tensor factorization

$$\mathscr{H} = \underbrace{\mathbb{C}^2 \otimes \cdots \otimes \mathbb{C}^2}_{n} \,.$$

The geometry of the set of (unit-determinant) unitary operators $\mathscr{U}(\mathscr{H})$ that acts on this Hilbert space. In this case, this set is

$$\mathscr{U}(\mathscr{H}) = \mathscr{U}\left(\mathbb{C}^{2^n}\right) = \mathrm{SU}(2^n) \,.$$

Now consider distinct ordered products $T_{a_1 \ldots a_m} = \gamma_{a_1} \ldots \gamma_{a_m}$ with $m \in \{1, \ldots, 2n\}$ and $a_p < a_q$ for $p < q$. We will often denote these operators as simply T_i, where i stands for the multi-index $a_1 \cdots a_m$. The total number of such ordered products is $\sum_{m=1}^{2n} {}^{2n}C_m = 2^{2n} - 1$. This is precisely the dimension of the Lie algebra $\mathfrak{su}(2^n)$. It is simply to make such ordered products of gamma matrices Hermitian by inserting appropriate factors of i. Such a construction is a basis for $\mathfrak{su}(2^n)$. Furthermore, k-local generators of the Lie algebra are simply those involving k or fewer gamma matrices.

Our next step is to come up with a right-invariant metric which penalize the motion in the direction of nonlocal unitary operators. In our case, we want to deter motion in directions which correspond to generators involving products of more than k gamma matrices. We begin with computing the structure constant f_{ij}^l of the Lie algebra defined as

This corresponds to a choice of gate set in the quantum computation picture, where we allow up to k-local gates in out circuit but do not allow more nonlocal gates.

$$[T_i, T_j] = i f_{ij}^l T_l \tag{5.2}$$

Using these, we calculate the Cartan-Killing form

$$K_{ij} = -\frac{1}{h} f_{im}^l f_{jl}^m \tag{5.3}$$

(where h is the dual Coxeter number) which is a positive-definite bilinear form. To build the notion of simple and hard directions in the Lie algebra, we construct a new positive-definite bilinear form on $\mathfrak{su}(2^n)$

$$G_{ij} = \frac{c_i + c_j}{2} K_{ij} \tag{5.4}$$

where the numbers c_i are "cost factors" which encode the information about our choice of local and nonlocal directions. Then a right-invariant metric g can be defined at an arbitrary point U on $\mathrm{SU}(2^n)$ by simply taking

$$g_U(X,Y) = G(XU^{-1}, YU^{-1}) \tag{5.5}$$

where we have used the group structure to transport the tangent vectors X and Y from U back to identity then applied. We will generally take $c_i = 1$ if the generator T_i consists of k or fewer gamma matrices, and $c_i = 1 + \mu$ with $\mu \geq 1$ otherwise.

Having chosen our cost factors, the geodesic equation on $\mathrm{SU}(2^n)$ with metric is given in terms of the Lie algebra metric and structure constants by the Euler-Arnold equation

$$G_{ij}\frac{dV^j}{ds} = f^p_{ij}V^jG_{pl}V^l \tag{5.6}$$

where the velocities $V^i(s)$ control the unitary path the geodesic follows via

$$U(s) = \mathcal{P}\exp\left[-i\int_0^s ds' V^i(s')T_i\right] \tag{5.7}$$

and we have made use of the path-ordered exponential to solve the matrix equation for the unitary operator

$$\frac{dU}{ds} = -iV^i(s)T_iU(s) \tag{5.8}$$

Finally, we impose the boundary condition $U(1) = U_{\text{target}}$ for some target unitary whose circuit complexity we wish to study. This complexity is given by the geodesic length

$$\mathcal{C}[U_{\text{target}}] = \min\int_0^1 ds\sqrt{G_{ij}V^i(s)V^j(s)} \tag{5.9}$$

where the minimization is over all geodesics from the identity to U_{target}. Having this preliminary required, we will talk about target unitary of our interest.

5.2 Setup

After a brief introduction to the circuit complexity and it's structure in $\mathrm{SU}(2^n)$, I'll setup the problem of interest i.e. a unitary U of interest. Consider one-dimensional discrete-time quantum walk (DTQW) governed by

$$U = S\cdot(C(\theta)\otimes I) \tag{5.10}$$

where S is the shift operator given by

$$S = \sum_x \left(|\uparrow\rangle\langle\uparrow|\otimes|x+1\rangle\langle x| + |\downarrow\rangle\langle\downarrow|\otimes|x-1\rangle\langle x|\right)\ . \tag{5.11}$$

and the coin operator $C(\theta)$

$$C(\theta) = \begin{bmatrix} \cos\theta & \sin\theta \\ -\sin\theta & \cos\theta \end{bmatrix}. \tag{5.12}$$

Due to large dimension of unitary, we can not directly find the complexity of the quantum-walk. However, as we will see, we will work with reduce dynamics in the coin space.

The unitary operator lives in $\mathscr{H}_2 \otimes \mathscr{H}_N$ which is a $(4N+2) \times (4N+2)$ dimensional space. The initial state is chosen to be positioned at the origin with an equal superposition of the coin states,

$$|\Psi(0)\rangle = \frac{|\uparrow\rangle + i|\downarrow\rangle}{\sqrt{2}} \otimes |0\rangle \tag{5.13}$$

After t-steps of evolution,

$$|\Psi(t)\rangle = U^t |\Psi(0)\rangle \tag{5.14}$$

can be written as a general superposition of the $|\uparrow\rangle$ and $|\downarrow\rangle$ states,

$$|\Psi(t)\rangle = \sum_x \psi^{\uparrow}_{x,t}|\uparrow\rangle|x\rangle + \psi^{\downarrow}_{x,t}|\downarrow\rangle|x\rangle\,. \tag{5.15}$$

The coefficients can be recursively solved from the relations,

$$\begin{aligned} \psi^{\uparrow}_{x,t} &= \cos\theta\psi^{\uparrow}_{x-1,t-1} + \sin\theta\psi^{\downarrow}_{x-1,t-1} \\ \psi^{\downarrow}_{x,t} &= -\sin\theta\psi^{\uparrow}_{x+1,t-1} + \cos\theta\psi^{\downarrow}_{x+1,t-1} \end{aligned} \tag{5.16}$$

The probability distribution as a function of the time and position is given by $p_{x,t} = |\psi^{\uparrow}_{x,t}|^2 + |\psi^{\downarrow}_{x,t}|^2$. In order to proceed, we consider the reduced density matrix,

$$\begin{aligned} \rho(t) &= \mathrm{tr}_x|\Psi(t)\rangle\langle\Psi(t)| = \sum_{i,j\in\uparrow,\downarrow} \rho_{ij}|i\rangle\langle j| \\ \rho_{\uparrow\uparrow} &= \sum_x |\psi^{\uparrow}_{x,t}|^2 \\ \rho_{\uparrow\downarrow} &= \sum_x \psi^{\uparrow}_{x,t}(\psi^{\downarrow}_{x,t})^* \\ \rho_{\downarrow\uparrow} &= \rho^*_{\uparrow\downarrow}, \qquad \rho_{\downarrow\downarrow} = 1 - \rho_{\uparrow\uparrow}\,. \end{aligned} \tag{5.17}$$

By construction, $\mathrm{tr}\rho(t) = 1$, and the resultant is a mixed state density matrix in the coin space ($\mathscr{H}_2$).

5.2.1 Canonical Purification

We start by canonically purifying the reduced density matrix which begins at computing the eigenvalues of the matrix $\rho(t)$ given by,

$$\lambda_{\pm}(t) = \frac{1 \pm \sqrt{1 - 4\det\rho}}{2}\,. \tag{5.18}$$

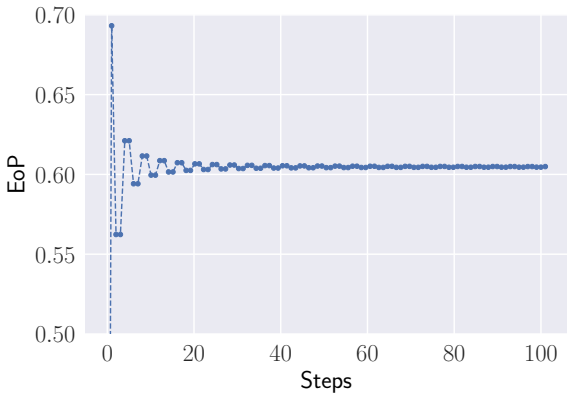

FIGURE 5.1: Entanglement of purification (EoP) with steps for canonical purification.

and corresponding eigenvectors $|\psi_\pm\rangle$. The resultant canonically purified state,

$$|\Phi(t)\rangle = \sqrt{\lambda_+(t)}|\psi_+,\psi_+\rangle + \sqrt{\lambda_-(t)}|\psi_-,\psi_-\rangle\,, \tag{5.19}$$

is a 2-qubit state where $|\psi,\psi\rangle = |\psi\rangle \otimes |\psi\rangle$. This is our starting point for the complexity computation. It is motivated by the following principle. Since complexity computation is known for pure states, the corresponding evaluation for mixed states entails an additional intermediate step of purifying the mixed state to a pure state at the cost of dimensional oxidation from $\mathscr{H}^{2^n} \to \mathscr{H}^{2^{2n}}$ space. The corresponding entanglement of purification as a function of time is,

$$\mathrm{EoP}(t) = -\mathrm{tr}\left(\rho_{\mathrm{pr}} \log \rho_{\mathrm{pr}}\right)\,, \tag{5.20}$$

where $\rho_{\mathrm{pr}} = \mathrm{tr}_2\left(|\Phi(t)\rangle\langle\Phi(t)|\right)$. The density matrix ρ_{pr} is the reduced density matrix from the purified state where tr_2 implies the partial trace of the second qubit. The functional dependence of entanglement of purification on steps is given in FIG. 5.1. It follows essentially the same behavior as the entanglement for the quantum walk.

To conclude the section, we would like to comment on the continuum limit of the walk and its implications on purification. As was established in [141, 142], the continuum limit of the one-dimensional walk is given by the Dirac-Hamiltonian for a single free fermion,

$$H(p) = -ip\begin{pmatrix} \cos\theta & \sin\theta \\ \sin\theta & -\cos\theta \end{pmatrix} + \begin{pmatrix} 0 & -i\sin\theta \\ i\sin\theta & 0 \end{pmatrix} \tag{5.21}$$

This Hamiltonian characterizes a pure fermionic state. To put this loosely, we can construct a 2-particle state (also a pure state) by,

$$H(p_1,p_2) = H(p_1)\otimes\mathbb{I}_2 + \mathbb{I}_2 \otimes H(p_2)\,. \tag{5.22}$$

5.2.2 Target Unitary Operator

Our starting point is the construction of a unitary operator U_{target} such that,

$$|\Phi(t)\rangle = U_{\text{target}}|\Phi_R\rangle\,, \tag{5.23}$$

where $|\Phi(t)\rangle$ is the target state given in EQ. (5.19) and $|\Phi_R\rangle$ is a reference state chosen to be the most simple 2-qubit state $|0\rangle \otimes |0\rangle$. We call U_{target} as the *target unitary operator* that converts the reference state into the target state. Since $|\Phi(t)\rangle$ is time-dependent, we expect U_{target} to be a time-dependent matrix as well. However, the matrix is not fully constrained by EQ. (5.23). We begin by constructing,

$$U_{\text{target}} = \begin{bmatrix}\mathbf{u}_0 & \mathbf{u}_1 & \mathbf{u}_2 & \mathbf{u}_3\end{bmatrix} \tag{5.24}$$

where $\mathbf{u}_i$ are column vectors of dimension 4×1. From EQ. (5.23), we get $\mathbf{u}_0 = |\Phi(t)\rangle$, satisfying $|\mathbf{u}_0|^2 = 1$ from normalization of $|\Phi(t)\rangle$. The unitarity constraint $UU^\dagger = \mathbb{I}$ enforces,

$$\mathbf{u}_i \cdot \mathbf{u}_j^\dagger = \delta_{ij}\,, \tag{5.25}$$

which is incidentally the condition for Gram-Schmidt orthonormalization. To start with,

$$\mathbf{u}_i = \mathbf{v}_i - \sum_{j=0}^{i-1} \frac{\langle \mathbf{u}_j, \mathbf{v}_i\rangle}{\|\mathbf{u}_j\|^2}\mathbf{u}_j\,. \tag{5.26}$$

where $\|\cdot\|$ is the norm of the vector. We choose $\mathbf{v}_i$ to be random vector,

$$\mathbf{v}_i = \mathbf{a}_i + i\mathbf{b}_i\,, \tag{5.27}$$

where $\mathbf{a}_i\,, \mathbf{b}_i \in \text{rand}_{(0,1)}$. Such a construction of target unitary U_{target} is not unique, therefore, in what follows, we will consider average of complexity taken over large number target unitaries so that the complexity is well converged.

This approach is identical to considering the vectors $\mathbf{u}_i \in \text{SU}(4)$ and then optimizing over the parameters. This optimization is over 15 parameters which coincide with the parameterization of $U_{\text{target}} \in \text{SU}(4)$. We perform the optimization numerically by sampling over n-samples of choices of the initial random vectors $\mathbf{v}_i$. The number of samples for this optimization depends on whether the standard deviation of the complexity computed from each sample reaches saturation. We will report on this saturation of standard deviation in the next section after discussing the notion of complexity.

5.3 Circuit Complexity

Once the unitary target operator U_{target} is determined, we proceed to compute the complexity of the operator $C[U_{\text{target}}]$ using the formulation presented in §5.1.

5.3.1 Two-qubit system

We begin by constructing a path ordered unitary operator for a 2-qubit circuit,

$$U(s) = \mathcal{P}\exp\left[-\int_0^s ds' V_i(s')T_i\right] \tag{5.28}$$

where $V_i(s)$ measures the response function for the generators $T_i \in \text{SU}(4)$ group and $\mathcal{P}$ denotes path ordering, which denotes the non-commutativity of quantum gates. The generators T_i are built from Majorana fermionic operators γ_a (satisfying

It is unclear, as of yet, how these response functions are connected to the strengths (or, more specifically, numbers) of quantum gates needed to construct an actual quantum circuit. However, at this point, we will refrain from addressing this issue and will come back to this at the end of the work.

EQ. (5.1)) are given by,

$$T_i = i^{{}^qC_2}\gamma_1^{b_1}\gamma_2^{b_2}\gamma_3^{b_3}\gamma_4^{b_4} \tag{5.29}$$

where b_i are the bitwise representation of the integers representing the generators,

$$1 \leq i = 2^3 b_4 + 2^2 b_3 + 2^1 b_2 + 2^0 b_1 \leq 15\,, \tag{5.30}$$

and $q = b_1 + b_2 + b_3 + b_4$. The fermionic generators γ_a [143] and explicit forms of the generators T_i are given in appendix 6. We also define the structure constant and the Cartan killing forms ($h = 32$ is the Coxeter number),

$$f_{ij}^k = -\frac{i}{4}\mathrm{tr}T_k[T_i, T_j]\,, \qquad K_{ij} = -\frac{1}{h}f_{il}^m f_{jm}^l\,. \tag{5.31}$$

With the choice of normalization $K_{ij} = \delta_{ij}$ and hence $G_{ij} = c_i\delta_{ij}$. The quadratic cost function that defines the complexity is given by,

Recall that c_i are cost functions such that $c_i = 1$ whenever T_i is built from k or fewer γ_a otherwise $c_i = 1 + \mu$ with $\mu \geq 1$.

$$C[U] = \min \int_0^1 ds\sqrt{G_{ij}V^i(s)V^j(s)}\,, \tag{5.32}$$

where the functions $V^i(s)$ satisfy the Euler-Arnold geodesic equations,

$$G_{ij}\frac{dV^j(s)}{ds} = f_{ik}^p G_{pl}V^k(s)V^l(s)\,. \tag{5.33}$$

The minimization is over all geodesics leading the affine path from $s = 0$ to $s = 1$. The minimization takes the geodesic solution to the Euler-Arnold equation EQ. (5.33). Note that the explicit solutions are relevant for the construction of the unitary matrix, but in so far as the complexity is concerned, only the sums of squares of the functions are important. However, depending on the solutions, the sum of squares of the functions form simple subsets which are constants and independent of s. In this sense,

$$C[U] = \sqrt{A^T A + B^T B + \cdots}\,, \tag{5.34}$$

where $A, B, \ldots$ are the subsets. These solutions can be obtained by matching,

$$U(s=1) = U_{\text{target}} \rightarrow V_i(s=1)T_i = i\log[U_{\text{target}}] \tag{5.35}$$

In the next few sections, we will solve EQ. (5.33) explicitly for $k = 1, 2, 3$ local cases and construct the complexity explicitly.

5.3.1.1 $k = 1$

For this case, we have the constants of motion ($V_i(s) = v_i$) in the subset $\mathcal{B} = \{v_i : 5 \leq i \leq 10\}$. The remaining equations are of the form,

$$\begin{aligned}\frac{d\mathcal{A}_1(s)}{ds} + 2\mu\mathcal{M}_1\mathcal{A}_1(s) &= 0\\ \frac{d\mathcal{A}_2(s)}{ds} + \frac{2\mu}{1+\mu}\mathcal{M}_2(s)\mathcal{A}_2(s) &= 0\end{aligned} \tag{5.36}$$

where

$$\begin{aligned}\mathcal{A}_1(s) &= \begin{bmatrix} V_1(s) & V_2(s) & V_3(s) & V_4(s) \end{bmatrix}^T \\ \mathcal{A}_2(s) &= \begin{bmatrix} V_{11}(s) & V_{12}(s) & V_{13}(s) & V_{15}(s) \end{bmatrix}^T \end{aligned} \tag{5.37}$$

and

$$\begin{aligned}\mathcal{M}_1(s) &= \begin{bmatrix} 0 & v_5 & v_6 & v_8 \\ -v_5 & 0 & v_7 & v_9 \\ -v_6 & -v_7 & 0 & v_{10} \\ -v_8 & -v_9 & -v_{10} & 0 \end{bmatrix} \\ \mathcal{M}_2(s) &= \begin{bmatrix} 0 & 0 & 0 & 0 & -V_4(s) \\ 0 & 0 & 0 & 0 & V_3(s) \\ 0 & 0 & 0 & 0 & -V_2(s) \\ 0 & 0 & 0 & 0 & V_1(s) \\ V_4(s) & -V_3(s) & V_2(s) & -V_1(s) & 0 \end{bmatrix}. \end{aligned} \tag{5.38}$$

which satisfy the property $\mathcal{M}_{1,2}^T = -\mathcal{M}_{1,2}$. The corresponding solutions are

$$\begin{aligned}\mathcal{A}_1(s) &= \exp\left[2\mu\mathcal{M}_1(1-s)\right]\mathcal{A}_1(s=1)\,, \\ \mathcal{A}_2(s) &= \exp\left[\alpha\int_s^1 ds'\,\mathcal{M}_2(s')\right]\mathcal{A}_2(s=1)\,. \end{aligned} \tag{5.39}$$

where $\alpha = 2\mu/(1+\mu)$. Using the properties of the matrices $\mathcal{M}_{1,2}$, we can write

$$\mathcal{A}_{1,2}^T(s)\mathcal{A}_{1,2}(s) = \mathcal{A}_{1,2}^T(s=1)\mathcal{A}_{1,2}(s=1) \tag{5.40}$$

as constants evaluated at $s = 1$. The metric of measure is independent of the affine parameter s and it follows that the complexity is

$$C[U] = \sqrt{\mathcal{A}_1^T\mathcal{A}_1 + (1+\mu)\left(\mathcal{B}^T\mathcal{B} + \mathcal{A}_2^T\mathcal{A}_2\right)}\,. \tag{5.41}$$

5.3.1.2 $k = 2$

In this case, the constants of motion form the subset $\mathcal{B} = \{v_i : 1 \le i \le 10\}$. The remaining variables form the vector

$$\mathcal{A}(s) = \begin{bmatrix} V_{11}(s) & V_{12}(s) & V_{13}(s) & V_{14}(s) & V_{15}(s) \end{bmatrix}^T \tag{5.42}$$

satisfying

$$\frac{d\mathcal{A}(s)}{ds} + \frac{2\mu}{1+\mu}\mathcal{M}\mathcal{A}(s) = 0 \tag{5.43}$$

where

$$\mathcal{M} = \begin{bmatrix} 0 & -v_{10} & v_9 & -v_8 & -v_4 \\ v_{10} & 0 & -v_7 & v_6 & v_3 \\ -v_9 & v_7 & 0 & -v_5 & -v_2 \\ v_8 & -v_6 & v_5 & 0 & v_1 \\ v_4 & -v_3 & v_2 & -v_1 & 0 \end{bmatrix} \tag{5.44}$$

which satisfies $\mathscr{M}^T = -\mathscr{M}$. The solution is given by

$$\mathscr{A}(s) = \exp\left(\alpha\mathscr{M}(1-s)\right)\mathscr{A}(s=1) \tag{5.45}$$

with $\alpha = 2\mu/(1+\mu)$. Again, the norm of the vector $\mathscr{A}(s)$ is independent of the affine parameter s, and the complexity,

$$C[U] = \sqrt{\mathscr{B}^T\mathscr{B} + (1+\mu)\mathscr{A}^T\mathscr{A}}\,. \tag{5.46}$$

5.3.1.3 $k = 3$

Finally, for the three local cases, the only constant of motion is a the subset $\mathscr{B} = \{v_{15}\}$ with only one element. The remaining variables form the vector,

$$\mathscr{A}(s) = \begin{bmatrix} V_1(s) & V_2(s) & \cdots & V_{14}(s) \end{bmatrix} \tag{5.47}$$

which satisfies

$$\mathscr{A}(s) = \exp\left(2\mu\mathscr{M}(1-s)\right)\mathscr{A}(s=1)\,. \tag{5.48}$$

where

$$\mathscr{M} = \begin{bmatrix} 0 & 0 & 0 & 0 & 0 & 0 & 0 & -v_{15} \\ 0 & 0 & 0 & 0 & 0 & 0 & v_{15} & 0 \\ 0 & 0 & 0 & 0 & 0 & -v_{15} & 0 & 0 \\ 0 & 0 & 0 & 0 & v_{15} & 0 & 0 & 0 \\ 0 & 0 & 0 & -v_{15} & 0 & 0 & 0 & 0 \\ 0 & 0 & v_{15} & 0 & 0 & 0 & 0 & 0 \\ 0 & -v_{15} & 0 & 0 & 0 & 0 & 0 & 0 \\ v_{15} & 0 & 0 & 0 & 0 & 0 & 0 & 0 \end{bmatrix} \tag{5.49}$$

In this case, the exponentiation can be done exactly, yielding the (8×8) dimensional "magic matrix". In this case, the complexity takes the simple form

$$C[U] = \sqrt{\mathscr{A}^T\mathscr{A} + (1+\mu)v_{15}^2}\,. \tag{5.50}$$

For 4-local case, $V_i(s) = v_i$ for all $i = 1 \ldots 15$.

5.3.2 Quantum-walk system

Given the circuit complexity of two-qubit system, we can proceed to find the complexity of the DTQW target unitary. Before proceeding, there is another subtly to care about. The two-qubit initial $|\psi(t_i)\rangle$ can be evolved to $|\psi(t_n)\rangle$ using two-ways: 1) Using the target unitary from reference state $|\psi(t_i)\rangle$ and target state $|\psi(t_n)\rangle$ 2) Using the set of target unitaries U_i from reference state $|\psi(t_{i-1})\rangle$ and target state $|\psi(t_i)\rangle$ so that the evolution operator becomes $U = \prod_i U_i$ (See Fig. 5.2). These two ways lead to two different definition of circuit complexity, explained below.

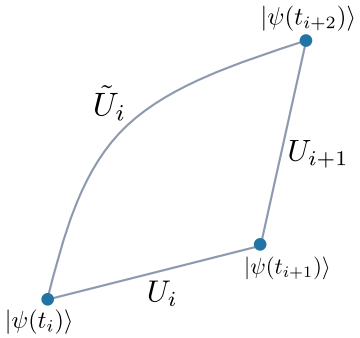

FIGURE 5.2: The two ways for computation of target unitary from state $|\psi(t_i)\rangle$ to $|\psi(t_{i+2})\rangle$. The direct target unitary corresponds to $\tilde{U}_i$ and step-wise target unitary corresponds to $U_{i+1}U_i$.

5.3.2.1 Direct complexity

In this case, we fix the reference state to the initial state $|\psi(t_0)\rangle = |0\rangle \otimes |0\rangle$. Then, we find the target unitary $U(t_n)$ by considering the target states $|\psi(t_n)\rangle$ – the state of quantum-walk at time t_n. The complexity (refers to as direct complexity) is, therefore, corresponds to target unitary $U(t_n)$. As apparent from the definition, this complexity doesn't affect by the path taken by the walk to reach $|\psi(t_n)\rangle$, but only the the final state.

The corresponding plots for the $k = 1,\ 2,\ 3$ local cases are shown in Fig. 5.3. We observe that the complexities for different timesteps with respect to the reference state behave in an uncorrelated, fluctuating way. However, it is worth noting that the fluctuating values decrease as we increase the notion of locality in the picture. In an explicit way, this basically means assigning fewer penalty factors to more and more generators of the SU(4) group. From a gate perspective, this can be understood as more and more quantum gates becoming easily available as we increase the locality.

5.3.2.2 Step-wise complexity

Another way is to consider the evolution in step-wise manner. More explicitly, the target state $|\psi(t_n)\rangle$ is obtained from the initial reference state $|\psi(t_0)\rangle$ as $|\psi(t_0)\rangle \to |\psi(t_1)\rangle \to \cdots \to |\psi(t_n)\rangle$ in step-wise manner such that

$$U(t_i)|\psi(t_i)\rangle = |\psi_{i+1}\rangle\,.$$

This is more significant from point of quantum circuit picture where the final state is obtained from set of unitary gates.

Therefore, the corresponding total complexity is the sum of individual complexities for each step. The step-wise complexity is shown in Fig. 5.3 which grows linearly as the number of steps. The growth persists forever, which is meaningful from a circuit construction point of view. This circuit successfully simulates all the states along the quantum walk at different steps. Here also, we find that the slope of the curves decreases as we increase the locality. It, therefore, seems to be universally true that as we make more and more generators (or equivalently quantum gates from a circuit perspective), it takes fewer number of gates to construct the optimized circuit.

From computational point of view, it is important to note that if $|\psi_i\rangle = U_i|\psi(t_0)\rangle$ and $|\psi(t_{i+1})\rangle = U_{i+1}|\psi(t_0)\rangle$, then, the $|\psi(t_{i+1})\rangle = U_{i+1}U_i^\dagger|\psi(t_i)\rangle$.

In FIG. 5.4, we plot the slope of the stepwise complexity plots for different locality notions with varying coin angles. Whereas the slope values increase with decreasing locality, which is expected from plots in FIG. 5.3 already, we notice that there is a dip in the slope for each of the cases around coin angle value $2\pi/3$. These plots, therefore, indicate that among different coin angles, the complexity is least for the coin with angle $\theta \approx 2\pi/3$.

As we pointed out in §5.2.2, the obtained target unitary operators are not unique, therefore, it is important to take sample average such that the complexity is well converged. In FIG. 5.5, we showed the standard deviation of the complexity for the time-step t_{100} as a function of number of samples. The standard deviation converges to unique value for large number of samples which ensures the convergence of the complexity.

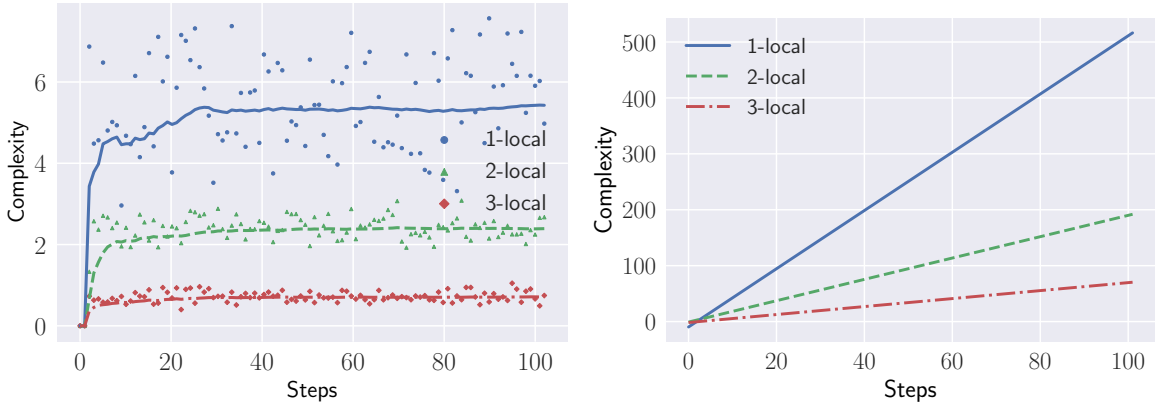

FIGURE 5.3: "Direct" complexity as function of unitary operator $U_{\text{target}}(t)$ for $\theta = \pi/4$ for $k = 1, 2, 3$ local operators. The scattered colored points are the actual values derived, whereas the dotted colored lines denote the stepwise averaged values.

5.3.3 Fermionic Hamiltonian in continuum limit

Before concluding the section, we would like to point out that diagonalization of the two-particle fermionic Hamiltonian in EQ. (5.22), leads to the following construction,

$$V(s) = v_5 T_5 + v_{10} T_{10} + v_{15} T_{15} = -iH_2(p_1, p_2)t \tag{5.51}$$

which solves for $v_5 = 0$ and

$$\begin{aligned} v_{10} &= -\frac{t}{2}\left(\sqrt{m^2 + p_1^2 + p_2^2 - \sqrt{\left(m^2 + 2p_1^2\right)\left(m^2 + 2p_2^2\right)}} + \sqrt{m^2 + p_1^2 + p_2^2 + \sqrt{\left(m^2 + 2p_1^2\right)\left(m^2 + 2p_2^2\right)}}\right) \\ v_{15} &= \frac{t}{2}\left(\sqrt{m^2 + p_1^2 + p_2^2 - \sqrt{\left(m^2 + 2p_1^2\right)\left(m^2 + 2p_2^2\right)}} - \sqrt{m^2 + p_1^2 + p_2^2 + \sqrt{\left(m^2 + 2p_1^2\right)\left(m^2 + 2p_2^2\right)}}\right) \end{aligned} \tag{5.52}$$

for $m = \sin\theta$. Consequently,

$$C = \int^{\Lambda_1}\int^{\Lambda_2} dp_1 dp_2 \sqrt{v_{10}^2 + v_{15}^2} \simeq \frac{5}{24}\, t\, \Lambda^3 \log\Lambda \tag{5.53}$$

This complexity grows linearly with time. However, this complexity does not indicate the quantum walk completely but only an approximation in the continuum limit. Hence the complexity does not demonstrate the nuances of the walk completely.

5.4 Quantum circuit

In this section, we connect the linear growth of cumulative step-wise complexity found in §5.3.2.2 to constant circuit depth of explicit quantum circuit associated with target unitary. The target unitary operator can be associated with a 2-qubit circuit, as shown in FIG. 5.6. To find the circuit depth of a quantum circuit, one

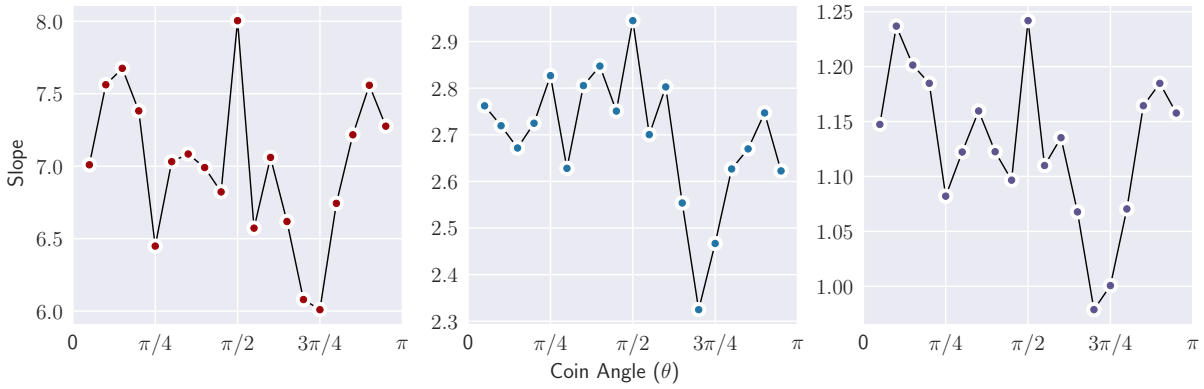

FIGURE 5.4: Slope of linear complexity with varying coin angle θ with **Left** : 1-local operators, **Middle** : 2-local operators and **Right** : 3-local operators.

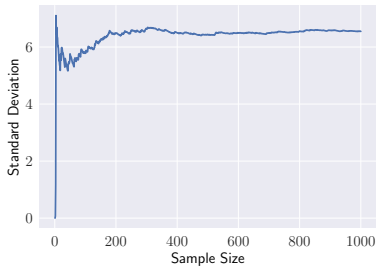

FIGURE 5.5: Standard deviation of the circuit complexity with an increasing sample size of target unitary operators calculated for the 10th step of DTQW.

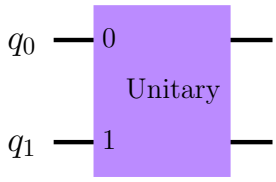

FIGURE 5.6: A general 2-qubit quantum circuit for the step-wise unitary operator.

is required to decompose the unitary into a universal set of gates. For our purpose, we will consider a 1-qubit gate $U_3(\theta, \phi, \lambda)$ and 2-qubit CNOT gate with the explicit forms as following

$$U_3(\theta, \phi, \lambda) = \begin{bmatrix} \cos\theta & e^{i\phi}\sin\theta \\ -e^{-i\phi}\sin\theta & e^{-i(\phi+\lambda)}\cos\theta \end{bmatrix} \tag{5.54}$$

and

$$\text{CNOT} = \begin{bmatrix} 1 & 0 & 0 & 0 \\ 0 & 0 & 0 & 1 \\ 0 & 0 & 1 & 0 \\ 0 & 1 & 0 & 0 \end{bmatrix}. \tag{5.55}$$

In FIG. 5.7, we showed the explicit circuit associated with the target unitary for a particular walk step constructed using Qiskit [144]. The circuit associated with the target unitary for different walk steps has a contact depth of 7 layers with parameters θ, ϕ, and λ changing values. Therefore, similar to the direct complexity study using Nielsen's proposal, the cost of constructing the unitary seems almost a constant function. Therefore, if we again construct the circuit stepwise and cumulatively sum the depth of the individual circuits, the depth grows linearly again with the steps (see FIG. 5.8), in agreement with the complexity computed from Nielsen's proposal.

It's important to emphasize that relation between k-local case in context of Nielsen's complexity (NC) and k-qubit gate in context of quantum circuit is not very well understood. If we naively consider that both are equivalent to each other, then $k = 1$ should correspond to single qubit quantum circuits for target unitary. However, since the universal set of quantum gates atleast requires a two-qubit gate [145] as known from the Solovay-Kitaev theorem, one can not construct a general n-qubit quantum circuit ($n > 1$) with just single qubit gates (unless target unitary is separable into n independent single qubit gates which is not true generally or in our case). The case $k = 3$ on the other hand can be realised for n qubit quantum circuits with

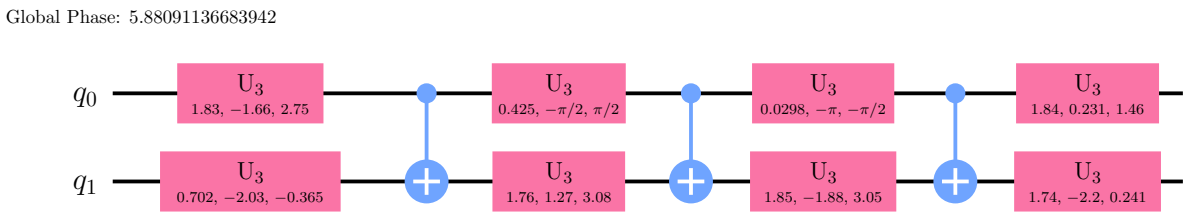

FIGURE 5.7: Representing a 2-qubit quantum circuit for the step wise unitary operator using QISKIT.

$n \geq 3$. However, in our case, we have a two-qubit target unitary, which can not be written in terms of three qubit quantum gates. These facts as mentioned above suggest that k-local operators should not in general be understood as k-qubit gates, and their exact relation needs further investigation. However, for the two-qubit circuit, our result indeed shows a qualitative similarity between the two concepts. It will be interesting to extend these studies to higher qubit circuits, where one can explicitly check if such similarities exist for $k \geq 3$.

5.5 Discussions

We conclude the chapter with a brief account of what has been answered and what more remains to be done. To begin with:

- We have computed the complexity for the one-dimensional quantum walk using a SU(2) coin. The walk entangles the position and internal degrees of freedom and produces a mixed state on partial tracing over the position degrees of freedom. Consequently to measure the complexity of the mixed state, we first canonically purify the mixed state and then evaluate the complexity using an approximate 2-qubit quantum circuit.
- We compute and compare the complexities of the purified state using both the direct evolution operator and the step-wise evolution in the quantum walk. The complexity function oscillates with the steps around a mean value which can be associated with the depth of an average quantum circuit. The step-wise evolution, however, connects more with the actual quantum circuit and the quantum walk picture since the direct evolution ignores the steps in connecting the geodesic from the initial to the final step. As such, the step-wise evolution is a direct implementation of time-ordering and a successful simulation of the DTQW using a quantum circuit. The complexity of the step-wise evolution cumulatively grows with the steps and is indicative of the growing size of an associated quantum circuit and its complexity.
- To give some context, we also implement a schematic quantum circuit using 1 and 2 qubit quantum gates to implement the step-wise unitary evolution. The circuit has constant depth and relates to the average complexity in FIG. 5.3.

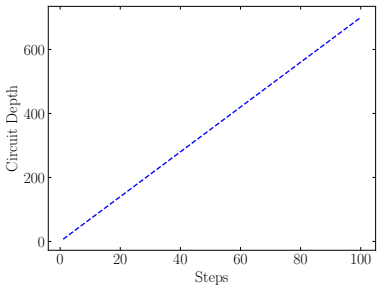

FIGURE 5.8: Quantum circuit depth corresponding to target unitary operator corresponding to two-local case (estimated with explicit construction of quantum circuit using QISKIT) with varying timesteps of DTQW.

- Another upshot of doing the stepwise evolution is that although we have stepwise geodesics instead of a full one, it can produce for us the stepwise response functions which are valid for individual timesteps. Let us say if we want to write the Hamiltonian acting between steps (t_{n-1}) and t_n, we can simply pick the corresponding step-wise unitary $U_n(t_n)$ and get an estimate of the Hamiltonian as

$$H(n) = -\frac{1}{i}\log[U(t_n)] \tag{5.56}$$

since each timestep is of length 1. Now we can write this Hamiltonian as

$$H(n) = \sum_i V_i(n)T_i \tag{5.57}$$

to figure out which generator was effective and how much during a particular time step. Finally, we can sum all those step-wise Hamiltonians with the corresponding step functions and write down a complete Hamiltonian that is time-independent step-wise but gives rise to all the purified states corresponding to the mixed one of the actual DTQW. This is somewhat analogous to finding out the response functions for different quantum gates in the Nielsen picture of complexity. This is a trivial task and the states being individually randomly distributed, these functions do not show up any particular nature of growth or decay. However, it might produce further interesting results in the case of an explicitly chaotic quantum walk [146] or for a time-dependent coin operator [136].

However, more questions have been uncovered by the exploration. Some of the pressing questions, which we could not answer in this work due to lack of resources, but intend to complete them in immediate future follow-up works are:

- First of all, the precise connection between the circuit picture and the continuum formulation is still largely opaque. We have just implemented an example circuit that can connect with the step-wise evolution. However, the exact nature of how the geodesic length is connected with the actual quantum circuit still remains to be explored further.

- The distinction between the step-wise evolution and the unitary evolution is based on the logic that one can view the step-wise evolution with some quantum circuits and hence the size of the circuit grows along with its complexity which exhibits itself in the linear growth. However, for real quantum systems, the complexity grows linearly with time for early time and smooths out to a constant. One reason for the discrepancy might be the fact that the dimension of the Hilbert space of the state in quantum walk linearly grows with time. In order to gain insights into this apparent conflict, one way to move forward would be to connect the quantum walk to the Hamiltonian of some physical system, to get a more realizable connection with real-time systems. Consequently designing quantum circuits for the quantum walk will act as

a bridge to gain more insights into the mapping of field theory complexity with the actual circuit compiling complexity.

Outlook 6

This thesis describes the wide range of ideas in quantum computing that are all linked together with the quantum-walks. Therefore, this thesis among others is one evidence of wide applicability of quantum-walks. Here, I'll briefly summarize the work and make comments on further possibility that remains to take care in the future.

On Chapter 3 Very few who have seen a quantum computer or let alone have one could tell that *at present, they are good for nothing.* But this should not deter us from seeing the fact that we have made a large progress from where we begin. The quantum computers does have shown a so called "quantum advantage" for few artificial problem, but it's important to ask if what practical we can do from what we currently have. Toward this direction, Quantum simulation holds a great promise – such as simulating different phase of matter. It is, therefore, becomes important to investigate efficient ways of quantum simulation. In this chapter, we propose a qubit efficient scheme to simulate discrete-time quantum walk based protocols. We explicit seen the implementation of the scheme for the problem of neutrino oscillations.

The simulation scheme exploits the interaction between the system and the environment. This interaction is chosen to be of particular form, therefore, is bit artificial at this point. Therefore, a possible way to probe such a interaction becomes viable goal for the future. In the context of neutrino oscillation, there are several direction could be explored. Among other is to incorporate the decoherence effects induced by new physics (e.g., quantum gravity, string theory) in neutrino oscillations in the scheme. It can be done by equipping new interaction between the system and the environment. Other direction which becomes important from computa-

A prominent example is related to high-temperature superconductivity: one of the important questions in this context is, which basic interaction between the electrons is responsible for the superconducting behaviour? In other words, which minimal Hamiltonian describes the phenomenon of high-temperature superconductivity? To answer this question, a quantum simulator could check the various candidate Hamiltonians for relevant phases. A quantum simulator may not only become a precious tool for tackling some specific problems in those fields, but should also prove a powerful instrument for developing, testing and benchmarking theoretical methods.

tion point of view is to consider collective neutrino oscillations – in which neutrino interact with one another.

On Chapter 4 A quantum computer can outperform the classical computer by running quantum algorithms. Despite the fact that the full-functional quantum computer are not yet developed, quantum algorithms became a popular avenue to explore the possibilities of what we can achieve with quantum computers. Search algorithm is for finding a data point from a unstructured data-base. One of the early work is that of Grover on data-base search in which a significant speed-up can be achieved compared to proposed classical algorithms. Since, then, several extension to this algorithm has been proposed to search for multiple data-points or set of points. These algorithms fall sort in several ways : 1) They do not provide a homogeneous amplification to marked points. 2) They neglect any inherent ordering (or category) in marked points.

In our work, we proposed a extension to of Grover's search algorithm for multiple marked data-points that overcome these problems. The underlying idea of the algorithm is to introduce extra dimension to data structure which is same as adding extra qubits. These qubits are then used to encode any additional information. The scheme can also be used to search of dynamical marked points (that can change position on their position on data-base). The work is complement by giving an explicit construction of quantum circuit for the algorithm and its complexity analysis. A possible extension of this work is to implement the idea for generic graph structures (as our analysis talks only about the two-dimensional lattices).

On Chapter 5 Finding a efficient quantum circuits that can perform unitary operation remain a challenging task. In this regard, the concept of circuit complexity is mathematically accessible way to talk about the complexity of the operation – which opens up the door to suggest new quantum algorithm or to prove limitations on the power of quantum computers. Although, the circuit complexity meant to describe the number of gates require to implement a unitary operation, it is still not very well understood the exact relation between these two quantities.

In this work, we tried to shed light on the relationship between the circuit complexity and circuit depth. To do this, we performed the two computations for a two-qubit system obtained from purification of reduced coin-space. Our results shows that the two quantities obey the same linear scaling. However, it is still unknown how does these two quantities can be put on the same ground which we aim to resolve in future.

Flip-Flop Shift Operator

In this appendix, we demonstrate the unitarity of flip-flop shift operator.

Open-boundary condition The flip-flop shift operator for open boundary condition is given by sum of interior term

To unclutter the notation, we will assume that the position labels x, y runs from $1, 2, \ldots N$. Furthermore, we define set of points $\phi_1 = \{1, 2, \ldots N-1\}$ and $\phi_2 = \{2, 3, \ldots, N\}$.

$$\begin{aligned} S_{\text{int}} &= |\downarrow\rangle\langle\uparrow| \otimes \sum_x \sum_{y\in\phi_1} |x, y+1\rangle\langle x, y| + |\uparrow\rangle\langle\downarrow| \otimes \sum_x \sum_{y\in\phi_2} |x, y-1\rangle\langle x, y| + |\leftarrow\rangle\langle\rightarrow| \otimes \sum_{x\in\phi_1} \sum_y |x+1, y\rangle\langle x, y| \\ &\quad + |\rightarrow\rangle\langle\leftarrow| \otimes \sum_{x\in\phi_2} \sum_y |x-1, y\rangle\langle x, y| \\ &= |\downarrow\rangle\langle\uparrow| \otimes I \otimes \sum_{y\in\phi_1} |y+1\rangle\langle y| + |\uparrow\rangle\langle\downarrow| \otimes I \otimes \sum_{y\in\phi_2} |y-1\rangle\langle y| + |\leftarrow\rangle\langle\rightarrow| \otimes \sum_{x\in\phi_1} |x+1\rangle\langle x| \otimes I \\ &\quad + |\rightarrow\rangle\langle\leftarrow| \otimes \sum_{x\in\phi_2} |x-1\rangle\langle x| \otimes I \end{aligned} \tag{1}$$

and boundary (exterior) term

$$\begin{aligned} S_{\text{ext}} = |\uparrow\rangle\langle\uparrow| \otimes I \otimes |N\rangle\langle N| + |\downarrow\rangle\langle\downarrow| \otimes I \otimes |1\rangle\langle 1| \\ + |\rightarrow\rangle\langle\rightarrow| \otimes |N\rangle\langle N| \otimes I + |\leftarrow\rangle\langle\leftarrow| \otimes |1\rangle\langle 1| \otimes I \end{aligned} \tag{2}$$

as $S_{\text{o}} = S_{\text{int}} + S_{\text{ext}}$. The form of S_{int} and S_{ext} is chosen so that the shift operator S_{o} is unitary i.e. $S_{\text{o}}(S_{\text{o}})^\dagger = (S_{\text{o}})^\dagger S_{\text{o}} = I$. To verify this, consider

$$\begin{aligned} S_{\text{o}}(S_{\text{o}})^\dagger &= (S_{\text{int}} + S_{\text{ext}})(S_{\text{int}}^\dagger + S_{\text{ext}}^\dagger) \\ &= S_{\text{int}}S_{\text{int}}^\dagger + S_{\text{int}}S_{\text{ext}}^\dagger + S_{\text{ext}}S_{\text{int}}^\dagger + S_{\text{ext}}S_{\text{ext}}^\dagger \\ &= S_{\text{int}}S_{\text{int}}^\dagger + S_{\text{ext}}S_{\text{ext}}^\dagger \end{aligned}$$

where we used $S_{\text{int}}S_{\text{ext}}^{\dagger} = 0 = S_{\text{ext}}S_{\text{int}}^{\dagger}$ — follows from the orthonormality of the position basis. The two terms can easily be found using the explicit form of S_{int} and S_{ext}.

$$\begin{aligned}
S_{\text{int}}S_{\text{int}}^{\dagger} &= |{\downarrow}\rangle\langle{\downarrow}| \otimes I \otimes \sum_{y\in\phi_1} |y\rangle\langle y| + |{\uparrow}\rangle\langle{\uparrow}| \otimes I \otimes \sum_{y=1}^{N-1} |y\rangle\langle y| \\
&\quad + |{\leftarrow}\rangle\langle{\leftarrow}| \otimes \sum_{x\in\phi_1} |x\rangle\langle x| \otimes I + |{\rightarrow}\rangle\langle{\rightarrow}| \otimes \sum_{x=1}^{N-1} |x\rangle\langle x| \otimes I \\
S_{\text{ext}}S_{\text{ext}}^{\dagger} &= |{\uparrow}\rangle\langle{\uparrow}| \otimes I \otimes |N\rangle\langle N| + |{\downarrow}\rangle\langle{\downarrow}| \otimes I \otimes |1\rangle\langle 1| \\
&\quad + |{\rightarrow}\rangle\langle{\rightarrow}| \otimes |N\rangle\langle N| \otimes I + |{\leftarrow}\rangle\langle{\leftarrow}| \otimes |1\rangle\langle 1| \otimes I
\end{aligned}$$

Adding the two terms together, we get $S_{\text{int}}S_{\text{int}}^{\dagger} + S_{\text{ext}}S_{\text{ext}}^{\dagger} = S_{\text{o}}(S_{\text{o}})^{\dagger} = I$. As required. Note that this unitarity breaks if we consider the exterior term to be

$$\begin{aligned}
S_{\text{ext}} &= |{\downarrow}\rangle\langle{\uparrow}| \otimes I \otimes |N\rangle\langle N| + |{\uparrow}\rangle\langle{\downarrow}| \otimes I \otimes |1\rangle\langle 1| \\
&\quad + |{\leftarrow}\rangle\langle{\rightarrow}| \otimes |N\rangle\langle N| \otimes I + |{\rightarrow}\rangle\langle{\leftarrow}| \otimes |1\rangle\langle 1| \otimes I
\end{aligned}$$

which gives

$$\begin{aligned}
S_{\text{ext}}S_{\text{ext}}^{\dagger} &= |{\downarrow}\rangle\langle{\downarrow}| \otimes I \otimes |N\rangle\langle N| + |{\uparrow}\rangle\langle{\uparrow}| \otimes I \otimes |1\rangle\langle 1| \\
&\quad + |{\leftarrow}\rangle\langle{\leftarrow}| \otimes |N\rangle\langle N| \otimes I + |{\rightarrow}\rangle\langle{\rightarrow}| \otimes |1\rangle\langle 1| \otimes I\,.
\end{aligned}$$

From which, it is easier to note that $S_{\text{int}}S_{\text{int}}^{\dagger} + S_{\text{ext}}S_{\text{ext}}^{\dagger} = S_{\text{o}}(S_{\text{o}})^{\dagger} \neq I$.

Details of generators

We provide the explicit form of the fermionic generators γ_a here. There are

$$\begin{aligned}
\gamma_1 &= \sigma_1 \otimes I_2 = \begin{bmatrix} 0 & 0 & 1 & 0 \\ 0 & 0 & 0 & 1 \\ 1 & 0 & 0 & 0 \\ 0 & 1 & 0 & 0 \end{bmatrix} \\
\gamma_2 &= \sigma_2 \otimes I_2 = \begin{bmatrix} 0 & 0 & -i & 0 \\ 0 & 0 & 0 & -i \\ i & 0 & 0 & 0 \\ 0 & i & 0 & 0 \end{bmatrix} \\
\gamma_3 &= \sigma_3 \otimes \sigma_1 = \begin{bmatrix} 0 & 1 & 0 & 0 \\ 1 & 0 & 0 & 0 \\ 0 & 0 & 0 & -1 \\ 0 & 0 & -1 & 0 \end{bmatrix} \\
\gamma_4 &= \sigma_3 \otimes \sigma_2 = \begin{bmatrix} 0 & -i & 0 & 0 \\ i & 0 & 0 & 0 \\ 0 & 0 & 0 & i \\ 0 & 0 & -i & 0 \end{bmatrix} .
\end{aligned} \tag{3}$$

The γ_a satisfy,

$$\{\gamma_a, \gamma_b\} = 2\eta_{ab} \, . \tag{4}$$

The explicit forms of the generators T_i for the $SU(4)$ group are then given by,

$$\begin{aligned}
T_i = \{&\gamma_1, \gamma_2, \gamma_3, \gamma_4, i\gamma_1\gamma_2, i\gamma_1\gamma_3, i\gamma_1\gamma_4, i\gamma_2\gamma_3, i\gamma_2\gamma_4, i\gamma_3\gamma_4, \\
&-i\gamma_1\gamma_2\gamma_3, -i\gamma_1\gamma_2\gamma_4, -i\gamma_1\gamma_3\gamma_4, -i\gamma_2\gamma_3\gamma_4, -\gamma_1\gamma_2\gamma_3\gamma_4\}
\end{aligned} \tag{5}$$

Bibliography

[1] Wikipedia contributors (2024), URL https://en.wikipedia.org/wiki/Random_walk.

[2] I. M. Georgescu, S. Ashhab, and F. Nori, Rev. Mod. Phys. **86**, 153 (2014), URL https://link.aps.org/doi/10.1103/RevModPhys.86.153.

[3] A. Browaeys and T. Lahaye, Nature Physics **16**, 132 (2020), URL https://www.nature.com/articles/s41567-019-0733-z.

[4] M. J. Hartmann, Journal of Optics **18**, 104005 (2016), ISSN 2040-8986, URL https://dx.doi.org/10.1088/2040-8978/18/10/104005.

[5] A. A. Houck, H. E. Türeci, and J. Koch, Nature Physics **8**, 292 (2012), ISSN 1745-2481, URL https://www.nature.com/articles/nphys2251.

[6] M. Greiner, O. Mandel, T. Esslinger, T. W. Hänsch, et al., Nature **415**, 39 (2002), ISSN 1476-4687, URL https://www.nature.com/articles/415039a.

[7] R. Blatt and C. F. Roos, Nature Physics **8**, 277 (2012), ISSN 1745-2481, URL https://www.nature.com/articles/nphys2252.

[8] C. Monroe, W. Campbell, L.-M. Duan, Z.-X. Gong, et al., Reviews of Modern Physics **93**, 025001 (2021), URL https://link.aps.org/doi/10.1103/RevModPhys.93.025001.

[9] A. Aspuru-Guzik and P. Walther, Nature Physics **8**, 285 (2012), ISSN 1745-2481, URL https://www.nature.com/articles/nphys2253.

[10] C. Gross and I. Bloch, Science **357**, 995 (2017), URL https://www.science.org/doi/10.1126/science.aal3837.

[11] A. G. White, Conference on Lasers and Electro-Optics (2016), URL https://opg.optica.org/abstract.cfm?URI=CLEO_QELS-2016-FTh4C.1.

[12] J. I. Cirac and P. Zoller, Nature Physics **8**, 264 (2012), ISSN 1745-2481, URL https://www.nature.com/articles/nphys2275.

[13] A. J. Daley, I. Bloch, C. Kokail, S. Flannigan, N. Pearson, et al., Nature **607**, 667 (2022), ISSN 1476-4687, URL https://www.nature.com/articles/s41586-022-04940-6.

[14] F. Verstraete, D. Porras, and J. I. Cirac, Physical Review Letters **93**, 227205 (2004), URL https://link.aps.org/doi/10.1103/PhysRevLett.93.227205.

[15] R. F. Nalewajski, Applied Sciences **9**, 1262 (2019), ISSN 2076-3417, URL https://www.mdpi.com/2076-3417/9/6/1262.

[16] M. R. Wasielewski, M. D. E. Forbes, N. L. Frank, K. Kowalski, et al., Nature Reviews Chemistry **4**, 490 (2020), ISSN 2397-3358, URL https://www.nature.com/articles/s41570-020-0200-5.

[17] R. J. Lewis-Swan, A. Safavi-Naini, A. M. Kaufman, and A. M. Rey, Nature Reviews Physics **1**, 627 (2019), ISSN 2522-5820, URL https://www.nature.com/articles/s42254-019-0090-y.

[18] R. Augusiak, F. M. Cucchietti, and M. Lewenstein, *Many body physics from a quantum information perspective* (2012), URL http://arxiv.org/abs/1003.3153.

[19] J. Goold, M. Huber, A. Riera, L. d. Rio, and P. Skrzypczyk, Journal of Physics A: Mathematical and Theoretical **49**, 143001 (2016), ISSN 1751-8121, URL https://dx.doi.org/10.1088/1751-8113/49/14/143001.

[20] S. Lloyd, Science **319**, 1209 (2008), URL https://www.science.org/doi/full/10.1126/science.1154732.

[21] S. E. Venegas-Andraca, Quantum Information Processing **11**, 1015 (2012), ISSN 1573-1332, URL https://doi.org/10.1007/s11128-012-0432-5.

[22] A. Ambainis, E. Bach, A. Nayak, A. Vishwanath, et al., Association for Computing Machinery p. 37–49 (2001), URL https://doi.org/10.1145/380752.380757.

[23] D. Aharonov, A. Ambainis, J. Kempe, and U. Vazirani, Association for Computing Machinery p. 50–59 (2001), URL https://doi.org/10.1145/380752.380758.

[24] S. Venegas-Andraca, International Journal of Quantum Information **2**, 365 (2004), URL https://doi.org/10.1142/S0219749903000383.

[25] T. Oka, N. Konno, R. Arita, and H. Aoki, Physical Review Letters **94**, 100602 (2005), URL https://link.aps.org/doi/10.1103/PhysRevLett.94.100602.

[26] G. S. Engel, T. R. Calhoun, E. L. Read, T.-K. Ahn, et al., Nature **446**, 782 (2007), ISSN 1476-4687, URL https://www.nature.com/articles/nature05678.

[27] M. Mohseni, P. Rebentrost, S. Lloyd, and A. Aspuru-Guzik, The Journal of Chemical Physics **129**, 174106 (2008), ISSN 0021-9606, URL https://aip.scitation.org/doi/10.1063/1.3002335.

[28] C. M. Chandrashekar and R. Laflamme, Phys. Rev. A **78**, 022314 (2008), URL https://link.aps.org/doi/10.1103/PhysRevA.78.022314.

[29] C. M. Chandrashekar, Physical Review A **83**, 022320 (2011), URL https://link.aps.org/doi/10.1103/PhysRevA.83.022320.

[30] T. Kitagawa, M. S. Rudner, E. Berg, and E. Demler, Physical Review A **82**, 033429 (2010), URL https://link.aps.org/doi/10.1103/PhysRevA.82.033429.

[31] N. Shenvi, J. Kempe, and K. B. Whaley, Physical Review A **67**, 052307 (2003), URL https://link.aps.org/doi/10.1103/PhysRevA.67.052307.

[32] A. M. Childs, R. Cleve, E. Deotto, E. Farhi, et al., Proceedings of the thirty-fifth annual ACM symposium on Theory of computing pp. 59–68 (2003), URL https://doi.org/10.1145/780542.780552.

[33] A. Ambainis, J. Kempe, and A. Rivosh, in *Proceedings of the Sixteenth Annual ACM-SIAM Symposium on Discrete Algorithms* (Society for Industrial and Applied Mathematics, USA, 2005), SODA '05, p. 1099–1108, ISBN 0898715857.

[34] C. M. Chandrashekar, *Discrete-Time Quantum Walk - Dynamics and Applications* (2010), arXiv:1001.5326 [quant-ph], URL http://arxiv.org/abs/1001.5326.

[35] O. Mülken and A. Blumen, Physics Reports **502**, 37 (2011), ISSN 0370-1573, URL https://www.sciencedirect.com/science/article/pii/S0370157311000184.

[36] C. M. Chandrashekar, Scientific Reports **3**, 2829 (2013), ISSN 2045-2322, URL https://www.nature.com/articles/srep02829.

[37] D. Xie, T.-S. Deng, T. Xiao, W. Gou, T. Chen, W. Yi, and B. Yan, Phys. Rev. Lett. **124**, 050502 (2020), URL https://link.aps.org/doi/10.1103/PhysRevLett.124.050502.

[38] J. Wu, W.-W. Zhang, and B. C. Sanders, Frontiers of Physics **14**, 61301 (2019), ISSN 2095-0470, URL https://doi.org/10.1007/s11467-019-0918-z.

[39] C. Huerta Alderete, S. Singh, N. H. Nguyen, et al., Nature Communications **11**, 3720 (2020), ISSN 2041-1723, URL https://www.nature.com/articles/s41467-020-17519-4.

[40] K. Manouchehri and J. Wang, *Physical Implementation of Quantum Walks* (Springer, Berlin, Heidelberg, 2014), ISBN 978-3-642-36013-8 978-3-642-36014-5, URL https://link.springer.com/10.1007/978-3-642-36014-5.

[41] J. Du, H. Li, X. Xu, M. Shi, J. Wu, X. Zhou, and R. Han, Phys. Rev. A **67**, 042316 (2003), URL https://link.aps.org/doi/10.1103/PhysRevA.67.042316.

[42] C. A. Ryan, M. Laforest, J. C. Boileau, and R. Laflamme, Phys. Rev. A **72**, 062317 (2005), URL https://link.aps.org/doi/10.1103/PhysRevA.72.062317.

[43] H. Schmitz, R. Matjeschk, C. Schneider, J. Glueckert, M. Enderlein, T. Huber, and T. Schaetz, Phys. Rev. Lett. **103**, 090504 (2009), URL https://link.aps.org/doi/10.1103/PhysRevLett.103.090504.

[44] F. Zähringer, G. Kirchmair, R. Gerritsma, E. Solano, R. Blatt, and C. F. Roos, Phys. Rev. Lett. **104**, 100503 (2010), URL https://link.aps.org/doi/10.1103/PhysRevLett.104.100503.

[45] M. Genske, W. Alt, A. Steffen, A. H. Werner, R. F. Werner, D. Meschede, and A. Alberti, Phys. Rev. Lett. **110**, 190601 (2013), URL https://link.aps.org/doi/10.1103/PhysRevLett.110.190601.

[46] D. Bouwmeester, I. Marzoli, G. P. Karman, W. Schleich, and J. P. Woerdman, Phys. Rev. A **61**, 013410 (1999), URL https://link.aps.org/doi/10.1103/PhysRevA.61.013410.

[47] T. Kitagawa, M. A. Broome, A. Fedrizzi, M. S. Rudner, E. Berg, I. Kassal, A. Aspuru-Guzik, E. Demler, and A. G. White, Nature Communications **3**, 882 (2012), ISSN 2041-1723, URL https://doi.org/10.1038/ncomms1872.

[48] P. Xue, R. Zhang, H. Qin, X. Zhan, Z. H. Bian, J. Li, and B. C. Sanders, Phys. Rev. Lett. **114**, 140502 (2015), URL https://link.aps.org/doi/10.1103/PhysRevLett.114.140502.

[49] H. B. Perets, Y. Lahini, F. Pozzi, M. Sorel, R. Morandotti, and Y. Silberberg, Phys. Rev. Lett. **100**, 170506 (2008), URL https://link.aps.org/doi/10.1103/PhysRevLett.100.170506.

[50] Y. Bromberg, Y. Lahini, R. Morandotti, and Y. Silberberg, Phys. Rev. Lett. **102**, 253904 (2009), URL https://link.aps.org/doi/10.1103/PhysRevLett.102.253904.

[51] L. Sansoni, F. Sciarrino, G. Vallone, P. Mataloni, A. Crespi, R. Ramponi, and R. Osellame, Phys. Rev. Lett. **108**, 010502 (2012), URL https://link.aps.org/doi/10.1103/PhysRevLett.108.010502.

[52] A. Mallick and C. M. Chandrashekar, Scientific Reports **6**, 25779 (2016), ISSN 2045-2322, URL https://www.nature.com/articles/srep25779.

[53] A. Mallick, S. Mandal, A. Karan, and C. M. Chandrashekar, Journal of Physics Communications **3**, 015012 (2019), ISSN 2399-6528, URL https://dx.doi.org/10.1088/2399-6528/aafe2f.

[54] F. W. Strauch, Phys. Rev. A **73**, 054302 (2006), URL https://link.aps.org/doi/10.1103/PhysRevA.73.054302.

[55] R. Gerritsma, G. Kirchmair, F. Zähringer, E. Solano, R. Blatt, and C. F. Roos, Nature **463**, 68 (2010), ISSN 1476-4687, URL https://doi.org/10.1038/nature08688.

[56] C. Qu, C. Hamner, M. Gong, C. Zhang, and P. Engels, Physical Review A **88**, 021604 (2013), URL https://link.aps.org/doi/10.1103/PhysRevA.88.021604.

[57] S. Lovett, P. M. Walker, A. Osipov, A. Yulin, P. U. Naik, C. E. Whittaker, I. A. Shelykh, M. S. Skolnick, and D. N. Krizhanovskii, *Observation of Zitterbewegung in photonic microcavities* (2023), arXiv:2211.09907 [cond-mat, physics:physics], URL http://arxiv.org/abs/2211.09907.

[58] T. Liu, M. Feng, W. Yang, L. Chen, F. Zhou, and K. Wang, Science China Physics, Mechanics & Astronomy **57**, 1250 (2014), ISSN 1869-1927, URL https://doi.org/10.1007/s11433-014-5458-5.

[59] T. A. Brun and L. Mlodinow, Physical Review A **102**, 062222 (2020), URL https://link.aps.org/doi/10.1103/PhysRevA.102.062222.

[60] P. Arrighi, S. Facchini, and M. Forets, Quantum Information Processing **15**, 3467 (2016), ISSN 1573-1332, URL https://doi.org/10.1007/s11128-016-1335-7.

[61] P. Arnault, G. Di Molfetta, M. Brachet, and F. Debbasch, Physical Review A **94**, 012335 (2016), URL https://link.aps.org/doi/10.1103/PhysRevA.94.012335.

[62] P. Arnault, A. Pérez, P. Arrighi, and T. Farrelly, Physical Review A **99**, 032110 (2019), URL https://link.aps.org/doi/10.1103/PhysRevA.99.032110.

[63] B. Hall, A. Roggero, A. Baroni, and J. Carlson, Phys. Rev. D **104**, 063009 (2021), URL https://link.aps.org/doi/10.1103/PhysRevD.104.063009.

[64] T. Kitagawa, M. S. Rudner, E. Berg, and E. Demler, Phys. Rev. A **82**, 033429 (2010), URL https://link.aps.org/doi/10.1103/PhysRevA.82.033429.

[65] S. Barkhofen, L. Lorz, T. Nitsche, C. Silberhorn, and H. Schomerus, Phys. Rev. Lett. **121**, 260501 (2018), URL https://link.aps.org/doi/10.1103/PhysRevLett.121.260501.

[66] T. Nitsche, S. Barkhofen, R. Kruse, L. Sansoni, M. Štefaňák, A. Gábris, V. Potoček, T. Kiss, I. Jex, and C. Silberhorn, Science Advances **4** (2018), URL https://www.science.org/doi/abs/10.1126/sciadv.aar6444.

[67] F. Elster, S. Barkhofen, T. Nitsche, J. Novotný, A. Gábris, I. Jex, and C. Silberhorn, Scientific Reports **5**, 13495 (2015), ISSN 2045-2322, URL https://doi.org/10.1038/srep13495.

[68] J. Lesgourgues and S. Pastor, New Journal of Physics **16**, 065002 (2014), ISSN 1367-2630, URL https://dx.doi.org/10.1088/1367-2630/16/6/065002.

[69] X. Qian and J.-C. Peng, Reports on Progress in Physics **82**, 036201 (2019), ISSN 0034-4885, URL https://dx.doi.org/10.1088/1361-6633/aae881.

[70] A. C. Hayes and P. Vogel, Annual Review of Nuclear and Particle Science **66**, 219 (2016), URL https://doi.org/10.1146/annurev-nucl-102115-044826.

[71] H. Duan, G. M. Fuller, and Y.-Z. Qian, Annual Review of Nuclear and Particle Science **60**, 569 (2010), URL https://doi.org/10.1146/annurev.nucl.012809.104524.

[72] A. Mirizzi, I. Tamborra, H.-T. Janka, N. Saviano, K. Scholberg, R. Bollig, L. Hüdepohl, and S. Chakraborty, La Rivista del Nuovo Cimento **39**, 1 (2016), ISSN 1826-9850, URL https://doi.org/10.1393/ncr/i2016-10120-8.

[73] J. N. Bahcall and C. Peña-Garay, New Journal of Physics **6**, 63 (2004), ISSN 1367-2630, URL https://dx.doi.org/10.1088/1367-2630/6/1/063.

[74] M. C. Gonzalez-Garcia and M. Maltoni, Physics Reports **460**, 1 (2008), ISSN 0370-1573, URL https://www.sciencedirect.com/science/article/pii/S0370157308000148.

[75] A. Mallick, S. Mandal, and C. M. Chandrashekar, The European Physical Journal C **77**, 85 (2017), ISSN 1434-6052, URL https://doi.org/10.1140/epjc/s10052-017-4636-9.

[76] G. D. Molfetta and A. Pérez, New Journal of Physics **18**, 103038 (2016), ISSN 1367-2630, URL https://dx.doi.org/10.1088/1367-2630/18/10/103038.

[77] T. Kajita and Y. Totsuka, Reviews of Modern Physics **73**, 85 (2001), URL https://link.aps.org/doi/10.1103/RevModPhys.73.85.

[78] R. Davis, D. S. Harmer, and K. C. Hoffman, Phys. Rev. Lett. **20**, 1205 (1968), URL https://link.aps.org/doi/10.1103/PhysRevLett.20.1205.

[79] M. C. Gonzalez-Garcia and M. Maltoni, Physics Reports **460**, 1 (2008), ISSN 0370-1573, URL https://www.sciencedirect.com/science/article/pii/S0370157308000148.

[80] S. M. Bilenky and S. T. Petcov, Rev. Mod. Phys. **59**, 671 (1987), URL https://link.aps.org/doi/10.1103/RevModPhys.59.671.

[81] S. M. Bilenky and B. Pontecorvo, Physics Reports **41**, 225 (1978), ISSN 0370-1573, URL https://www.sciencedirect.com/science/article/pii/0370157378900959.

[82] S. Bilenky, Journal of Physics: Conference Series **718**, 062005 (2016), ISSN 1742-6596, URL https://dx.doi.org/10.1088/1742-6596/718/6/062005.

[83] Z. Maki, M. Nakagawa, and S. Sakata, Progress of Theoretical Physics **28**, 870 (1962), ISSN 0033-068X, URL https://doi.org/10.1143/PTP.28.870.

[84] T. Kajita, Reviews of Modern Physics **88**, 030501 (2016), URL https://link.aps.org/doi/10.1103/RevModPhys.88.030501.

[85] S. Fukuda, Y. Fukuda, M. Ishitsuka, Y. Itow, et al., Physics Letters B **539**, 179 (2002), ISSN 0370-2693, URL https://www.sciencedirect.com/science/article/pii/S0370269302020907.

[86] J. Naikoo, S. Banerjee, and C. M. Chandrashekar, Physical Review A **102**, 062209 (2020), URL https://link.aps.org/doi/10.1103/PhysRevA.102.062209.

[87] S. Banerjee, A. K. Alok, R. Srikanth, and B. C. Hiesmayr, The European Physical Journal C **75**, 487 (2015), ISSN 1434-6052, URL https://doi.org/10.1140/epjc/s10052-015-3717-x.

[88] Wikipedia, *Neutrino oscillation* (2023), URL http://en.wikipedia.org/w/index.php?title=Neutrino%20oscillation&oldid=1143844099.

[89] L. Amico, R. Fazio, A. Osterloh, and V. Vedral, Rev. Mod. Phys. **80**, 517 (2008), URL https://link.aps.org/doi/10.1103/RevModPhys.80.517.

[90] M. Blasone, F. Dell'Anno, S. D. Siena, and F. Illuminati, Europhysics Letters **85**, 50002 (2009), URL https://dx.doi.org/10.1209/0295-5075/85/50002.

[91] Z. Hu, R. Xia, and S. Kais, Scientific Reports 2020 10:1 **10**, 1 (2020), ISSN 2045-2322, URL https://www.nature.com/articles/s41598-020-60321-x.

[92] Z. Hu, K. Head-Marsden, D. A. Mazziotti, P. Narang, and S. Kais, Quantum **6**, 726 (2022), ISSN 2521-327X, URL https://doi.org/10.22331/q-2022-05-30-726.

[93] F. Benatti and R. Floreanini, Journal of High Energy Physics **2000**, 032 (2000), URL https://dx.doi.org/10.1088/1126-6708/2000/02/032.

[94] E. Lisi, A. Marrone, and D. Montanino, Phys. Rev. Lett. **85**, 1166 (2000), URL https://link.aps.org/doi/10.1103/PhysRevLett.85.1166.

[95] G. B. Gomes, D. V. Forero, M. M. Guzzo, P. C. de Holanda, and R. L. N. Oliveira, Phys. Rev. D **100**, 055023 (2019), URL https://link.aps.org/doi/10.1103/PhysRevD.100.055023.

[96] D. Bacon and W. van Dam, Communications of the ACM **53**, 84 (2010), ISSN 0001-0782, URL https://dl.acm.org/doi/10.1145/1646353.1646375.

[97] A. Montanaro, npj Quantum Information **2**, 15023 (2016), ISSN 2056-6387, URL https://doi.org/10.1038/npjqi.2015.23.

[98] T. D. Ladd, F. Jelezko, R. Laflamme, Y. Nakamura, C. Monroe, and J. L. O'Brien, Nature **464**, 45 (2010), ISSN 1476-4687, URL https://doi.org/10.1038/nature08812.

[99] N. Gisin, G. Ribordy, W. Tittel, and H. Zbinden, Reviews of Modern Physics **74**, 145 (2002), URL https://link.aps.org/doi/10.1103/RevModPhys.74.145.

[100] F. Magniez, A. Nayak, J. Roland, and M. Santha, Proceedings of the thirty-ninth annual ACM symposium on Theory of computing pp. 575–584 (2007), URL https://dl.acm.org/doi/10.1145/1250790.1250874.

[101] M. Cerezo, A. Arrasmith, R. Babbush, S. C. Benjamin, S. Endo, K. Fujii, J. R. McClean, K. Mitarai, X. Yuan, L. Cincio, et al., Nature Reviews Physics **3**, 625 (2021), ISSN 2522-5820, URL https://www.nature.com/articles/s42254-021-00348-9.

[102] P. Shor, in *Proceedings 35th Annual Symposium on Foundations of Computer Science* (1994), pp. 124–134, URL https://ieeexplore.ieee.org/document/365700.

[103] S. Lloyd, Science **273**, 1073 (1996), URL https://www.science.org/doi/10.1126/science.273.5278.1073.

[104] A. W. Harrow, A. Hassidim, and S. Lloyd, Physical Review Letters **103**, 150502 (2009), URL https://link.aps.org/doi/10.1103/PhysRevLett.103.150502.

[105] A. M. Childs and W. van Dam, Reviews of Modern Physics **82**, 1 (2010), URL https://link.aps.org/doi/10.1103/RevModPhys.82.1.

[106] S. P. Jordan, K. S. M. Lee, and J. Preskill, Science **336**, 1130 (2012), URL https://www.science.org/doi/abs/10.1126/science.1217069.

[107] B. Bauer, S. Bravyi, M. Motta, and G. K.-L. Chan, Chemical Reviews **120**, 12685 (2020), ISSN 0009-2665, URL https://doi.org/10.1021/acs.chemrev.9b00829.

[108] A. Ambainis, ACM SIGACT News **35**, 22 (2004), ISSN 0163-5700, URL https://dl.acm.org/doi/10.1145/992287.992296.

[109] I. M. Georgescu, S. Ashhab, and F. Nori, Rev. Mod. Phys. **86**, 153 (2014), URL https://link.aps.org/doi/10.1103/RevModPhys.86.153.

[110] A. Trabesinger, Nature Physics **8**, 263 (2012), ISSN 1745-2481, URL https://doi.org/10.1038/nphys2258.

[111] L. K. Grover, Proceedings of the twenty-eighth annual ACM symposium on Theory of Computing pp. 212–219 (1996), URL https://dl.acm.org/doi/10.1145/237814.237866.

[112] R. A. M. Santos, Quantum Information Processing **15**, 4461 (2016), ISSN 1573-1332, URL https://doi.org/10.1007/s11128-016-1427-4.

[113] M. Santha, in *Theory and Applications of Models of Computation*, edited by M. Agrawal, D. Du, Z. Duan, and A. Li (Springer, Berlin, Heidelberg, 2008), Lecture Notes in Computer Science, pp. 31–46, ISBN 978-3-540-79228-4.

[114] R. Portugal, *Quantum Walks and Search Algorithms* (Springer, New York, NY, 2013), ISBN 978-1-4614-6335-1 978-1-4614-6336-8, URL https://link.springer.com/10.1007/978-1-4614-6336-8.

[115] A. Ambainis, International Journal of Quantum Information **01**, 507 (2003), ISSN 0219-7499, URL https://www.worldscientific.com/doi/10.1142/S0219749903000383.

[116] Y. Xu, D. Zhang, and L. Li, Physical Review A **106**, 052207 (2022), URL https://link.aps.org/doi/10.1103/PhysRevA.106.052207.

[117] T. G. Wong and R. A. M. Santos, Quantum Information Processing **16**, 154 (2017), ISSN 1573-1332, URL https://doi.org/10.1007/s11128-017-1606-y.

[118] A. J. and A. Patel, Quantum Information and Computation **18**, 1295 (2018), ISSN 15337146, 15337146, URL http://www.rintonpress.com/journals/doi/QIC18.15-16-3.html.

[119] M. Li and Y. Shang, New Journal of Physics **22**, 123030 (2020), ISSN 1367-2630, URL https://dx.doi.org/10.1088/1367-2630/abca5d.

[120] A. Glos, N. Nahimovs, K. Balakirev, and K. Khadiev, Quantum Information Processing **20**, 6 (2021), ISSN 1573-1332, URL https://doi.org/10.1007/s11128-020-02939-4.

[121] G. A. Bezerra, P. H. G. Lugão, and R. Portugal, Phys. Rev. A **103**, 062202 (2021), URL https://link.aps.org/doi/10.1103/PhysRevA.103.062202.

[122] P. Kaye, R. Laflamme, M. Mosca, P. Kaye, R. Laflamme, and M. Mosca, *An Introduction to Quantum Computing* (Oxford University Press, Oxford, New York, 2006), ISBN 978-0-19-857049-3.

[123] B. Tregenna, W. Flanagan, R. Maile, and V. Kendon, New Journal of Physics **5**, 83 (2003), URL https://dx.doi.org/10.1088/1367-2630/5/1/383.

[124] K. Watabe, N. Kobayashi, M. Katori, and N. Konno, Phys. Rev. A **77**, 062331 (2008), URL https://link.aps.org/doi/10.1103/PhysRevA.77.062331.

[125] F. Fillion-Gourdeau, S. MacLean, and R. Laflamme, Physical Review A **95**, 042343 (2017), URL https://link.aps.org/doi/10.1103/PhysRevA.95.042343.

[126] W. Puengtambol, P. Prechaprapranwong, and U. Taetragool, Journal of Physics: Conference Series **1719**, 012103 (2021), ISSN 1742-6596, URL https://dx.doi.org/10.1088/1742-6596/1719/1/012103.

[127] A. Bhattacharya, H. Sahu, A. Zahed, and K. Sen (2023), arXiv:2307.13450 [quant-ph], URL http://arxiv.org/abs/2307.13450.

[128] F. Vatan and C. Williams, Phys. Rev. A **69**, 032315 (2004), URL https://link.aps.org/doi/10.1103/PhysRevA.69.032315.

[129] S. Aaronson, *Introduction to Quantum Information Science* , https://www.scottaaronson.com/ (2016), [Online; accessed 01-12-2023].

[130] C. Gidney (2015), URL https://algassert.com/circuits/2015/06/05/Constructing-Large-Controlled-Nots.html.

[131] V. V. Shende and I. L. Markov, Quantum Information & Computation **9**, 461 (2009), ISSN 1533-7146.

[132] S. Chakraborty, L. Novo, S. Di Giorgio, and Y. Omar, Phys. Rev. Lett. **119**, 220503 (2017), URL https://link.aps.org/doi/10.1103/PhysRevLett.119.220503.

[133] P. W. Anderson, Phys. Rev. **109**, 1492 (1958), URL https://link.aps.org/doi/10.1103/PhysRev.109.1492.

[134] M. Zeng and E. H. Yong, Scientific Reports **7**, 12024 (2017), ISSN 2045-2322, URL https://doi.org/10.1038/s41598-017-12077-0.

[135] S. Derevyanko, Scientific Reports **8**, 1795 (2018), ISSN 2045-2322, URL https://doi.org/10.1038/s41598-017-18498-1.

[136] K. Sen (2023), URL http://arxiv.org/abs/2303.06769.

[137] J. I. Cirac, P. Zoller, H. J. Kimble, and H. Mabuchi, Phys. Rev. Lett. **78**, 3221 (1997), URL https://link.aps.org/doi/10.1103/PhysRevLett.78.3221.

[138] M. Christandl, N. Datta, A. Ekert, and A. J. Landahl, Phys. Rev. Lett. **92**, 187902 (2004), URL https://link.aps.org/doi/10.1103/PhysRevLett.92.187902.

[139] M. A. Nielsen, M. R. Dowling, M. Gu, and A. C. Doherty, Science **311**, 1133 (2006), URL https://doi.org/10.1126%2Fscience.1121541.

[140] M. R. Dowling and M. A. Nielsen, Quant. Inf. Comput. **8**, 0861 (2008), URL https://doi.org/10.26421/QIC8.10-1.

[141] G. Di Molfetta and P. Arrighi (2019), URL https://doi.org/10.48550/arXiv.1906.04483.

[142] C. M. Chandrashekar, Scientific Reports **3**, 2829 (2013), URL https://doi.org/10.1038/srep02829.

[143] P. Kuusela (2019), URL https://arxiv.org/pdf/1905.00429.pdf.

[144] Qiskit contributors, *Qiskit: An open-source framework for quantum computing* (2023).

[145] M. A. Nielsen and I. L. Chuang, *Quantum Computation and Quantum Information: 10th Anniversary Edition* (Cambridge University Press, 2010).

[146] S. Omanakuttan and A. Lakshminarayan, Phys. Rev. E **103**, 012207 (2021), URL https://arxiv.org/pdf/2008.11318.pdf.